The Effect of Amines on the Electrode Potential of Mild Steel in Tap Water and Acid Solutions[1]

NORMAN HACKERMAN AND J. D. SUDBURY[2]

The University of Texas, Austin, Texas

ABSTRACT

Potentials of SAE 1020 steel were measured in 1.0*N* H_2SO_4 and tap water, each with added amines. The steady state potential was found to be a function of the nature and concentration of the amine additives. The effect could not be completely reversed in all cases when the metal was placed in amine-free solutions. Anodic and cathodic polarization measurements in the presence of the amines showed that both anodic and cathodic areas were affected by the inhibitor. Decomposition potential curves for those systems pointed to the same conclusion.

The data are discussed in terms of a generalized theory of corrosion inhibition. It is postulated that the measured changes are due to adsorption of the polar compounds on the metal surface. The lack of complete reversibility is attributed to the heterogeneity of the surface giving rise to a variety of adsorption energies. Inhibition at the anodic areas is considered to be due to an actual reduction in tendency for the iron ions to go into solution due to a displacement of electrons from the metal toward the positively charged particle rather than toward the cathodic areas within the metal. The amines may act as inhibitors at the cathodic areas by virtue of diffusion effects, increased resistance, and overvoltage.

INTRODUCTION

There is a growing belief among many investigators that the mechanism of corrosion inhibition by organic compounds involves adsorption which is not limited to either anode or cathode regions (1, 2, 3, 4). Most of the earlier workers suggested that inhibition was due principally to adsorption of the inhibitor on the cathodic areas. In a recent paper, Hoar (5) concluded that inhibition takes place through a general adsorption which interferes with both the anodic and cathodic processes with the effect on the former generally being greater. His conclusions were based on weight loss and single electrode potential measurements of mild steel corroding in dilute sulfuric acid using varying concentrations of beta-naphthoquinoline and ortho-tolylthiourea as additives. Cavallaro (6) and his coworkers have recently made a study of the electrochemical mechanism of corrosion processes by determining the effect of anodic and cathodic polarizations on the electrode potential of steel. They also reported inhibition to be due to both cathodic and anodic effects. A study of anodic and cathodic polarization curves led Kuznetsov and Iofa (7) to the conclusion that the inhibitor was adsorbed. They stated that the adsorbed inhibitor retards hydrogen evolution at the cathodic areas and solution of iron at the anodic areas.

Bockris and Conway (8) related corrosion inhibition to the activation overpotential of hydrogen at an iron surface in a solution containing inhibitors. Overpotential measurements were made on iron electrodes in 0.1*N* HCl by direct and indirect methods to distinguish between hydrogen activation overpotential and increase in resistance at the cathode-solution interface due to the presence of an adsorbed film. Measurements were made with varying polarizing currents. The increase in overpotential was generally greater with increasing complexity of inhibition molecule and at higher concentration. It was shown that the presence of certain inhibitors caused a considerable increase in the hydrogen activation overpotential but that ohmic resistances were negligible. Corrosion inhibition was thus attributed to an increase in hydrogen overpotential. They also showed that corrosion activators such as nitrobenzene caused the hydrogen overpotential to decrease. The claim was made that the prevention of ionic diffusion could not be a factor in the inhibition process.

A study of the effect of the addition of amines on the electrode potential of copper in buffered acid solutions was discussed in an earlier paper from this laboratory (9). Those data were discussed in terms of a generalized theory for the mechanism of organic corrosion inhibitors (10). It seemed advisable to extend the previous work to a study of the effect of various amines on the electrode potential of mild steel.

[1] Manuscript received October 11, 1949. This paper prepared for delivery before the Chicago Meeting, October 12 to 15, 1949. This work was carried out under Contract N5ori-136, Task Order II, with the Office of Naval Research.

[2] Present address: Continental Oil Company, Ponca City, Oklahoma.

The adsorption of cationic materials (e.g., amines) on the surface generally may be explained by a mechanism in which the positive inhibitor particle (oxidizing agent) offers competition for the electrons flowing from anodic to cathodic regions within the metal. The displacement of electrons toward the positively charged particle may, in a sense, cause equipotentialization of the surface with consequent decreased tendency for galvanic corrosion. By such a mechanism, the most active (most nearly oxidized) atoms may actually be fully oxidized and dissolve at very low concentrations of inhibitor. However, at slightly higher inhibitor concentrations the next most active atoms might be partially oxidized, thus further decreasing the flow of electrons in the metal. It is likely, though, that only a very small fraction of the surface atoms are involved in actual electronic transfers (11). Essentially, then, the effect is one of partial polarization from the solution side. At cathodic areas the particle may be adsorbed by Van der Waals forces or held by electrostatic forces, thereby providing a diffusion barrier or ohmic resistance.

If the above is true, it appears that it should be possible to get surface effects using either homogeneous anodic or cathodic surfaces, as well as ordinary surfaces. Homogeneous anodic and cathodic surfaces could be obtained by anodic and cathodic polarization of steel coupons. Adsorption isotherm type curves already have been described for amines on cathodically polarized mild steel in 1*N* sulfuric acid (12). Evidence of adsorption on anodically polarized coupons would lend further support to the idea that the inhibition mechanism involves adsorption less specifically than at cathode areas alone.

Experimental

Equipment and Materials

Potential measurements were made using a Type K-2 Leeds & Northrup potentiometer as described previously (9). Changes in pH were obtained with a Model G Beckman pH meter which could be read to 0.02 pH units. Optical density measurements were made with a Model DU Beckman Photoelectric Quartz Spectrophotometer. A tungsten lamp supplied light of 500 mμ wavelength.

The tap water used was slightly alkaline with a chloride content of 2–3 ppm. The calcium and magnesium content was relatively small. The sulfuric acid used was obtained from the E. I. du Pont Company and contained very small amounts of iron, ammonium ion, heavy metals (chiefly lead), reducing materials (chiefly SO_2), and nonvolatile materials. The n-octyl and n-decyl amines (Armeen 8D and Armeen 10D) were furnished by Armour and Company. They were purified by distillation and were better than 90 per cent pure. The impurities consisted of the amines with two carbons more or less than in the subject compound. The other amines were all made by Eastman Kodak Company and were all of the highest purity available except for the dibenzyl amine which was "technical" grade.

Coupons, 2.5 x 5.0 x 0.6 cm, were prepared from SAE 1020 sheet steel. The coupons were cleaned by abrasion with a fine grade emery belt (Grit No. 100), scrubbed with pumice, rinsed with distilled water, and then rubbed carefully with a towel to remove clinging particles of emery, pumice, and droplets of water. They were then coupled in the electric circuit as described previously (9). A saturated calomel cell was used as the reference electrode.

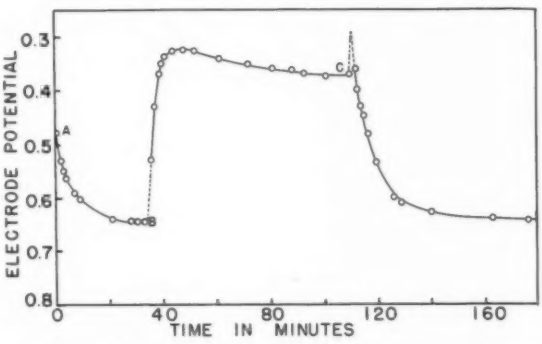

Fig. 1. Effect of adsorption and desorption of 0.047 molar diethyl amine on the electrode potential of 1020 steel at 25°.

Potentials in Tap Water

A steel coupon was placed in a cell containing 200 ml of tap water at 25 ± 0.2°C and the potential was observed at various time intervals until a steady state value was reached. At this point a weighed amount of diethyl amine was added to the system to give a 0.047 molar solution and a very rapid change of potential in the more noble direction was observed. It was found that the steady potential was dependent on the concentration of amine added, as had been the case with copper (9). After the potential had reached a reasonably steady value, an attempt was made to reverse the potential shift by transferring the inhibited coupon to a beaker containing tap water free of amine. If the adsorbed amine were completely removed, the final potential should have been very nearly the same as that of the uninhibited coupon.

An interesting outcome of this work was the observation that after exposure of the steel to higher inhibitor concentrations (0.017–0.047 molar), the potential shift could be reversed completely, but, for lower concentrations (0.0028–0.014 molar), the effect did not appear to be entirely reversible. These experiments are illustrated by Fig. 1 and 2. At point A

the coupon was placed in the solution; at point B the inhibitor was added, and at point C the washing process was begun; points D and E on Fig. 2 represent successive washings. Note that the initial change in the noble direction in the case of the 0.047 molar diethyl amine (Fig. 1) was quite high, but that the final steady potential after desorption indicated complete reversal of the potential shift. On the other hand, the rise due to the 0.014 molar diethyl amine was much smaller, but the final equilibrium value after three successive washings indicated that not all of the adsorbed material had been removed by the simple washing process. Similar observations have been made in two other independent investigations here; first, using a procedure in which the extent of adsorption of polar organic molecules on steel powder from benzene was measured gravimetrically (13), and second, in an electron diffraction study of steel surfaces as an alkyl substituted succinimide was adsorbed and desorbed from benzene solutions (14). These suggested that adsorption rate, steric factors, and different types of surface forces were involved.

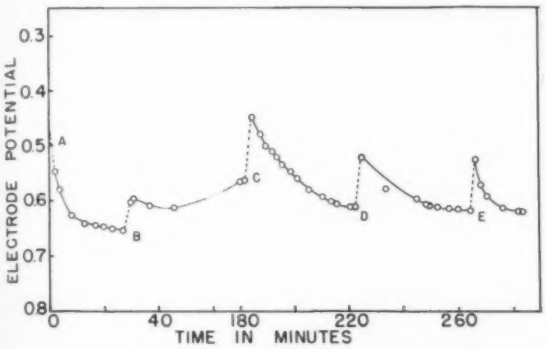

FIG. 2. Effect of adsorption and desorption of 0.014 molar diethyl amine on the electrode potential of 1020 steel at 25°.

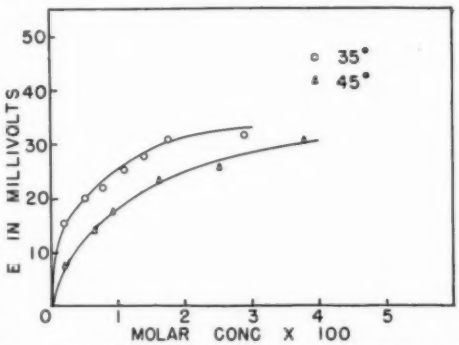

FIG. 3. Triethyl amine adsorption on 1020 steel from 1.0*N* H_2SO_4.

Potentials in Sulfuric Acid

A more complete study was then made of the potential of the steel in 1*N* H_2SO_4 as a function of the nature and concentration of added amine. Experiments were made using varying concentration of nine amines at 35°C and at 45°C. The solutions were prepared by dissolving weighed amounts of inhibitor in 1.0*N* H_2SO_4. The steady state potential of the coupon in an amine-free acid solution at each temperature was determined first. The steady state potentials in the various inhibitor solutions were then measured and were again found to be somewhat more noble. The difference between the potential of the inhibited and uninhibited coupon was taken to be a measure of the extent of adsorption. Plotting this difference in potential against the inhibitor concentration for each amine at each temperature gave "adsorption isotherms." As an illustration, Fig. 3 shows the curve for triethyl amine. Fig. 4 and 5 show these data plotted according to equations modeled after the linear forms of the Langmuir and the Freundlich equations (9). According to Halsey (11), the agreement with the Langmuir equation indicates the presence of less than a monolayer and the existence of chemisorption forces. Table I contains a compilation of the results obtained with the nine amines.

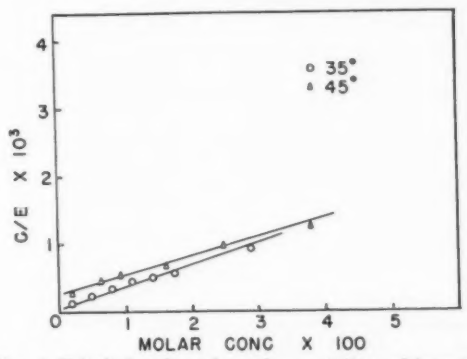

FIG. 4. Triethyl amine adsorption on 1020 steel from 1.0*N* H_2SO_4.

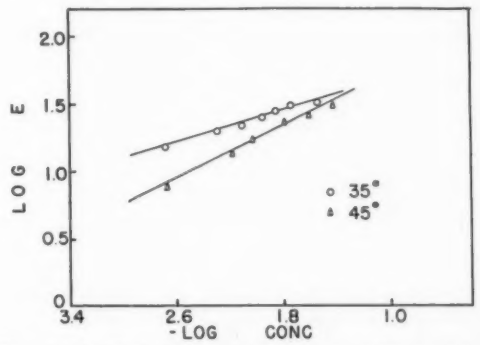

FIG. 5. Triethyl amine adsorption on 1020 steel from 1.0*N* H_2SO_4.

Constants of the Langmuir and Freundlich equation were determined from the linear forms using

the best apparent straight line through the experimental points. Calculated isotherms using these constants fitted only moderately well. By fitting the linear form by the method of averages, constants were obtained for the triethyl amine system at 45° which gave a calculated isotherm coincident with the lower curve in Fig. 3. The actual values of a', k, and n are not of great significance although the n values are of the usual order of magnitude. The values of b' (column 5, Table I) are the highest potentials attained according to the modified form of the Langmuir equation and compare reasonably

TABLE I

Amine	Temp	Peak	Temp coef	Langmuir constants		Freundlich constants	
				b'	a'	n	k
	°C	mv	mv/°C	mv			
diethyl	35	7.5	+0.55	9.7	129	2.17	37
	45	13.0		15	121	2.17	92
di-n-butyl	35	44	−1.2	46	210	2.22	162
	45	32		29	438	2.00	220
di-n-amyl	35	25	+0.60	29	292	1.59	450
	45	31		32	387	1.72	365
isobutyl	35	17	−0.95	14	355	0.94	49
	45	7.5		9.2	273	2.33	47
isoamyl	35	26	—	29	117	2.17	125
triethyl	35	35	−0.20	31	1600	3.33	98
	45	31		38	96	2.08	175
tri-n-butyl	35	42	+1.50	42	∞	3.84	170
	45	57		56	600	2.70	380
benzyl	35	43	−0.20	50	222	1.75	290
	45	41		48	420	1.89	310
dibenzyl	35	56	−0.40	53	1900	5.88	124
	45	52		50	2000	12.50	76

well with the experimental values in column 3 of Table I. Brunauer (15) has stated that, for Langmuir type adsorption, a' should change markedly and b' only slightly with temperature. The tabulated values are in agreement with such effects. The constants n and k of the Freundlich equation also vary somewhat as described by Brunauer. The data appear to obey both of the adsorption equations reasonably well, especially the Langmuir equation. This is not proof that adsorption is involved. However, such a step is either specified or is tacitly assumed by many workers, and the parallelism between potential changes and adsorption with concentrations is of interest.

Attempts were made to desorb the amine in each of these systems by washing the coupons in amine-free sulfuric acid. The results were somewhat erratic but showed that, in general, reversal was not complete. Although these results were qualitatively repetitive, quantitative checks could not be obtained. The chief problem appeared to be the difficulty in finding a method of preparing the coupon surface reproducibly.

Potentials after Improved Surface Preparation

In an attempt to improve the method of coupon preparation, cylindrical coupons, 1.8 cm diameter x 6.7 cm long, were prepared from a rod of SAE 1020 steel. The surface was prepared while the coupons rotated in a chuck mounted on the shaft of a motor

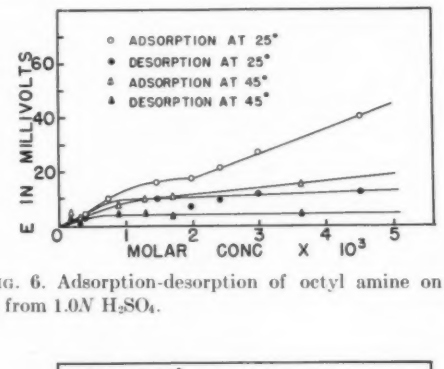

FIG. 6. Adsorption-desorption of octyl amine on 1020 steel from 1.0*N* H_2SO_4.

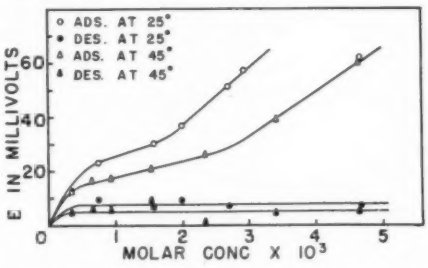

FIG. 7. Adsorption-desorption of decyl amine on 1020 steel from 1.0*N* H_2SO_4.

(1150 rpm). Steps in the surface preparation included abrasion with 2/0 and then 4/0 Behr-Manning emery polishing paper, rubbing with lens paper, and coating the flat surfaces and about 1 cm of the top and bottom of the cylindrical surface with Ucilon. A saturated KCl-3 per cent agar bridge was used between the solution and the reference calomel electrode.

The effect of n-octyl and n-decyl amines on the potential of these coupons is shown in Fig. 6 and 7. These curves were quite reproducible. They are somewhat sigmoidal except that the second change in slope is quite sharp. Assuming saturation concentration values for the amines, an attempt was made to

fit these data to a linear form of the BET[3] equation. This was not successful, the resulting curves being convex to the abscissa.

The first breaks occur possibly at concentration at which all sites available for Langmuir adsorption were filled (11) and the subsequent linear rise may indicate polylayer formation. At each concentration, desorption caused a decrease in potential due to removal of less firmly held solute particles. From the essentially horizontal nature of the desorption curves, it seems likely that all of the piled-on molecules were removed by the washing process. In addition, some of the directly adsorbed layer must have come off since the horizontal "desorption" curve lies below the just change in slope of the "adsorption" curve.

Study of Concentration of Fe(II) and Fe(III)

Before proceeding further it was necessary to prove that the changes in steady state potential were actually due to adsorption of the inhibitor and not to a change in iron ion concentration in the system. Qualitative tests (16) using alpha, alpha′ dipyridyl, and potassium thiocyanate showed the presence of both Fe(II) and Fe(III) in solutions resulting from adsorption and desorption experiments with various inhibitor concentrations. A quantitative determination was then made spectrophotometrically using a method according to Foley and Anderson (17). The method is based on the fact that Fe(III) forms a violet colored complex with sulfosalicylic acid. It was found that solutions with smaller total iron ion concentrations were those in which steel had exhibited the more noble potentials. This is contrary to effects expected from larger iron ion concentrations and also shows that the nobler potential and inhibition are related. It was also determined that a sudden large increase in iron ion concentration by addition of Fe(II) and Fe(III) salts did not cause a correponding change in potential in the more noble direction. Further, if the potential changes were due to iron ions in the solutions, positive temperature coefficients would be expected. However, negative temperature coefficients are shown in Fig. 6 and 7. Therefore the changes in steady state potentials of the steel coupons do not appear to be due in any large measure to changes in iron ion concentration.

Use of Polarized Coupons

Exploratory potential measurements on anodically and cathodically polarized steel coupons were made to show the effect of varying current density and inhibitor concentration on the potential of SAE 1020 steel coupons in 1.0*N* H_2SO_4. The exposed area of the steel coupon was flat and circular (diameter = 1.90 cm). A platinum wire was used as the inert electrode in both anodic and cathodic polarizations. The electrodes were placed 5 cm apart in the inhibitor solution. A 6-volt lead storage battery served as a source of current. The solutions

[3] See "Pittsburgh International Conference on Surface Reactions," Corrosion Publishing Co., Pittsburgh, 1948, p. 82, for details about this equation.

TABLE II. *The effect of n-octyl amine concentration on the electrode potential of SAE 1020 steel in 1.0N H_2SO_4 during and after anodic polarization at 35°C*

Amine conc molar × 1000	Polarizing current			
	15 milliamperes		30 milliamperes	
	Potential during polarization	Potential after polarization	Potential during polarization	Potential after polarization
0	0.463	0.498		
0.49	0.453	0.498		
1.15	0.445	0.494		
1.66	0.439	0.492		
2.57	0.427	0.483		
2.93	0.424	0.488		
3.28	0.412	0.486		
3.35	0.414	0.483		
3.48	0.417	0.479		
3.54	0.414	0.465		
0			0.445	0.504
0.60			0.444	0.504
1.22			0.424	0.503
1.35			0.422	0.503
1.76			0.429	0.500
2.47			0.409	0.496
2.87			0.417	0.491
3.13			0.421	0.494
3.46			0.404	0.479

TABLE III. *The effect of n-octyl amine concentration on the electrode potential of SAE 1020 steel in 1.0N H_2SO_4 during and after cathodic polarization at 35°C*

Amine conc molar × 1000	Polarizing current			
	5 milliamperes		10 milliamperes	
	Potential during polarization	Potential after polarization	Potential during polarization	Potential after polarization
0	0.553	0.509		
0	0.547	0.502		
0.45	0.575	0.498		
1.08	0.613	0.494		
2.06	0.641	0.497		
2.44	0.640	0.492		
3.39	0.641	0.483		
0			0.582	0.508
0.67			0.620	0.499
1.31			0.641	0.494
1.65			0.648	0.492
2.06			0.689	0.494
2.47			0.669	0.493
3.19			0.699	0.508
3.34			0.699	0.510
3.38			0.699	0.504

contained weighed amounts of n-octyl amine in 1800 ml of 1.0*N* H_2SO_4.

On anodically polarizing the steel, the electrode potential changed quite rapidly in the more noble direction and reached an essentially steady value after about one hour. The steady state value was dependent on the concentration of inhibitor. The electrode potential attained a less noble value with cathodic polarization. When the polarization currents were stopped the potentials changed rapidly at first toward the original potential of the unpolarized coupons and then slowly attained new steady state values which were dependent on the amine concentration. Tables II and III summarize the data obtained in the polarization work. Data were obtained also at 40 and 70 milliamperes for both anodic and cathodic polarization but these results were much more erratic and are not included here.

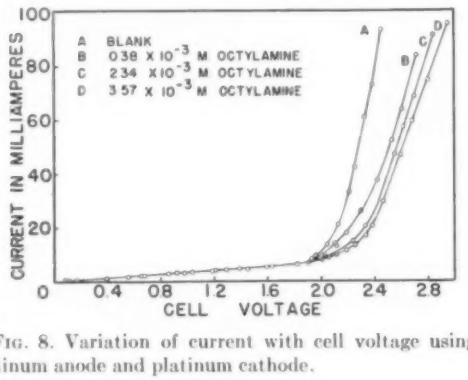

FIG. 8. Variation of current with cell voltage using a platinum anode and platinum cathode.

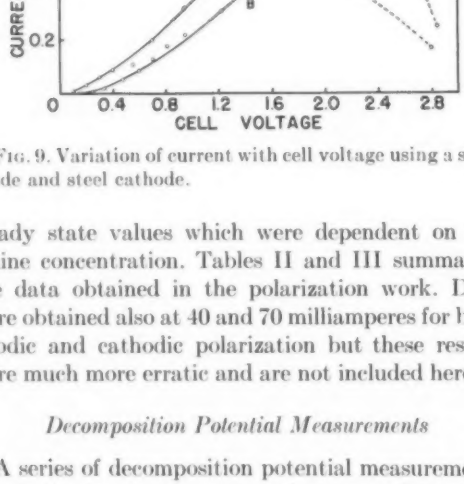

FIG. 9. Variation of current with cell voltage using a steel anode and steel cathode.

Decomposition Potential Measurements

A series of decomposition potential measurements (applied voltage versus current) were made in 1.0*N* H_2SO_4. Fig. 8 shows the effect of concentration of n-octyl amine on the decomposition potential curves using a platinum anode and a platinum cathode. The amine had no effect until the region of decomposition potential was reached, at which time the current rise was retarded by the presence of the amine. Increasing concentration of amine increased the effect. The presence of the amine retarded the formation of either H_2 or O_2 (since the effect did not appear until after the decomposition of water began as evidenced by the evolution of hydrogen and oxygen). Curves for steel coupons as both anode and cathode are given in Fig. 9. The residual current portion was very narrow and the current rose much more rapidly than when platinum electrodes were used. In addition, with steel, values 10 times as high were attained for equal voltages. Again the presence of an amine retarded the current rise. At about 2 volts the current decreased rapidly with increasing voltage. This was apparently because of passivation and the beginning of oxygen evolution (18).

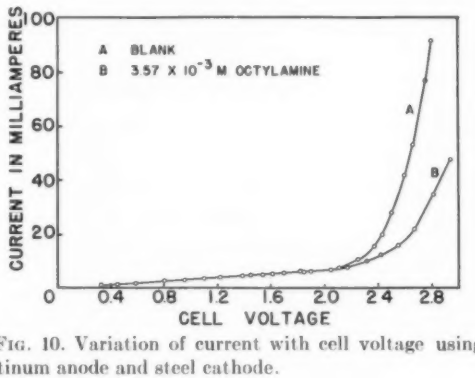

FIG. 10. Variation of current with cell voltage using a platinum anode and steel cathode.

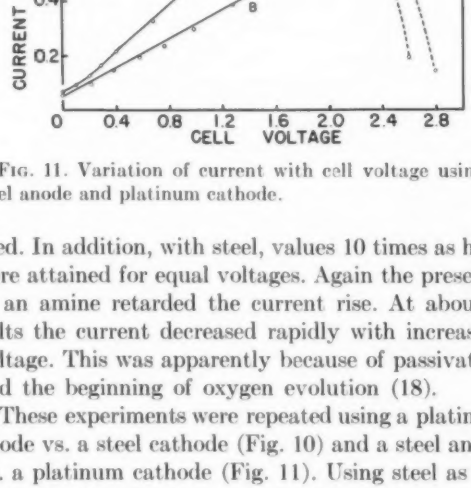

FIG. 11. Variation of current with cell voltage using a steel anode and platinum cathode.

These experiments were repeated using a platinum anode vs. a steel cathode (Fig. 10) and a steel anode vs. a platinum cathode (Fig. 11). Using steel as the cathode, the curves were essentially the same as when platinum was used as both the anode and cathode. Using steel as the anode, the curves were essentially the same as when steel was used as the anode and cathode.

Discussion

The experiments just described show that the addition of amine inhibitors causes the electrode potential of steel to become more noble in an acid solution. This shift increased with increasing molecular size and concentration of inhibitor. The increasingly cathodic potential may be ascribed partly to a decrease in solution tendency of the most anodic portions of the surface. This could occur by "partial oxidation" of the active atoms by displacement of electrons toward the positive amine molecules, thereby decreasing the tendency for flow of current into the metal and thus forming a more nearly homogeneous metal surface. Leveling off of the curves indicates that essentially all of the Langmuir sites have been filled. From the desorption data, it appears that a portion of the surface has irreversibly adsorbed the inhibitor. Cavallaro (6) reported similar residual effects when his polarized coupons were transferred from inhibitor to inhibitor-free solutions. This portion of the surface presumably consists of the anodic sites since the largest potential increments come with the lower amine concentrations. In nearly all cases, a much larger percentage of the potential rise remained on desorption after immersion at the lower concentrations (Fig. 1 and 2). The reason possibly lies in the submicroscopic roughness of the surface of the metal. Undoubtedly, considerable bridging occurs and a large part of the metal surface is blocked. Trurnit (19) reached such a conclusion on the basis of a series of interesting experiments in which monolayers were transferred from a liquid to a metal surface by dipping at constant surfaces pressure. For lower surface pressures, and likewise concentrations, the transferred layer could not be completely removed by re-immersion although complete removal was possible when starting with high surface pressures. These effects due to surface roughness should disappear if the system remained static until complete equilibrium was attained. A more fundamental change may have taken place, however, but what it could be is not yet clear. In any event, the effect might be important in practical corrosion problems, for example, where there are flow processes involved.

The polarization studies bear out the earlier predictions that the electrode potentials of both anodic and cathodic areas are affected by the addition of inhibitors. Although the data were not smooth, the change in the noble direction appeared to be dependent on the inhibitor concentration in both cases. Hoar (5) has stated that the ratio of anodic to cathodic effect is greater at higher inhibitor concentrations. Calculations show that a similar effect may have been found here.

The decomposition potential curves do not adequately separate anodic and cathodic effects, but the similarity of Fig. 8 and 10 and of Fig. 9 and 11 indicate that electrode processes of steel polarized either anodically or cathodically are affected by the presence of amines.

If the processes postulated are true, for maximum reduction in metal reactivity, it seems necessary to find compounds and conditions whereby the surface remains equipotentialized to the greatest extent even after desorption.

Conclusions

The effects of adsorption and desorption of a series of amines on the electrode potential of steel in tap water and in acid solutions were studied by determining electrode potentials of steel coupons. It was shown that increasing inhibitor concentrations caused the steel coupons to assume more noble potentials. The change in potential was taken to be a measure of the extent of adsorption. Desorption experiments showed that only a portion of the adsorbate could be readily removed indicating that at least two types of adsorption process occurred. Polarization and decomposition potential studies indicated that both the anodic and cathodic areas were affected by the amines. It is postulated that the effect on the anodic surfaces may actually cause a decrease in solution tendency, whereas adsorption at the cathodic regions probably inhibits by means of diffusion, resistance, or overvoltage effects.

Acknowledgement

The authors are happy to take this opportunity to express their gratitude to the Office of Naval Research for their support of this work.

Any discussion of this paper will appear in a Discussion Section, to be published in the December 1950 issue of the Journal.

References

1. R. W. Lawrence and J. H. Walton, *J. Phys. Chem.*, **46**, 609 (1942).
2. W. Machu, *Trans. Electrochem. Soc.*, **72**, 353 (1937).
3. G. E. Ardagh, R. M. B. Roome, and H. H. Owens, *Ind. Eng. Chem.*, **25**, 1116 (1933).
4. H. H. Uhlig, *Chem. Eng. News*, **24**, 3154 (1946).
5. T. P. Hoar, "Pittsburgh International Conference on Surface Reactions," pp. 127–34, The Corrosion Publishing Company, Pittsburgh (1948).
6. Leo Cavallaro, *Atti. acad. sci. Ferrara*, **24**, No. 2 (1946–47).
7. V. A. Kuznetsov and Z. A. Iofa, *J. Phys. Chem. U.S.S.R.*, **21**, 201 (1947); *C. A.*, **41**, 6115C (1947).
8. J. O'M. Bockris and B. E. Conway, *J. Phys. & Colloid Chem.*, **53**, 527 (1949).
9. Norman Hackerman and J. D. Sudbury, *J. (and Trans.) Electrochem. Soc.*, **93**, 191 (1948).
10. Norman Hackerman and H. R. Schmidt, *Corrosion*, **5**, 237 (1949).
11. G. J. Halsey, *J. Chem. Phys.*, **16**, 931 (1948).

12. C. A. Mann and Shih-Jen Ch'iao, *Ind. Eng. Chem.*, **39,** 910 (1947).
13. E. L. Cook, Ph.D. Dissertation, The University of Texas, Austin (May, 1949).
14. Norman Hackerman and E. E. Glenn, *J. Phys. & Colloid Chem.* (In Press).
15. Stephen Brunauer, "The Adsorption of Gases and Vapors," Volume I, "Physical Adsorption," Princeton University Press (1943).
16. Fritz Fiegel, "Qualtitative Analysis by Spot Tests," (Translated by Ralph Oesper), 3rd edition, Elsevier Publishing Company, New York and Amsterdam (1946).
17. R. T. Foley and R. C. Anderson, *J. Am. Chem. Soc.*, **70,** 1195 (1948).
18. Samuel Glasstone, "An Introduction to Electrochemistry," D. Van Nostrand Company, New York (1942).
19. H. J. Trurnit, *Angew. Chem.*, **59A,** 273 (1948).

Calcium Antimonates[1]

KEITH H. BUTLER, MARTHA J. BERGIN, AND VIRGINIA M. B. HANNAFORD

Sylvania Electric Products, Inc., Salem, Massachusetts, and Bayside, New York

ABSTRACT

A review of the literature on calcium antimonates reveals numerous discrepancies among results of various investigators, particularly in reference to the composition and crystal structure of calcium fluoantimonate and calcium pyroantimonate. A study of the preparation of these two compounds has been made and it has been established that $Ca_2Sb_2O_7$ is orthorhombic. Calcium fluoantimonate has been synthesized for the first time and found to have the cubic structure of the mineral romeite. The probable formula is $Ca_4Sb_4O_{11}F_2$. Powder diffraction data are given for these two materials as well as for calcium metaantimonate. The behavior of antimony during the firing of calcium halophosphate phosphors is discussed briefly with special reference to the formation of calcium antimonates during the processing.

INTRODUCTION

The literature on calcium antimonates gives a rather confused picture of the possible compounds and their crystal structure, even though they have received considerable study. Two antimonates are reported, a metaantimonate having the formula $CaSb_2O_6$ and a pyroantimonate having the formula $Ca_2Sb_2O_7$. The literature on this latter material shows that either several forms may exist or that the compounds investigated were incorrectly identified. The present investigation was undertaken in an attempt to clear up some of the discrepancies apparent in the literature. It resulted from a study of the acid insoluble residues in calcium halophosphate phosphors.

The earliest investigation of the calcium antimonates, in which modern x-ray diffraction methods of determining crystal structure were used, is that by Natta and Baccaredda (1–4), who reported the results of studies of various naturally occurring minerals, which approximated calcium pyroantimonate on analysis. In all cases, a cubic structure was obtained with slight variation from a lattice constant of 10.25 Å. The fourth paper dealt with the synthetic preparation of calcium pyroantimonate. A mixture of antimonic acid and calcium nitrate was fused at a low temperature and finally fired to a red heat, but the final temperature was not specified. Reaction started at 400°C and the product was a yellow powder with an apparent density of 4.30. The crystal structure was cubic with a lattice constant of $a_0 = 10.30$; the density calculated from the crystal structure was approximately 25 per cent higher than the experimental values and this difference was attributed to the fineness and imperfect condition of the experimental product.

In an independent investigation of the crystal structure of romeite and schneebergite, Zedlitz (5) concluded that the composition of romeite was (Ca, Na, Mn)$_2$ Sb_2(O, OH, F)$_7$. His basis was the assumption that these materials are isomorphous with pyrochlore for which the ideal formula is $CaNaCb_2O_6F$. In Zedlitz's structure, the presence of OH or F is essential and his formula for an ideal romeite is $CaNaSb_2O_6OH$, with 16 Na and Ca ions being statistically distributed in the 16 *c* positions of the O_h^7 (Fd3m) cubic lattice.

The next investigation of calcium antimonates was made by Magneli (6) as part of a rather extensive study of antimonates and arsenates. Calcium metaantimonate, prepared by reacting calcium carbonate and antimony trioxide for 20 hours at 1000°C, has the space group D_3^1 (C312). The unit cell contains 1 molecule of the compound with the edges being $a_0 = 5.22$ and $c_0 = 5.01$.[2] The structure is built up of sheets composed of Sb_2O_6 groups between which the bivalent cations are inserted.

In a second investigation by the Stockholm Institute of General and Inorganic Chemistry, an x-ray analysis of calcium pyroantimonate was made as part of a study of the antimonates, columbates (niobates), and tantalates of calcium, strontium, and cadmium. In this paper by Brystrom (7), calcium pyroantimonate was reported to be orthorhombic. The sample studied was made by heating calcium carbonate and antimony trioxide in the required proportions for 15 hours at 1200°C, but supporting analytical data are lacking. The dimensions of the unit cell are $a_0 = 7.28$, $b_0 = 7.44$, and $c_0 = 10.18$.

The structure assumed for calcium pyroantimonate was that of weberite Na_2MgAlF_7, and the paper contains an interesting discussion of the dif-

[1] Manuscript received October 25, 1949. This paper prepared for delivery before the Cleveland Meeting, April 19 to 22, 1950.

[2] These parameters hold for the hexagonal representation of the rhombohedral cell.

ference between the weberite and the pyrochlore structures.

Three compounds were found to have the orthorhombic weberite structure, composed of sheets of Sb_2O_7 groups, namely $Ca_2Sb_2O_7$, $Sr_2Sb_2O_7$, $Cd_2Sb_2O_7$, while four compounds, namely $Pb_2Sb_2O_7$, $Ca_2Ta_2O_7$, $Cd_2Ta_2O_7$, and $Cd_2Cb_2O_7$, were reported to have the pyrochlore structure, composed of a three dimensional framework of X_2O_6 groups, whereas X = Sb, Ta or Cb.

Experimental

Preparation of Calcium Pyroantimonate

In the present investigation a reaction mixture was made by ballmilling in acetone suspension the theoretical amounts of cp calcium carbonate and antimony tetroxide required for calcium pyroantimonate. The antimony tetroxide was prepared by carefully controlled oxidation of cp antimony trioxide. The ballmilled mixture was dried at 100°C, and then fired in open porcelain crucibles for various times and temperatures. The resulting product was submitted to x-ray powder diffraction examination and the phases identified are shown in Table I together with per cent insoluble in nitric acid.[3]

It is apparent that the reaction between calcium carbonate and antimony tetroxides starts at temperatures of approximately 800°C and goes to completion at temperatures as low as 925°C.

Since some unreacted material is apparently present, as shown by partial solubility in nitric acid, a preparation of higher purity was made by firing together calcium carbonate and antimony tetroxide, using a slight excess of calcium carbonate, at 980°C. The product was mortar ground and refired at 1200°C to remove any unreacted Sb_2O_4 by decomposition and volatilization. The refired material, which contained 1 per cent acid soluble material, was again mortar ground and leached in boiling 10 per cent hydrochloric acid to remove any unreacted calcium oxide.

The crystal structure of the pyroantimonate prepared in this way is identical with the orthorhombic form of Bystrom and no foreign material was found in the x-ray examination. Table II lists the interatomic spacings and the intensity of the lines observed for this pyroantimonate, compared by Bystrom's listing of intensities.[4] Bystrom reports: $a_0 = 7.28$, $b_0 = 7.44$, $c_0 = 10.18$, while we find $a_0 = 7.28$, $b_0 = 7.43$, $c_0 = 10.17$, averaged from the spacings for our best sample. The powder obtained by this method of preparation is nearly white in color with a slight yellowish undertone. It is insoluble in boiling dilute hydrochloric or nitric acid, but may be dissolved in concentrated sulfuric acid at its boiling point. The analysis of the product was made by dissolving in concentrated sulfuric acid and using the usual oxalate precipitation for calcium content and a titration method for the antimony content.

[3] Our standard test was treatment with boiling 10% nitric acid for ½ hour. Longer time of treatment did not change the results.

TABLE I. *Calcium pyroantimonate*

Firing temperature	% Insoluble in HNO_3	Phases found by x-ray		
		$Ca_2Sb_2O_7$	$CaSb_2O_6$	Sb_2O_4
°C				
593	No test	None	None	Very strong
704	No test	None	None	Very strong
815	56.8	Weak	None	Strong
871	74.1	No test	No test	No test
927	92.6	Very strong	None	None
1038	93.2	No test	No test	No test
1094	No test	Very strong	Weak	None

TABLE II. *Powder diffraction patterns on $Ca_2Sb_2O_7$*

h, k, l	Bystrom* intensity	Indexed lines of present data	
		d (*kx* units)	Intensity†
001	—	10.05	0.4
011	—	5.97	0.7
110	—	5.19	0.6
112, 200	M	3.633	0.5
211	M	3.105	0.4
012, 103	W	—	—
022	V.S.	3.009	0.9
202	V.S.	2.960	0.9
220	S	2.607	0.6
004	M	2.551	0.4
130	V.W.	2.351	0.1
310	V.W.	—	—
114	V.W.	2.290	0.1
132	W	2.132	0.1
312	W+	2.106	0.2
231, 033	M	2.009	0.4
015	V.W.	—	—
040	M	1.867	0.4
400, 224	S	1.824	1.0

* Bystrom does not list *d* values.

† Arbitrary scale, not comparable to ASTM scale.

The results of the analyses were:

	Experimental	Theoretical for $Ca_2Sb_2O_7$
Ca	18.6	18.40
Sb	56.6	55.89
O (by difference)	24.8	25.71
Density	4.97	5.19

Preparation of Calcium Metaantimonate

Calcium metaantimonate was also prepared from cp calcium carbonate and antimony tetroxide, ballmilled together in acetone. A study was first made of the reaction rates, as for calcium pyroantimonate, by firing mixtures at various temperatures as shown in Table III. Here reaction starts at 800°C with the formation of the pyroantimonates and on the basis of solubility is complete at 925°C, but the x-ray diffraction patterns indicate that the pyroantimonate, which is an intermediate product, persists up to 1100°C. We have not been able to prepare a calcium metaantimonate which does not contain a little pyroantimonate as a contaminant.

A high purity preparation was made by using a slight excess of antimony tetroxide and firing twice, at 985°C and 1200°C, with mortar grinding between firings. The resulting product was leached with hydrochloric acid before examination, 0.5 per cent of acid soluble material being removed. The powder diagram of this product is free of extraneous lines except for those due to pyroantimonate and is in full agreement with Magneli's structure as shown in Table IV. All of the lines present could be accounted for when indexed by the Davey charts and the observed intensities agreed reasonably well with Magneli's reported intensities for calcium metaarsenate. Magneli gives no *d* values for any compound studied.

TABLE III. *Calcium metaantimonate*

Firing temp	% Insoluble in HNO_3	Phases found by x-ray		
		$Ca_2Sb_2O_7$	$CaSb_2O_6$	Sb_2O_4
°C				
593	No test	None	None	V. strong
704	No test	None	None	V. strong
815	76.1	V. weak	None	Strong
927	99.5	Med.	Med.	None
1038	99.3	No test	No test	No test
1094	No test	Weak	V. strong	None

The powder is almost pure white and is soluble in boiling 98 per cent sulfuric acid. The analysis shows:

	Experimental	Theoretical for $CaSb_2O_6$
Ca	11.6	10.56
Sb	63.5	64.15
O (by difference)	24.9	25.29
Density	5.65	5.29

Preparation of Romeite Type Antimonates

From Zedlitz's discussion of the structure of romeite it appears that the presence of fluoride or hydroxyl ions is necessary to formation of a romeite type antimonate. To eliminate the possibility that it might be a modification stable at a different temperature, samples of the pyroantimonate were held 16 hours at 700°C and for 1 hour at 1250°C. No change in the powder diffraction pattern was observed in either case.

Acting on the assumption that a romeite type pyroantimonate has the chemical formula $Ca_2Sb_2O_6F$, a mixture of calcium carbonate, calcium fluoride, and antimony trioxide in stoichiometric amounts for the equation

$$3CaCO_3 + CaF_2 + 2Sb_2O_3 + 3/2\ O_2 \rightarrow 2Ca_2Sb_2O_6F + 3CO_2$$

was ballmilled in water. The dried mixture was held for 1 hour at 500°C, and then portions were fired. The amount insoluble in nitric acid and the x-ray identification of the phases present are shown in Table V.

It seems apparent from this test that a romeite type lattice is formed when one of the oxygen atoms of calcium pyroantimonate is replaced by fluoride and that the reaction progresses at lower temperatures than those required for the formation of the normal antimonates.

TABLE IV. *Powder diffraction patterns on $CaSb_2O_6$*

Magneli $CaAs_2O_6$		Present indexed lines of $CaSb_2O_6$	
h, *k*, *l*	Intensity	*d* (*kx* units)	Intensity*
00.1	—	4.99	0.9
10.0	—	4.49	0.5
10.1	V.S.	3.353	0.9
11.0	S	2.614	0.7
00.2	W	2.503	0.3
11.1	S	2.322	0.8
10.2	—	2.191	0.2
20.1	S	2.062	0.6
11.2	V.S.	1.811	1.0
21.0	V.W.	1.713	0.2
00.3	—	1.681	0.3
20.2	W	—	—
21.1	S	1.622	0.6
10.3	M	1.568	0.4
30.0	S	1.512	0.6
30.1	M	1.448	0.5
11.3	M	1.409	0.5
21.2	V.W.	—	—
20.3	M	1.347	0.4
22.0	M	1.309	0.4
30.2	M	1.296	0.4
22.1	—	1.269	0.4
00.4	W	1.256	0.3

Hex. parameters	Magneli		Present $CaSb_2O_6$
	$CaAs_2O_6$	$CaSb_2O_6$	
A_0	4.814	5.222	5.224
C_0	5.069	5.010	5.015

* Not on ASTM scale.

To follow the preferential reaction of the three component mixture, a series of samples was prepared using a variable amount of calcium fluoride, constant amount of calcium carbonate, and an excess of antimony trioxide sufficient to give the metaantimonate. These mixtures were ballmilled and fired at 500°C for 1 hour and then for 1 hour at 1040°C. The results for this series are found in Table VI.

TABLE V. *Romeite type pyroantimonate, containing fluorine*

Firing temp	% Insoluble in HNO_3	Phases identified
°C		
800	93.0	Romeite A_0 = 10.33
900	95.2	Romeite A_0 = 10.33
1000	95.7	Romeite A_0 = 10.33

TABLE VI. *Romeite type antimonates*

Mole composition of mixture			% Insoluble in HNO_3	Phases found by x-ray			
$CaCO_3$	CaF_2	Sb_2O_5		$Ca_2Sb_2O_7$	Romeite	$CaSb_2O_6$	Sb_2O_4
4.0	0.5	4.0	98.8	None	Medium	Strong	None
4.0	1.0	4.0	98.1	None	Medium	Strong	None
4.0	1.5	4.0	94.8	None	Very strong	Medium	None
4.0	2.0	4.0	96.4	None	Medium	Strong	Very weak

TABLE VII. *Romeite type antimonates*

Mole composition of mixture			% Insoluble in HNO_3	Phases found by x-ray	
$CaCO_3$	CaF_2	Sb_2O_5		$Ca_2Sb_2O_7$	Romeite
2.1	0.0	1.0	75.8	Strong	None
2.0	0.1	1.0	84.3	Strong	None
1.9	0.2	1.0	86.0	Mixture of both	
1.8	0.3	1.0	80.5	Trace	Strong
1.7	0.4	1.0	79.4	None	Strong
1.6	0.5	1.0	77.9	None	Strong

It is obvious that any pyroantimonate formed is converted into the romeite type antimonate or into the metaantimonate. It is also obvious that both of these latter materials can coexist and that the fluoride ion either does not enter the metaantimonate lattice or else does not affect the lattice spacing if it does enter the crystal structure.

These experiments show that replacement of one oxygen atom is sufficient to convert the pyroantimonate to a romeite type lattice. To test the possibility that only partial replacement was needed, mixtures were made of calcium carbonate, calcium fluoride, and antimony tetroxide in which the total calcium was sufficient to form the pyroantimonate while the fluorine varied from zero to one atom per molecule. These mixtures were fired at 1000°C, acid leached, and examined by x-ray powder diffraction methods with results shown in Table VII.

It is again evident that fluoride increases the speed of reaction and that romeite is preferentially formed at 1000°C but that the reaction is incomplete. The absence of $Ca_2Sb_2O_7$ when the CaF_2 content is 0.3 or 0.4 mole may be due to the possibility that formation of the romeite structure requires less than one atom of fluorine per molecule, but it is more probable that a very fine $Ca_2Sb_2O_7$ was formed giving a diffuse x-ray pattern which was not detectable.

TABLE VIII. *Romeite type antimonates*

Mole composition of mixture			% Insoluble in HNO_3	X-ray identification on acid insoluble portion
$CaCO_3$	CaF_2	Sb_2O_4		
1.7	0.5	1.0	92.4	Romeite, fair pattern
1.1	1.0	1.0	98.9	Romeite, excellent pattern

TABLE IX. *Analyses of Romeite type antimonates*

Sample No.	*36C*	*62L*
X-ray pattern	Good	Excellent
a_0	10.3_3	10.3_0
% Ca	19.2	18.5
% Sb	55.8	56.6
% F	4.1	4.5
% O (by difference)	20.9	20.4
Equiv. atoms Ca	2.08	2.00
Sb	2.00	2.00
F	0.94	1.03
O	5.70	5.50
Density observed	4.79	4.94

Two further preparations were made by ballmilling calcium carbonate, calcium fluoride, and antimony tetroxide. These were fired at 985°C, mortar ground, and refired at 1175°C to volatilize excess antimony oxide.

It is apparent that an excess of calcium fluoride gives a romeite with a well defined crystal structure. Table IX gives the chemical analysis of two romeite samples made by different procedures and Table X gives powder diffraction data on Sample 62L.

While there is still some uncertainty about the exact composition of fluoromeite, we believe that sample 62L most nearly approaches the true compound and from the analytical data the chemical formula should be $Ca_4Sb_4O_{11}F_2$.

Attempts were made to prepare hydroxyromeite by firing together calcium hydroxide and antimony trioxide and to prepare chlororomeite by firing together calcium chloride, calcium carbonate, and antimony trioxide. In both cases the x-ray examination

showed only the normal calcium pyroantimonate structure.

Method of Analysis

Calcium antimonates can be brought into solution by a fuming sulfuric acid attack using K_2SO_4 to raise the boiling point and using carbon reduction of the antimony. The sample was placed in a 250 ml Kjeldahl flask together with filter paper, 20 ml of concentrated sulfuric acid, and 15 grams of potassium sulfate. The mixture was heated until a water white solution remained, the heating being stopped as soon as the solution cleared. Excessive treatment

TABLE X. *Powder diffraction pattern of fluoromeite*

d	Intensity, arbitrary scale
kx units	
5.873	0.7
3.095	0.7
2.960	1.0
2.564	0.6
2.359	0.1
1.979	0.5
1.820	0.9
1.739	0.5
1.569	0.4
1.552	0.8
1.487	0.5
1.442	0.4
1.342	0.5
1.290	0.4
1.188	0.1
1.180	0.6
1.151	0.6
1.130	0.3
1.079	0.3
1.050	0.6
1.034	0.3
0.986	0.6

of antimony with fuming sulfuric acid is reported to convert Sb^{III} to Sb^{V} but our results show that this conversion is not rapid.

The solution was cooled and diluted by pouring into 200 ml of water and was now ready for either antimony (10) or calcium (11) determination.

The fluorine in calcium fluoantimonate was determined by means of a double distillation (12). The sample was placed in an all glass distilling apparatus with 100 ml of 1:1 sulfuric acid and 15 grams of potassium sulfate. The mixture was distilled until 75 ml distillate collected. At the end of the distillation the solution was perfectly clear indicating the attack was complete. The distillate was then redistilled, using steam distillation, after 10 ml of perchloric acid had been added. This distillation was continued until 150 ml had collected. The distillate was neutralized to a phenolphthalein end point with sodium hydroxide and adjusted to a volume of 250 ml. To a 50 ml aliquot alizarin red S indicator (0.1%) was added, and $N/10$ hydrochloric acid until the solution became yellow, followed by the addition of 1 ml of $0.4M$ acetic acid. The fluorine was titrated with thorium nitrate solution (13) (standardized with a known pure sodium fluoride solution) until a pink color was obtained.

Discussion of Results

Calcium pyroantimonate is readily prepared by the reaction of calcium carbonate or calcium hydroxide with antimony tetroxide with the reaction going early to completion at 925°C. The x-ray diffraction pattern agrees with that reported by Bystrom and the chemical analysis is in reasonable agreement with the formula $Ca_2Sb_2O_7$. The observed density is somewhat below the theoretical density. There seems to be little doubt that all the antimony is in the pentavalent state and that Bystrom's structure is plausible.

In the preparation of calcium metaantimonate from calcium carbonate and antimony tetraoxide, the pyroantimonate is an intermediate compound and it has proved almost impossible to obtain complete elimination of this material. The reaction to form the metaantimonate requires a higher temperature, about 1050°C, before conversion is complete. The chemical analysis agrees well with the formula $CaSb_2O_6$ and all the antimony is in the pentavalent state. The x-ray diffraction pattern is in good agreement with the rhombohedral cell suggested by Magneli, although the observed density is somewhat above the theoretical value calculated from the cell dimensions.

Calcium fluoantimonate (fluoromeite) is obtained by the reaction of antimony tetraoxide with a mixture of calcium carbonate and calcium fluoride. The reaction approaches completion at 825°C and fluoromeite is formed in preference to either pyroantimonate or metaantimonate.

The maximum amount of fluorine found by analysis is slightly over 1 atom for each 2 atoms of antimony or calcium, while equal numbers of calcium and antimony atoms are present. The amount of oxygen present is definitely below that needed to satisfy the valence of pentavalent antimony and we believe that fluoromeite has the composition:

$$Ca_4Sb_2^{III}Sb_2^{V}O_{11}F_2$$

The composition given would invalidate the structure assumed by Zedlitz, which is based on pentavalent antimony and would suggest a closer relation to the structures suggested by Dihlstrom (8, 9) for antimony tetroxide and its hydrate, in both of which part of the antimony is trivalent and part

pentavalent. However, the present analytical data are not felt to be sufficiently precise to establish the composition with the definiteness needed for structure determination work and no hypothesis on the arrangement of the atoms in the crystal will be put forth.

Calcium hydroxyantimonate (romeite) has not been obtained in the present investigation, but it is believed that it could be synthesized by the reaction of an active calcium oxide and antimonic acid at a low temperature following the procedure of Baccaredda. We believe that this compound also has a definite composition with OH replacing the F of fluoromeite, giving $Ca_4Sb_4O_{11}(OH)_2$ with two antimony atoms being trivalent and two pentavalent.

Behavior of Antimony Oxide in Calcium Halophosphate

As mentioned in the introduction, the presence of insoluble residues in calcium halophosphate phosphors motivated this study of calcium antimonates. Calcium pyroantimonate is not formed during phosphor preparation while fluoromeite and calcium metaantimonate are formed only as incidental steps in the complex chemical reactions taking place during the firing. Their presence is not necessary to phosphor development, although most methods of phosphor manufacture result in their formation.

In making these phosphors, the antimony, which is essential as an activator, is generally added as antimony trioxide, while the other ingredients include relatively large amounts of calcium fluoride and calcium carbonate, as well as calcium phosphate.

The following paragraphs describe a working hypothesis on the behavior of antimony in calcium halophosphates. Data to substantiate the reactions are not sufficiently complete to present at this time, but all experimental data obtained agree with the theories proposed.

As the temperature of the mixture gradually increases during the firing of the phosphor, antimony trioxide begins to oxidize to the tetraoxide at 450°C with the oxidation being complete below 520°C.

The tetraoxide then reacts with the large excess of calcium fluoride and calcium carbonate in the phosphor mixture, with the formation of fluoromeite. This reaction starts below 700°C and is completed at 875°C, the formation being apparently catalyzed by the other components of the phosphor mixture. Practically all the original antimony becomes converted into this acid insoluble compound and only a trace goes directly into the halophosphate lattice or into calcium metaantimonate.

The development of good fluorescence in the calcium halophosphate phosphors seems to require the presence of a certain amount of acid soluble antimony, which our tests indicate to be trivalent rather than pentavalent. This soluble antimony results from reactions at higher temperatures between the antimonates and the phosphates.

As a first step, the fluoromeite reacts with other components of the phosphor being converted into a mixture of acid insoluble calcium metaantimonate and the acid soluble form of antimony which is believed to be in solid solution in the halophosphate lattice, probably substituting for calcium. By continued heating some or all of the calcium metaantimonate also is converted into this type of acid soluble antimony, with the balance remaining as a separate phase.

Summary

Previous work on calcium pyroantimonate and calcium metaantimonate has been confirmed and x-ray powder diffraction for these two materials have been obtained. The hypothesis of Zedlitz that fluoride or hydroxide is an essential constituent of romeite has been confirmed for the fluoride ion and fluoromeite has been synthesized. It is apparently a compound of definite composition and a formula has been suggested.

Any discussion of this paper will appear in a Discussion Section, to be published in the December 1950 issue of the Journal.

REFERENCES

1. G. Natta and M. Baccaredda, *Atti. accad. Lincei.*, **15,** 389–95 (1932).
2. G. Natta and M. Baccaredda, *Atti. congr. naz. chim. pura applicata, 4th Congr. Rome and Abruzzo,* 537–46 (1933).
3. G. Natta and M. Baccaredda, *Z. Krist,* **85,** 271–96 (1933).
4. M. Baccaredda, *Gass. Chim. Ital,* **65,** 539–43 (1936).
5. O. Zedlitz, *Z. Krist,* **81,** 253 (1932).
6. A. Magneli, *Arkiv. Kemi, Mineral. Geol.*, **15B,** #3 (1941).
7. A. Bystrom, *Arkiv. Kemi. Mineral. Geol.*, **18A,** #21 (1944).
8. K. Dihlstrom, *Z. anorg. allgem Chem.*, **239,** 57 (1938).
9. K. Dihlstrom and A. Westgren, *Z. anorg. allgem. Chem.*, **235,** 153 (1937).
10. W. F. Hildebrand and G. E. F. Lundell, "Applied Inorganic Analysis," p. 228, John Wiley & Sons, Inc., New York (1929).
11. W. W. Scott and N. H. Furman, "Standard Methods of Chemical Analysis," 5th Ed., p. 211, D. Van Nostrand Co., Inc., New York (1939).
12. H. A. Lepper, Chairman, "Methods of Analysis of the Association of Official Agricultural Chemists," 6th Ed., p. 58, Association of Official Agricultural Chemists (1945).
13. D. S. Reynolds and W. L. Hill, *Ind. Eng. Chem. Anal. Ed.*, **11,** 21–22 (1939).

A Study of the Mechanism of Sensitized Luminescence of Solids[1]

JAMES H. SCHULMAN, ROBERT J. GINTHER, AND CLIFFORD C. KLICK

Crystal Branch, Naval Research Laboratory, Washington, D. C.

ABSTRACT

Reflection, excitation, and emission spectra of $CaSiO_3$:(Pb)and $CaSiO_3$:(Pb + Mn) are reported, as well as measurements of the dependence of luminescence intensity on exciting intensity for $CaSiO_3$:(Pb + Mn) and NaCl:(Pb + Mn). It is shown that the data support the conventional concept of sensitization, where all the ultraviolet absorption is due to the sensitizer, and that Butler's picture, where the activator absorbs ultraviolet, is invalid. An interpretation of the data on the $CaSiO_3$:(Pb + Mn) system is proposed, and the distance over which Pb^{+2} and Mn^{+2} interact in this phosphor is calculated on the basis of this interpretation.

INTRODUCTION

The sensitized luminescence of phosphors, first discovered by Rothschild (1), has recently been the subject of a number of investigations (2–8). The interest displayed in these systems is due partly to the practical applications found for some of them and partly to the theoretical problems they raise concerning the transport and transfer of energy.

With but one exception, all the recent investigations of this subject assume that the mechanism of sensitized luminescence in solids is roughly analogous to that in gases, i.e., that the incident radiant energy is absorbed by the "sensitizer" impurity and then transferred to the emitting impurity or "activator."

A contrary opinion is held by Butler (9). He postulates a configuration coordinate diagram for the activator which requires absorption of a far ultraviolet quantum to produce excitation of the activator from its ground state, A°, to some higher state A*, at normal temperatures and in the absence of sensitization (Fig. 1). His picture of sensitization is the following: Vibrational energy is lost to the crystal lattice by the sensitizer following light absorption or emission by this impurity. The vibrational energy imparted to the lattice is assumed to shift the position of the activator on its configuration coordinate diagram. It is proposed that this shift then enables the transition $A^\circ \rightarrow A^*$ to occur by absorption of a less energetic ultraviolet quantum, say in the same spectral region which causes excitation of the sensitizer. This picture thus requires that the activator itself directly absorb exciting ultraviolet radiation of the same, or nearly the same, frequency as that absorbed by the sensitizer, absorption in the sensitizer serving only to "trigger" the activator absorption. It follows from this picture that (*a*) the luminescence intensity should vary with the square of the intensity of exciting ultraviolet light at low values of the latter, and (*b*) if the concentration of sensitizer ions is kept constant, incorporation of the activator in the crystal should increase the concentration of absorbers by a factor calculable from the quantum efficiency of the activator luminescence. In contrast to this, the generally accepted view—that there is no direct absorption of radiation by the activator, and that all the ultraviolet absorption is due to the sensitizer—predicts: (*a*) a linear dependence of

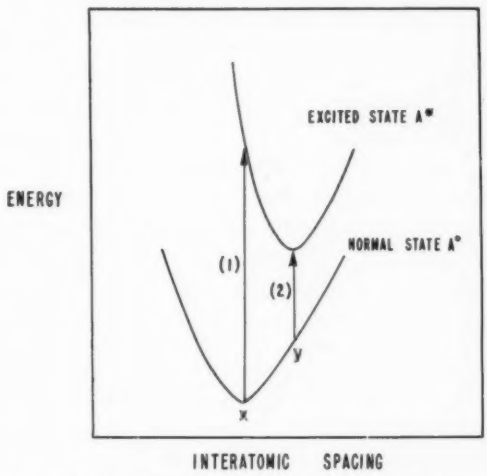

FIG. 1. Mechanism of sensitized luminescence according to Butler. (1) Transition $A^\circ \rightarrow A^*$ in absence of sensitizer requiring far ultraviolet quantum, (2) transition $A^\circ \rightarrow A^*$ in presence of sensitizer requiring less energetic ultraviolet quantum. $x \rightarrow y$ = shift of activator position due to absorption or emission by sensitizer.

[1] Manuscript received December 9, 1949. This paper prepared for delivery before the Cleveland Meeting, April 19 to 22, 1950.

luminescence intensity on the intensity of exciting ultraviolet, and (*b*) no dependence of the number of absorbers on the activator concentration.

Besides these basic differences in the interpretation of the elementary mechanism of sensitized luminescence, there are other questions concerning this phenomenon that call for an answer. Among the most important of these is the question of the maximum distance over which interaction (or energy transfer) between the sensitizer and the activator is possible. The main result of the present investigation is the calculation of this distance for the $CaSiO_3$:(Pb + Mn) phosphor, confirming an earlier hypothesis that the Pb and Mn must be near neighbors in the lattice (2, 3) before energy transfer is possible.

Experimental

Luminescence Intensity vs. Exciting Intensity

As mentioned above, analysis of Bulter's proposal shows that the intensity of the activator emission should depend on the square of the exciting ultraviolet intensity, in the limit of low exciting intensity. We have accordingly measured this dependence for $CaSiO_3$:(Pb + Mn) and NaCl:(Pb + Mn)[2] which have been shown to be Pb-sensitized Mn-activated phosphors (3, 8). The exciting source was a low-pressure Hg-discharge lamp equipped with two standard-thickness Corning 9863 filters to cut out visible light from the lamp. The lamp was diaphragmed so that only a 1 cm^2 section was effective as a source. Variation in ultraviolet (2537 Å) intensity was accomplished by means of the inverse square law, the lamp aperture being treated as a point source. Luminescence of the phosphors was measured by a conventional 1P21 photomultiplier and galvanometer arrangement, a red filter (Corning # 2424) being used in front of the phototube. As shown in Fig. 2, the dependence of luminescence emission intensity on exciting intensity was found with both phosphors to be very accurately linear down to the lowest levels of luminescence emission (i.e., of exciting intensity) that we could measure.[3] This result shows that Butler's proposed mechanism of sensitization is untenable.

[2] The $CaSiO_3$:(Pb + Mn) phosphors were prepared by the method of Merrill and Schulman (3). The powdered NaCl:(Pb + Mn) phosphors were prepared by the precipitation method of Schulman, *et al.* (8).

[3] Botden and Kroeger (5) report also that the luminescence intensities of $CaSiO_3$:(Pb + Mn) and $Ca_3(PO_4)_2$:(Ce + Mn) do not depend quadratically on the exciting intensity, which observation they use as evidence against transfer of the energy from sensitizer via the base lattice to the activator.

Absorption and Luminescence of $CaSiO_3$:Pb

In order to obtain information about the spatial separation of the sensitizer and activator in $CaSiO_3$:(Pb + Mn) extensive absorption and excitation measurements were undertaken with systematic variations in Pb and Mn content. A few such measurements have recently been reported (5, 16), but more comprehensive data were needed for our purpose.

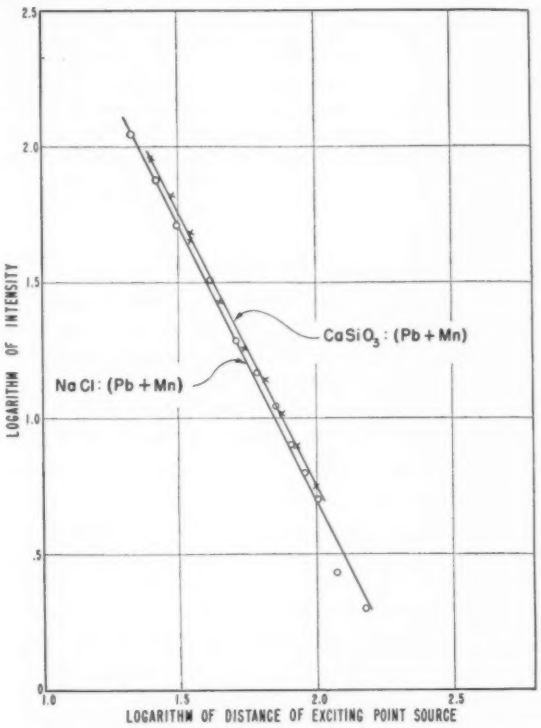

FIG. 2. Dependence of luminescence intensity on exciting intensity for $CaSiO_3$:(Pb + Mn) and NaCl:(Pb + Mn).

Information concerning the absorption of the phosphors was obtained by the reflection method. For the measurements, a Gaertner ultraviolet monochromator was used with a 1P28 phototube at the exit slit. Plaques of the various phosphors were placed before the entrance slit of the monochromator and irradiated by the light from a Beckman hydrogen lamp. A plaque of $MgCO_3$, smoked with MgO, was used as a reference standard, and it was assumed to have approximately 100 per cent reflectance over the wavelength range studied, 2200–4000 Å (10). The reproducibility of the reflectance data was found to be at worst ± 10 per cent by repeated measurement on several different phosphor samples against a number of different plaques of $MgCO_3$. These error limits include variations in preparation of the plaques by different individuals.

It will be noted that the experimental arrangement employed in this work leads to error if the specimen emits luminescent light in the ultraviolet region being studied. The error arises from the fact that the sample is constantly being irradiated by the continuous ultraviolet from the H_2 lamp. Because of excitation by the short-wave ultraviolet present in the continuum, the sample continually fluoresces during the measurement. The apparent reflectances exceeding 100 per cent observed in many of our curves are due to such luminescence.

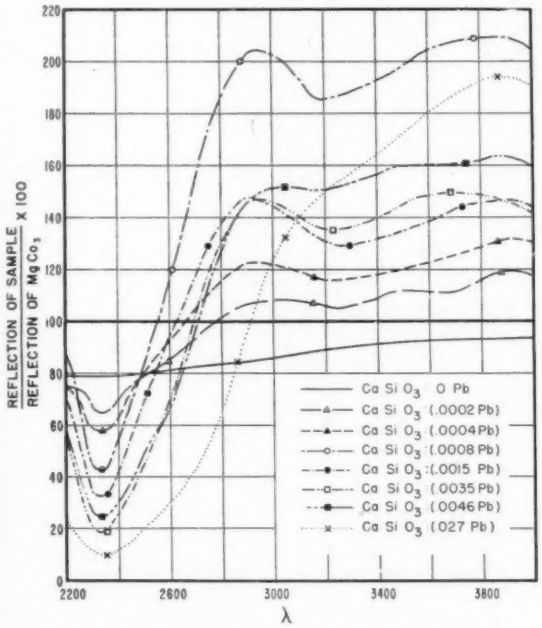
REFLECTION OF SAMPLE / REFLECTION OF MgCO3 X 100
λ
Ca Si O3 0 Pb
Ca Si O3 (.0002 Pb)
Ca Si O3 (.0004 Pb)
Ca Si O3 (.0008 Pb)
Ca Si O3 (.0015 Pb)
Ca Si O3 (.0035 Pb)
Ca Si O3 (.0046 Pb)
Ca Si O3 (.027 Pb)

FIG. 3. Reflection spectra of $CaSiO_3$:Pb phosphors

Fig. 3 shows the results of reflectance measurements of $CASiO_3$:Pb as a function of Pb concentration.[4] It may be seen that pure $CaSiO_3$ has only a feeble absorption over the spectral range investigated. The incorporation of as little as 2×10^{-4} moles Pb/mole Ca produces a distinct reflection minimum (absorption peak) at 2350 Å, and, at the same time, gives luminescence emission, as evidenced by the apparent reflectances greater than 100 per cent at wavelengths greater than about 2800 Å. Three such emission peaks appear in this lowest Pb sample, but we are inclined to question the apparent emission band structure in this sample because of the experimental errors involved. As the Pb concentration is increased to 4×10^{-4}, the reflection minimum at 2350 Å grows somewhat deeper and the emission is correspondingly increased in intensity. In this case, there appear to be quite definitely only two emission bands with peaks at 2900 Å and 3900 Å, respectively. With further Pb concentration increase to 8×10^{-4} moles Pb/mole Ca, the 2350 Å reflection minimum is even deeper and the luminescence emission is very intense, consisting of two peaks as in the preceding case. Increase of Pb concentration to 1.5×10^{-3} Pb/Ca further deepens the 2350 Å minimum, but the intensity of luminescence decreases, presumably due to the onset of concentration quenching. At 4.6 (10^{-3}) Pb/Ca there is a suggestion of the growth of a second reflection minimum at 2550 Å in addition to a further deepening of the 2350 Å minimum. In the 2.7×10^{-2} Pb/Ca preparation this new absorption minimum is even more strongly indicated, but it is still not well resolved. In this highest Pb-bearing sample the 2900 Å emission peak is practically gone, probably as a consequence of the increased width of the new 2550 Å absorption band. The 3900 Å emission peak is present, however, and there is a suggestion of a new emission peak in this sample near 3300 Å.

For the purpose of this work it was of interest to determine to what extent the depth of the reflection minimum could be used as a measure of the number of absorbing centers. Urbach, Hemmendinger, and Pearlman (11) have derived an approximate relationship between the reflection of a powdered sample, its absorption coefficient, and its "scattering coefficient." The relationship they have used is

$$\frac{\alpha}{\sigma} = \frac{(1-R)^2}{2R}$$

where: α = absorption coefficient, σ = scattering coefficient, and R is the reflection. They have shown that this relation gives good results with alkaline earth sulfide phosphors and other materials. Fig. 4 shows a plot of $\frac{\alpha}{\sigma}$ at 2350 Å vs. Pb concentration for the $CaSiO_3$:Pb samples described in Fig. 3. As is seen from Fig. 4, $\frac{\alpha}{\sigma}$ is proportional to the concentration of Pb absorbers when this concentration is below 4×10^{-3} Pb/Ca. Use will be made of this result in the discussion section of this paper.

In order to check the deductions from the reflection measurements concerning the emission spectra of the $CaSiO_3$:Pb phosphors, direct studies of the emission and excitation spectra of these phosphors were made.

[4] The Pb concentrations are noted in moles Pb/mole Ca. Due to the volatility of Pb compounds, the Pb concentration in a fired $CaSiO_3$:Pb preparation is always less than that in the unfired mixture (3, 4). The Pb concentrations given above are the actual values found by polarographic analysis of the final phosphors using a procedure to be described elsewhere.

Fig. 5 shows the emission spectra of three $CaSiO_3$:Pb phosphors of varying Pb concentration under 2350 A excitation. It is seen that the emission under 2350 Å irradiation does indeed consist of two well-resolved bands peaking at about 2900 Å and 3900 Å, respectively. Fig. 6 shows the variation in emission spectrum of $CaSiO_3$:0.0046Pb with variation in exciting wavelength. Excitation at 2350 A gives the two-band emission spectrum, while excitation at 2600 Å, i.e., in the new 2550 Å-peaked absorption band, gives essentially a single-band emission spectrum. The peak of the 2600 Å-excited emission lies at about 3400 Å, almost coincident with the minimum between the two emission bands excited by 2350 Å. Since there is an overlap between the 2350 Å and 2550 Å absorption (and excitation) bands, it was of interest to see what sort of emission would be produced by 2537 Å excitation. With sufficiently high Pb concentration the emission of $CaSiO_3$:Pb under 2537 Å excitation was very

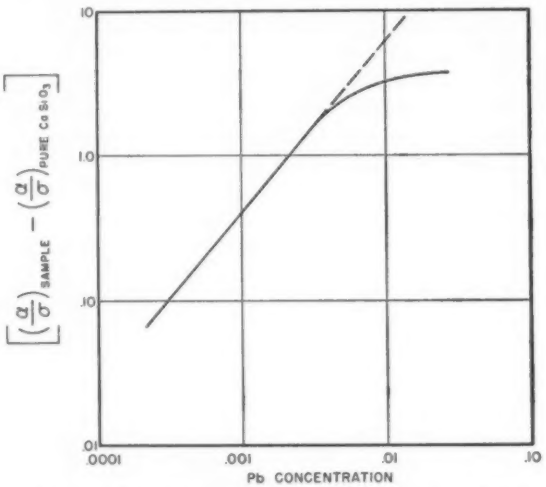

FIG. 4. Absorption coefficient at 2350 Å of $CaSiO_3$:Pb phosphors vs. Pb concentration.

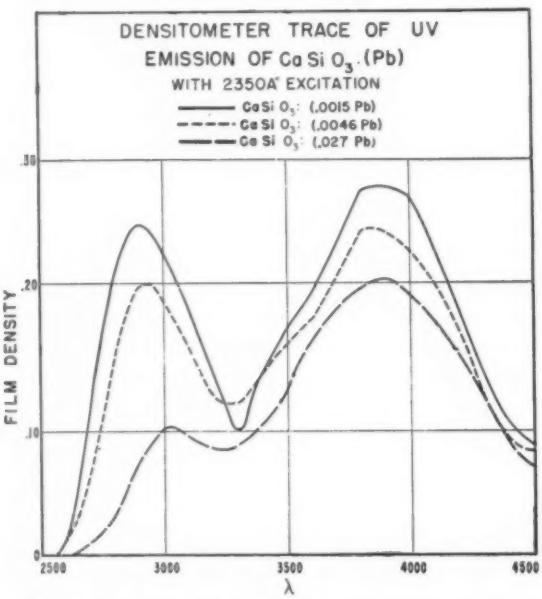

FIG. 5. Emission of $CaSiO_3$:Pb phosphors under 2350 Å excitation.

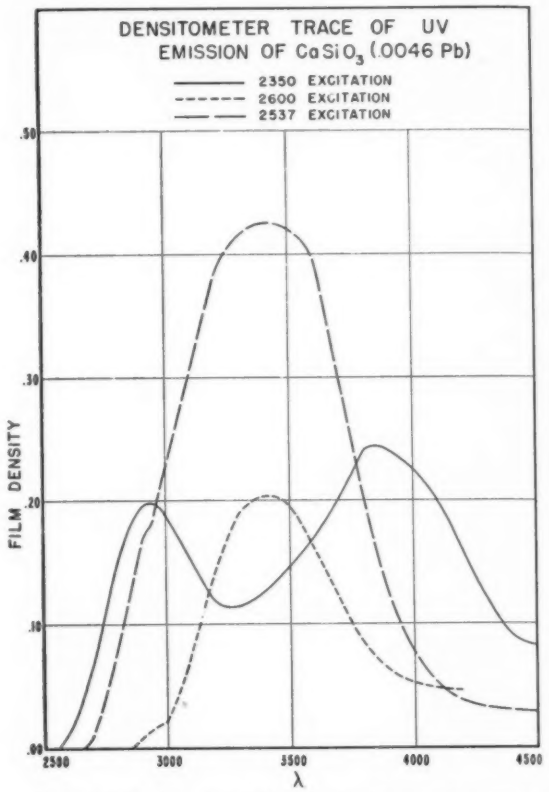

FIG. 6. Emission of $CaSiO_3$:Pb phosphor under various excitations.

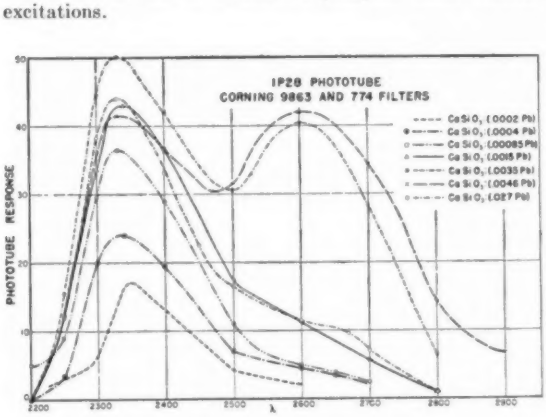

FIG. 7. Excitation spectra of $CaSiO_3$:Pb phosphors

similar to that under 2600 Å, i.e., a single band peaking at 3400 Å (cf. Fig. 6). In some samples of low Pb concentration, however, 2537 Å excitation gave, in addition, the two-band emission spectrum.

Fig. 7 shows the excitation spectra for the ultraviolet emission of a series of $CaSiO_3$:Pb phosphors. As the reflection measurements had indicated, there are indeed two distinct excitation peaks, one at 2350 Å and the second at 2550–2600 Å, the latter

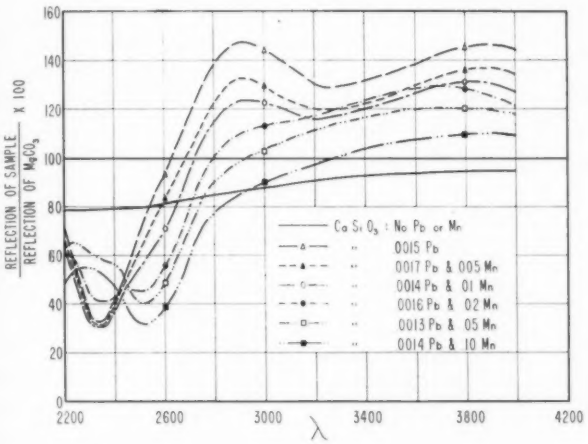
REFLECTION OF SAMPLE / REFLECTION OF MgCO3 X 100
Ca Si O3 : No Pb or Mn
" 0015 Pb
" 0017 Pb & 005 Mn
" 0014 Pb & 01 Mn
" 0016 Pb & 02 Mn
" 0013 Pb & 05 Mn
" 0014 Pb & 10 Mn
λ

FIG. 8. Reflection spectra of $CaSiO_3$:(Pb + Mn) phosphors.

increasing in prominence with increase in Pb concentration.

In summary, then, pure $CaSiO_3$ is essentially transparent down to 2200 Å. Introduction of Pb causes the appearance of a characteristic absorption peak at 2350 Å. Irradiation into this band causes luminescence, the emission consisting of two well-resolved bands with peaks at 2900 Å and 3900 Å, respectively. Increase of Pb concentration increases the characteristic absorption and finally produces a second absorption peak at 2550 Å, irradiation into which gives a single-band ultraviolet emission with a peak at about 3400 Å.

Effect of Manganese on the Absorption and Luminescence of $CaSiO_3$:Pb

The next question to be investigated was the effect of the Mn activator concentration on the absorption spectrum of $CaSiO_3$:Pb. Results of this study are given in Fig. 8 for $CaSiO_3$ phosphors containing about $1.5 \pm 0.2 \times 10^{-3}$Pb/Ca and manganese concentrations up to 0.10 Mn/Ca. The sample containing no manganese has a reflection minimum at 2350 Å and emits the double-peaked emission spectrum, as reported in the previous section. Incorporation of manganese reduces the depth of this minimum and causes the growth of a distinctly resolved second reflection minimum at about 2550 Å. With Pb/Ca = $1.6(10^{-3})$ and Mn/Ca = 0.02, the 2350 Å and 2550 Å reflection minima are about equal; with Mn/Ca = 0.10 the 2350 Å minimum has completely vanished as such, the absorption in this region being apparently due to overlap between the 2550 Å absorption band and the long-wave extension of a new absorption band (peak below 2200 Å) which was not observed before and which was not further investigated. The depth of the 2550 Å reflection minimum in the presence of

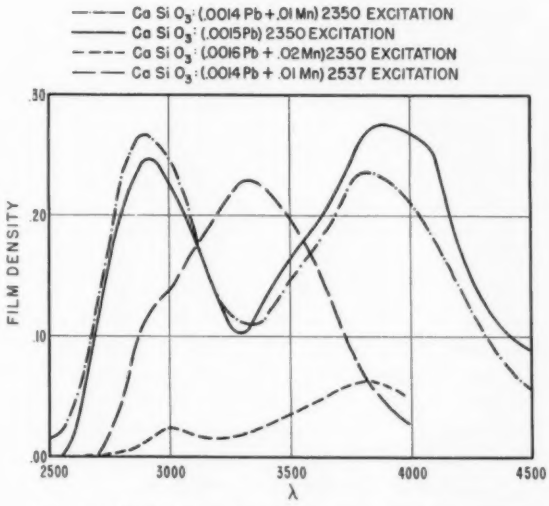
Ca Si O3 (.0014 Pb + .01 Mn) 2350 EXCITATION
Ca Si O3 (.0015Pb) 2350 EXCITATION
Ca Si O3 (.0016 Pb + .02Mn)2350 EXCITATION
Ca Si O3 (.0014 Pb + .01 Mn) 2537 EXCITATION
FILM DENSITY
λ

FIG. 9. Ultraviolet emission spectra of various $CaSiO_3$:(Pb + Mn) phosphors under 2350 Å and 2537 Å excitation.

0.10 Mn/Ca is the same as the depth of the 2350 Å reflection minimum of the manganese-free sample containing the same amount of lead.

The ultraviolet emission spectra of various $CaSiO_3$:(Pb + Mn) phosphors are shown in Fig. 9. It is seen that 2350 Å excitation calls forth the same double-peaked ultraviolet emission from a $CaSiO_3$:(0.0014Pb,0.01Mn) phosphor as it does from

a $CaSiO_3$:(0.0015Pb) phosphor containing no manganese. Increase of manganese concentration to 0.02 Mn/Ca seriously reduces the intensity of the ultraviolet emission, but the double-peaked spectrum is still recognizable. Excitation of $CaSiO_3$:(0.0014Pb, 0.01 Mn) at 2537 Å, however, gives essentially a single-band ultraviolet emission peaked at about 3400 Å. This is almost identical with the behavior of $CaSiO_3$:(Pb), containing sufficient Pb^{+2} to bring out the 2550 Å absorption band, when irradiated with 2537 Å.

Fig. 10 illustrates the effect of Mn^{+2} concentration on the excitation spectra for ultraviolet emission of $CaSiO_3$:(Pb + Mn). With low Mn^{+2} concentration there is a strong excitation peak at 2350 Å (leading, of course, to the double-band ultraviolet

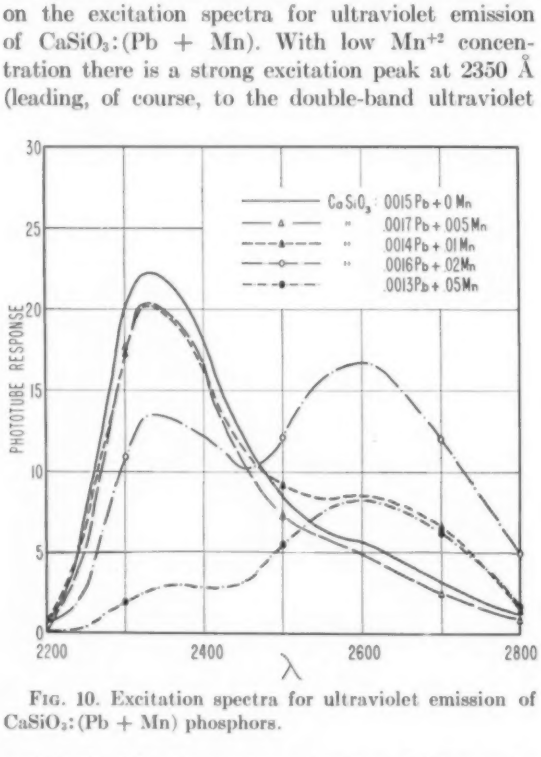

FIG. 10. Excitation spectra for ultraviolet emission of $CaSiO_3$:(Pb + Mn) phosphors.

emission) with a long-wave extension which may be the start of the 2550 Å excitation band (leading to the single-band ultraviolet emission). With increase in manganese concentration, the former excitation band decreases in height and the latter increases correspondingly. The overall intensity of the ultraviolet emission is decreased, however, by incorporation of Mn^{+2}. At a Mn/Ca ratio of 0.10 (not shown) the ultraviolet emission could not be detected with our arrangement.

The emission spectra of $CaSiO_3$:(Pb + Mn) phosphors in the visible have already been described (3–5), hence it remained only to investigate the excitation spectra of these phosphors. The behavior is shown in Fig. 11. *It is noteworthy that irradiation into the 2350 Å absorption band does not excite the visible Mn^{+2} emission; only irradiation into the 2550 Å absorption is effective in this regard.* The 2550 Å excitation band for the Mn^{+2} emission of $CaSiO_3$:(Pb + Mn) is identical with the excitation band for the 3400 Å-peaked single-band ultraviolet emission of $CaSiO_3$:(Pb) or $CaSiO_3$:(Pb + Mn).

The effects of Mn^{+2} on the characteristics of the $CaSiO_3$:(Pb) phosphor are then as follows: (*a*) Excitation of $CaSiO_3$:(Pb + Mn) in its 2350 Å absorption band produces only the double-peaked ultraviolet emission obtained by similar excitation of $CaSiO_3$:(Pb). (*b*) Incorporation of Mn^{+2} acts like a simple increase in Pb^{+2} concentration in that it calls forth a new absorption band at 2550 Å. Irradiation into this band in $CaSiO_3$:(Pb + Mn) yields both the single band 3400 Å-peaked ultraviolet emission obtained by similar excitation of

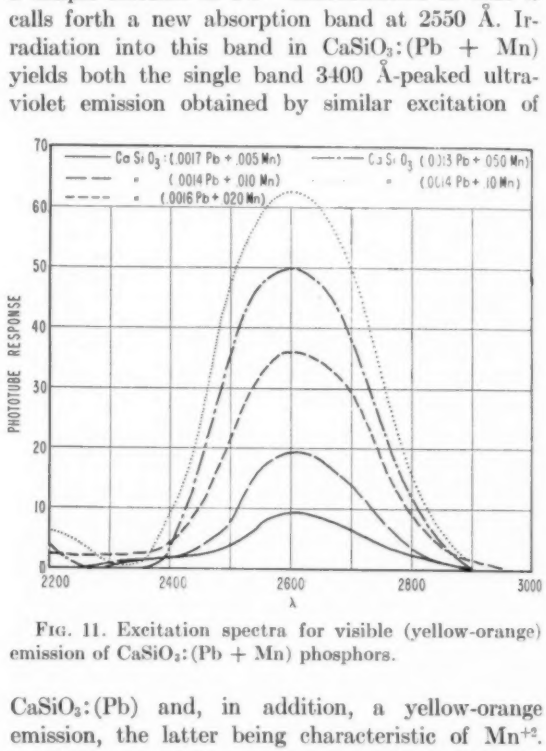

FIG. 11. Excitation spectra for visible (yellow-orange) emission of $CaSiO_3$:(Pb + Mn) phosphors.

$CaSiO_3$:(Pb) and, in addition, a yellow-orange emission, the latter being characteristic of Mn^{+2}. (*c*) Increase of Mn^{+2} concentration in $CaSiO_3$:(Pb + Mn) differs from a simple increase of Pb^{+2} concentration in $CaSiO_3$:(Pb) in that the 2550 A absorption band increases in intensity at the expense of the 2350 Å band in the former case, while both the 2350 Å and the 2550 Å absorption band grow more intense in the latter case.

DISCUSSION

In this discussion we assume that the "scattering coefficient" σ in the Urbach, Hemmendinger, and Pearlman relation

$$\frac{\alpha}{\sigma} = \frac{(1 - R^2)}{2R}$$

is constant over the wavelength range 2300–2600 Å for the different phosphors we have investigated.

We also assume that the number of absorbers giving rise to a particular absorption band is proportional to the value of $\frac{\alpha}{\sigma}$ calculated from the reflection at the wavelength of peak absorption in that band. The bases for these assumptions have already been mentioned.

It will be seen by reference to the reflection data of Fig. 8 that at constant Pb^{+2} concentration, the total number of absorbers in the 2350 Å and 2550 Å absorption bands is unaffected by changes in the Mn^{+2} concentration. With no Mn^{+2}, all the absorption is in the 2350 Å band, while with high Mn^{+2} concentration, practically all the absorption is in the 2550 Å band. The depths of the reflection minima in these two limiting cases are equal, however, showing that the total number of absorbers has remained constant. This is additional disproof of Butler's mechanism of sensitization, it being impossible to reconcile this mechanism with our experimental data without additional purely *ad hoc* assumptions. Our data confirm the generally accepted idea that absorption of ultraviolet light in sensitized phosphors is performed entirely by the sensitizer and that the absorber energy is subsequently transferred to the activator or emitter, as in the sensitized luminescence of gases.[5]

[5] All previous writers (1–8) on sensitization of phosphors have considered the situation to be very similar to that existing in gases, i.e., that energy transfer occurs between an *excited* sensitizer ion and a near-by activat or ion. Jenkins, McKeag, and Ranby (12) have recently suggested another interpretation involving *ionization* of the sensitizer and activator. Where previous writers assumed that direct excitation of the activator by ultraviolet absorption is not observed because it corresponds to a forbidden transition within the activator itself, Jenkins, *et al.*, assume that it is the direct transfer of an electron from the activator to the conduction band that is forbidden. Instead of assuming that absorption of ultraviolet by the sensitizer places this impurity in an excited state, Jenkins, *et al.*, assume that such absorption ionizes the sensitizer. In place of the assumption that energy transfer takes place by a process analogous to collisions of the second kind (overlap of wave functions of the excited states of sensitizer and activator), Jenkins, *et al.*, assume that this takes place by the following sequence: (*a*) the activator donates an electron directly to the ionized sensitizer, and (*b*) the activator captures an electron from the conduction band. From the view of Jenkins, *et al.*, one might expect photoconductivity in the phosphor containing the sensitizer alone. We have failed to find such photoconductivity in NaCl:(Pb) under 2730 Å excitation, which indicates at least that there is no reason to assume ionization of the sensitizer by absorption in its characteristic ultraviolet absorption bands.

Botden and Kroeger (5) have already pointed out that the restriction on energy transfer is the same whether one assumes only excitation of the impurities or their ionization. In both cases, sensitization requires proximity of the sensitizer and activator in order to make energy transfer possible.

We propose the following interpretation of the sensitized luminescence of the $CaSiO_3$:(Pb + Mn) phosphor: The 2350 Å-peaked absorption band in $CaSiO_3$:(Pb) is due to the absorption of "singlet" Pb^{+2}-ions, i.e., Pb^{+2}-ions that have no other Pb^{+2} ions as neighbors.[6]

The evidence for this is the occurrence of this absorption band at very low Pb^{+2} concentrations, where practically all the Pb^{+2}-ions would be "singlets" if they were distributed randomly, replacing Ca^{+2}. The emission of "singlet" Pb^{+2} is excited only by absorption in the 2350 Å band, and is a double band with peaks at 2900 Å and 3900 Å. The 2550 Å absorption band in high Pb-bearing $CaSiO_3$:(Pb) we assign to Pb^{+2}-Pb^{+2} "doublets" or higher aggregates of Pb^{+2} -ions, i.e., centers consisting of a Pb^{+2} which has at least one other and perhaps several Pb^{+2}-ions in neighboring cation positions. The single-band emission peaking at 3400 Å we ascribe to the "doublet" Pb^{+2} centers. Increase of Pb^{+2} concentration in $CaSiO_3$:(Pb) increases both the number of Pb^{+2} singlets and the number of Pb^{+2} doublets, the rate of this increase varying with the concentration. Below 4×10^{-3}Pb/Ca practically all the Pb^{+2}-ions are singlets, and the absorption coefficient at 2350 Å (or rather $\frac{\alpha}{\sigma}$) increases linearly with the Pb^{+2} concentration; above this concentration "doublets" become increasingly important, causing a nonlinear dependence of $\left(\frac{\alpha}{\sigma}\right)$ 2350 Å on the Pb^{+2} concentration and growth of the 2550 Å absorption band.

The 2350 Å absorption band in $CaSiO_3$:(Pb + Mn) we ascribe again to singlet Pb^{+2}-ions, and specify that these singlets have *neither another Pb^{+2} nor a Mn^{+2}-ion as a neighboring*[7] *cation*. The emission of singlet Pb^{+2} in $CaSiO_3$:(Pb + Mn) is the same double-banded emission as in $CaSiO_3$:(Pb), and is excited only by the 2350 Å band absorption. The 2550 Å absorption band in $CaSiO_3$:(Pb + Mn) we ascribe to Pb^{+2}-ions which have *either a Pb^{+2} neighbor or a Mn^{+2} neighbor*, i.e., Pb^{+2}-Pb^{+2} "doublets" or aggregates, or Pb^{+2}-Mn^{+2} "doublets" or aggregates. The ultraviolet emission of Pb^{+2} in a Pb^{+2}-Mn^{+2} doublet we assume is indistinguishable from that of Pb^{+2} in a Pb^{+2}-Pb^{+2} doublet, both con-

[6] By a "neighboring" position we mean a cation position near enough to the one in question so that there will be appreciable interaction between the two Pb^{+2} ions, resulting in modification of the absorption energy. Positions in the nearest cation shell surrounding the given Pb^{+2} would certainly be "neighbors," and perhaps the second, third, or further shells might also be "neighbors" in this respect. We leave open for the time being the actual number of cation sites effective as neighbors.

[7] See footnote 6.

sisting of the single band peaking at 3400 Å. Excitation of this ultraviolet emission can occur only by radiation into the 2550 Å absorption band. This is true likewise of the visible manganese emission, which can be excited only by absorption in Pb^{+2}-ions that interact with Mn^{+2}, and not by the "isolated" or "singlet" Pb^{+2}. Our interpretation thus agrees with the conventional concept of sensitization in that, at a given Pb^{+2} concentration, the total concentration of absorbing centers is thus independent of the manganese concentration, the absorbing centers being singlet Pb^{+2}, Pb^{+2} in Pb^{+2}-Pb^{+2} aggregates, or Pb^{+2} in Pb^{+2}-Mn^{+2} aggregates. At the low Pb^{+2} concentration of the samples in Fig. 8, those Pb^{+2} -ions which are not singlets are principally Pb^{+2}-Mn^{+2} aggregates, and the absorption at 2550 Å is due almost entirely to such groups. Increase in Mn^{+2} concentration decreases the number of singlet Pb^{+2}-ions, thus decreasing the 2350 Å absorption band intensity; simultaneously an equal number of Pb^{+2}-Mn^{+2} doublets are created, which increases the 2550 Å absorption band intensity by an equal amount.

We shall assume that there are K cation positions around a given Pb^{+2} ion, such that interaction between a Pb^{+2} and a Mn^{+2} can occur only if a Mn^{+2}-ion occupies one of the K sites. We assume this interaction is what causes modification of both the absorption and emission spectra of the Pb^{+2} and is the prerequisite for energy transfer between Pb^{+2} and Mn^{+2}. We now ask for an estimate of the value of K.

For a random distribution of Pb^{+2} and Mn^{+2} replacing Ca^{+2} in the crystal, the probability of a given Pb^{+2}-ion having a Mn^{+2} occupy a particular one of the "effective" K sites is X_{Mn}, where X_{Mn} is the mole fraction of Mn^{+2} in the phosphor. The probability of a given Pb^{+2}-ion having no Mn^{+2} neighbors in any of the total K effective sites is $(1\text{-}X_{Mn})^K$, while the probability of its having at least one Mn^{+2} neighbor among these K effective sites is $1\text{-}(1\text{-}X_{Mn})^K$.

When singlet Pb^{+2}, Pb^{+2}-Pb^{+2} "pairs," and Pb^{+2}-Mn^{+2} "pairs" are present, the ratio of the number of the Pb^{+2} singlets to the number of Pb^{+2}-Mn^{+2} "pairs" is

$$\frac{N_{\text{singlet Pb}^{+2}}}{N_{\text{Pb}^{2+}\text{as Pb}^{+2}\text{-Mn}^{+2}}} = \frac{(1 - X_{Mn})^K - (N_{\text{Pb}^{+2}\text{ as Pb}^{+2}\text{-Pb}^{+2}})}{1 - (1 - X_{Mn})^K}$$

At low Pb^{+2} concentration and reasonably high Mn^{+2} concentrations, the number of Pb^{+2}-Pb^{+2} pairs will be much smaller than the number of Pb^{+2}-Mn^{+2} pairs. Although, according to our interpretation, both these types of centers give rise to the 2550 Å-peaked absorption, the contribution of the Pb^{+2}-Pb^{+2} pairs to this absorption can be neglected in this case. We can then say

$$\frac{N_{\text{singlet Pb}^{+2}}}{N_{\text{Pb}^{+2}\text{ as Pb}^{+2}\text{-Mn}^{+2}}} = \frac{\left[\left(\frac{\alpha}{\sigma}\right)_{2350\text{ Å CaSiO}_3\text{:(Pb+Mn)}} - \left(\frac{\alpha}{\sigma}\right)_{2350\text{ Å CaSiO}_3}\right]}{\left[\left(\frac{\alpha}{\sigma}\right)_{2550\text{ Å CaSiO}_3\text{:(Pb+Mn)}} - \left(\frac{\alpha}{\sigma}\right)_{2550\text{ Å CaSiO}_3}\right]} = \frac{(1 - X_{Mn})^K}{1 - (1 - X_{Mn})^K}$$

Using the data on the $CaSiO_3$:(0.0016 Pb + 0.02 Mn) phosphor, Fig. 8, where both the 2350 Å and 2550 Å reflection minima appear about equal, we have:

$$\left[\left(\frac{\alpha}{\sigma}\right)_{2350\text{ Å CaSiO}_3\text{:(0.0016Pb+0.02Mn)}} - \left(\frac{\alpha}{\sigma}\right)_{2350\text{ Å CaSiO}_3}\right] = 0.384$$

$$\left[\left(\frac{\alpha}{\sigma}\right)_{2550\text{ Å CaSiO}_3\text{:(0.0016Pb+0.02Mn)}} - \left(\frac{\alpha}{\sigma}\right)_{2550\text{ Å CaSiO}_3}\right] = 0.310$$

$$X_{Mn} = 0.02$$

Whence $K \cong 28$.

A fairly good check for the above value of K is obtained using the data for $CaSiO_3$:(0.0013 Pb + 0.05 Mn) (Fig. 8), although here there is less accuracy in reading reflection at 2350 Å. A similar check was obtained with $CaSiO_3$:(0.00042 Pb + 0.02 Mn).[8]

From the value of K found above we may estimate that a Pb^{+2} -ion interacts effectively with Mn^{+2}-ions situated in the first two neighboring rings of cation sites around the Pb^{+2}-ion, and consequently that energy transfer is possible over this distance.

We can suggest the following questions concerning our interpretation of the experimental data. We have assumed substitutional solid solution of Pb^{+2}

[8] A corresponding calculation can be made, in principle, for the value of K corresponding to a Pb^{+2}-Pb^{+2} interaction in $CaSiO_3$:(Pb). We have not attempted such a calculation because of the much poorer resolution of the 2550 Å reflection minimum in $CaSiO_3$:(Pb) compared to the resolution of this minimum in $CaSiO_3$:(Pb + Mn) (cf. Fig. 3 and 8). Also, the apparent depth of the 2550 Å reflection minima in $CaSiO_3$:(Pb) may be subject to considerable interference from overlap of the nearby Pb^{+2} emission band, which peaks at 2900 Å but which extends to shorter wavelengths. With $CaSiO_3$:(Pb + Mn) there is less likelihood of such interference, for the ultraviolet emission from the Mn^{+2}-bearing phosphor is less intense than from the Mn^{+2}-free phosphor.

and Mn^{+2} for Ca^{+2}, but have given no reason why the Pb^{+2} absorption and emission should be affected upon replacement of one divalent near neighbor, Ca^{+2}, by another divalent near neighbor, Mn^{+2}. Nor have we given any reason why the effect of a Mn^{+2} near neighbor should be the same as that of a Pb^{+2}-ion near neighbor on the absorption and emission spectrum of a given Pb^{+2}-ion. With regard to the first question, we suggest that the difference between the effect of a Ca^{+2} near neighbor vs. that of a Mn^{+2} near neighbor on the energy levels of a Pb^{+2}-ion is related to the fact that the Ca^{+2}-ion has an inert gas configuration while the Mn^{+2} has not. The same difference exists between the electronic configuration of the Pb^{+2}-ion vs. that of the Ca^{+2}-ion. The difference between ions of inert gas configuration and those of non-noble gas configuration has been pointed out by Fajans (13) and has been recently emphasized repeatedly in publications by Weyl (14). The assumed identity with respect to absorption and emission of a Pb^{+2}-Pb^{+2} configuration and a Pb^{+2}-Mn^{+2} configuration is forced upon us by the data. It is not unreasonable that the difference between a Pb^{+2}-Pb^{+2} interaction and a Pb^{+2}-Mn^{+2} may be of a lower order of magnitude than the difference between either of them and a Ca^{+2}-Pb^{+2} interaction, making it difficult to distinguish between the first two.

Another objection that may be raised concerning our interpretation is that our picture assigns no influence to the difference in crystal structure which has been shown to exist (15) between $CaSiO_3$:Pb and $CaSiO_3$:Mn. We have confirmed the findings of Fonda and Froelich (15) that such differences do exist, $CaSiO_3$:Pb having the α-wollastonite structure, $CaSiO_3$:Mn having the β-wollastonite structure, while $CaSiO_3$:(Pb + Mn) may have either of the two structures depending on the relative amounts of Pb and Mn. In a recent publication, Studer and Fonda (16) have ascribed differences in the excitation and emission spectra of various $CaSiO_3$:Pb and $CaSiO_3$:(Pb + Mn) phosphors to this difference in structure, occasioned by different proportions in their phosphors and by differences in firing conditions. They also ascribe some of the excitation and emission phenomena to a Ca_2SiO_4 host structure which can be shown to be one of the first products of the reaction between CaO or $CaCO_3$ and SiO_2.

We believe that the above structural differences have no appreciable effect on our results or our interpretation, for the following reasons: (*a*) Increase of Pb^{+2} concentration in $CaSiO_3$:Pb causes the growth of the 2550 Å excitation band for the ultraviolet Pb^{+2} emission in addition to the 2350 Å excitation band found at low Pb^{+2} concentrations. No structural change is produced by this increase in Pb^{+2} concentration, the α-wollastonite structure being maintained at both low and high Pb^{+2} concentrations; (*b*) The ultraviolet emission excited by irradiation into the 2550 Å band in high Pb^{+2}-bearing $CaSiO_3$:Pb (α-wollastonite structure) is the same 3400 Å-peaked emission excited by irradiation into the 2550 Å band of Mn^{+2}-bearing $CaSiO_3$:(Pb + Mn) (β-wollastonite structure); (*c*) In order to explain some of their results Studer and Fonda have to assume the existence of an "aggregate" $CaSiO_3$·SiO_2 as a separate phase. There is no x-ray or other evidence for the existence of such a phase, nor is the structural nature of this "aggregate" defined in any way by them; (*d*) The assumption of a mixture of phases fails to explain the emission of a 3850 Å band (equivalent to our 3900 Å band) on irradiation of $CaSiO_3$:Pb with 2288 Å light (equivalent to our irradiation with 2350 Å light). Studer and Fonda admit that x-ray examination showed only α-wollastonite in this phosphor, and the foregoing observation is left completely unexplained; (*e*) Our preparations were made using 10 mole per cent excess SiO_2, and PbF_2 as a catalyst. Firing was at 1150° for 6 hours, followed by grinding and refiring 6 more hours at 1150°. Under these conditions the existence of Ca_2SiO_4 in the final product, as assumed by Studer and Fonda in their preparations, is extremely unlikely.

Our final comments concern the calculations of Botden and Kroeger (5) on the efficiency of energy transfer between Pb^{+2} and Mn^{+2} in $CaSiO_3$:(Pb + Mn) and between Ce and Mn in $Ca_3(PO_4)_2$:(Ce + Mn). The considerations advanced by these investigators are perfectly valid for the case where the introduction of the activator leaves the position of the sensitizer absorption band unchanged. In this case, there are the following possible dispositions of the absorbed energy: (*a*) return of the sensitizer to the ground state with emission of its characteristic luminescence; (*b*) radiationless return of the sensitizer to its ground state; (*c*) transfer of energy from sensitizer to activator followed by luminescence emission characteristic of the activator; and (*d*) transfer from the sensitizer to activator followed by radiationless dissipation of the energy by the activator. Processes (*b*) and (*d*) are indistinguishable to the observer. Calculations such as Botden and Kroeger make are, therefore, possible under these circumstances, it being necessary only to make the reasonable assumptions that: (1) ultraviolet absorption occurs exclusively in the sensitizer ions; (2) all the sensitizer ions absorb regardless of their location in the lattice; (3) they can dissipate the absorbed energy by processes (*a*), (*b*), or (*c*) above; and (4) there is some restriction on process

(*c*), for example, that only those Pb^{+2}-ions which have Mn^{+2}-ions among their nearest cation neighbors can get rid of their energy by this process. The foregoing assumptions make it possible to calculate a theoretical maximum efficiency of sensitization in the case described. If there is a change in absorption spectrum upon incorporation of the activator, and if emission from the activator is produced only by irradiation into the new band, the *a priori* calculation of sensitization efficiency cannot be made on the foregoing basis. That this is the situation with regard to the Pb^{+2} absorption and the Mn^{+2} excitation in $CaSiO_3$ was unknown to Botden and Kroeger since their reflection measurements extended only to 2500 Å. The disagreement between their calculated value and the observed sensitization efficiency in $CaSiO_3$:(Pb + Mn) is, therefore, understandable, and their inference of *preferential* pair formation accordingly need not be resorted to. For $Ca_3(PO_4)2$:(Ce + Mn) their calculation of sensitization efficiency (corrected for the existence of $Ce^{+3}-Ce^{+3}$ pairs) amounts to 50 per cent of the experimentally determined sensitization efficiency. This is reasonably good agreement, in our opinion, considering their assumption that the number of neighboring cation sites over which energy transfer is possible is 10. If this number is taken as 20, which is more in line with our value of K, an excellent check is obtained for this system. The success of such a calculation for this phosphor implies that the introduction of Mn^{+2} in $Ca_3(PO_4)_2$:Ce does not alter the position of the Ce^{+3} absorption band (or bands). From Botden and Kroeger's data, this appears to be true.

In our interpretation of systems like $CaSiO_3$:(Pb + Mn), where the position of the sensitizer absorption is altered by the activator, it is impossible to calculate *a priori* maximum sensitization efficiencies. In these cases, the sensitizer atoms which absorb in the new band are all coupled with the activator atoms to begin with, and all these sensitizer atoms are in a position to transfer energy to the latter. The probability that they will do so, based solely on considerations of activator-sensitizer proximity, is unity. The actual probability of energy transfer is, however, a function of properties of the system other than the proximity of the sensitizer and activator. Bases for calculating this energy transfer probability are likely to be derived, as Botden and Kroeger point out, by applying to solids the criteria for such transfer known to hold for gases.

Acknowledgments

We wish to express our indebtedness to Mrs. Esther W. Claffy for the polarographic analyses of the $CaSiO_3$ phosphors and for the x-ray diffraction studies of these preparations. We also wish to thank Legrand Van Uitert and Seymour Londoner for their assistance in the preparation of material.

Any discussion of this paper will appear in a Discussion Section, to be published in the December 1950 issue of the JOURNAL.

REFERENCES

1. S. ROTHSCHILD, *Physik. Z.*, **35,** 557 (1934); **37,** 757 (1936).
2. J. H. SCHULMAN, L. W. EVANS, R. J. GINTHER, AND K. J. MURATA, *J. Applied Phys.*, **18,** 732 (1947).
3. J. B. MERRILL AND J. H. SCHULMAN, *J. Optical Soc. Am.*, **38,** 471 (1948).
4. H. C. FROELICH, *J.* (*and Trans.*) *Electrochem. Soc.*, **93,** 101 (1948).
5. TH. P. J. BOTDEN AND F. A. KROEGER. *Physica*, **14,** 553 (1948).
6. R. NAGY, R. W. WOLLENTIN, AND C. K. LUI, *J.* (*and Trans.*) *Electrochem. Soc.*, **95,** 187 (1949).
7. H. C. FROELICH, *J.* (*and Trans.*) *Electrochem. Soc.*, **95,** 254 (1949).
8. J. H. SCHULMAN, E. BURSTEIN, L. W. EVANS, R. J. GINTHER, AND M. WHITE, *Bull. Am. Phys. Soc.*, **24,** (No. 4, Paper Q1), 25 (1949).
9. K. H. BUTLER, *J.* (*and Trans.*) *Electrochem. Soc.*, **95,** 267 (1949).
10. C. F. GOODEVE AND J. A. KITCHENER, *Trans. Faraday Soc.*, **34,** 902 (1938).
11. F. URBACH, H. HEMMENDINGER, AND D. PEARLMAN, "Solid Luminescent Materials," (Cornell Symposium), Paper #16, John Wiley & Sons, Inc., New York (1948).
12. H. G. JENKINS, A. H. MCKEAG, AND R. W. RANBY, *J.* (*and Trans.*) *Electrochem. Soc.*, **96,** 1 (1949).
13. K. FAJANS, "Radio Elements in Isotopes; Chemical Forces and Optical Properties of Substances," McGraw-Hill Book Co., Inc., New York (1931).
14. J. K. INMAN, A. M. MRAZ, AND W. A. WEYL, "Solid Luminescent Materials," (Cornell Symposium), pp. 182–9, John Wiley & Sons, Inc., New York (1948).
15. G. R. FONDA AND H. FROELICH, *J.* (*and Trans.*) *Electrochem. Soc.*, **93,** 114 (1948).
16. F. J. STUDER AND G. R. FONDA, *Bull. Am. Phys. Soc.*, **23,** 48 (1948); *J. Optical Soc. Am.*, **39,** 655 (1949).

Anode Effect in Aqueous Electrolysis[1]

HERBERT H. KELLOGG

School of Mines, Columbia University, New York, New York

ABSTRACT

A phenomenon which closely resembles "anode effect" in molten electrolysis can be developed in the electrolysis of aqueous solutions at high current density. Normal operation of the electrode ceases and a so-called "transition period" begins when the electrode temperature reaches the boiling point of the electrolyte. When the applied voltage is increased beyond a critical value the transition behavior suddenly changes to the "aqueous anode-effect." During this effect the surface temperature of the anode rises far above the boiling point of the electrolyte. Evidence is provided which indicates that the gaseous envelope surrounding the anode during the aqueous anode-effect is maintained by the vaporization of the electrolyte against the hot anode surface. An aqueous cathode-effect was also obtained. The relation between aqueous anode-effect and anode effect in molten media is discussed.

INTRODUCTION

Since the earliest experiments with the electrolysis of molten salts, the behavior called "anode effect" has been reported and many investigators have attempted explanations of this peculiar and troublesome phenomenon. The description of anode effect by C. S. Taylor (1) is quoted below:

"The anode, during the normal course of electrolysis, is surrounded with a large number of gas bubbles which are constantly escaping from it. These small bubbles seem to form on the anode, and then break away easily and escape from the electrolyte by breaking through the surface film. This smooth, even evolution of gas around the anode is always a sign of normal operation. The moment the anode effect occurs, however, conditions are entirely different. The anode appears to be entirely surrounded by a film of gas, which, by covering the surface of the anode, pushes the fused electrolyte away, and thus produces the so-called 'non wetting' of the anode. As the electrolyte is pushed away, small arcs form between the electrolyte and the anode."

The literature on anode effect is rich in factual information on the occurrence and control of the phenomenon in a variety of molten electrolyses (2, 3, 4). Noticeably lacking, however, is a satisfactory hypothesis concerning the anode effect which will explain what forces are responsible for holding the molten electrolyte away from the anode in the form of a gaseous envelope despite the ever present hydrostatic forces which tend to collapse this envelope. To the best of the author's knowledge, the idea that this envelope is maintained by the rush of gases evolved at the anode is the most widely held hypothesis at the present time.

[1] Manuscript received August 2, 1949. This paper prepared for delivery before the Cleveland Meeting, April 19 to 22, 1950.

This paper shows that a phenomenon can be obtained with electrodes which evolve gas in aqueous electrolysis, which phenomenon closely fits the previously cited description of anode effect in molten electrolysis. Furthermore, by analysis of pertinent data on this "aqueous anode-effect," an explanation of the forces which form and maintain the gaseous envelope has been arrived at. It seems very likely that the explanations of aqueous anode-effect may also be valid for the anode effect in molten electrolysis, and it is contemplated to investigate this possibility in a future paper.

EXPERIMENTAL

The experiments on aqueous anode-effect were made with the following circuit: The cell was an 800-ml Pyrex beaker in which were placed the anode to be investigated (in most instances a platinum wire, 1.25 mm diameter, immersed to a depth of 8 mm) and a platinum cathode (4 x 6 cm sheet). The electrolyte (usually 1.0*N* H_2SO_4) was added so as to almost fill the cell. A glass stirring-rod, bent into a loop at the bottom, was attached to a motor and rotated at 450 rpm. A mercury thermometer was used to record the temperature of the electrolyte. Direct current was supplied to the electrodes by means of a voltage divider connected across a 115 volt source. An ammeter was placed in series with the cell, and the total cell voltage was measured across the electrodes with a voltmeter.

The measurements of electrode temperature were made with an electrode constructed in the following manner: A tube of 25-20 chromium-nickel steel, closed at one end, 3.5 mm OD, 2.7 mm ID, and 50 mm long comprised the electrode. A copper-constantan thermocouple (30 gauge wire) was threaded through a two-hole ceramic insulator and inserted into the steel tube so that the junction was in contact with

the closed end of the tube. An efficient thermal contact between the thermocouple junction and the tube was made by placing about 50 mg of a low melting (80°C) alloy of lead, tin, and bismuth in the bottom

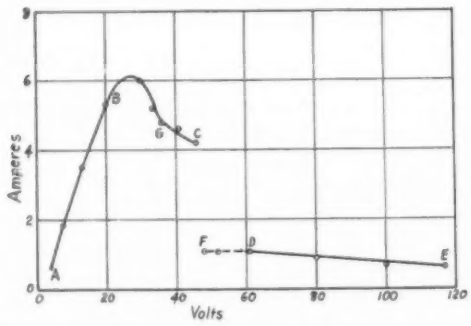

FIG. 1. Anode effect with platinum-wire anode (0.314 cm² immersed area) in normal H_2SO_4 at 66° ± 4° C.

FIG. 2. Normal operation of platinum-wire anode. 1*N* H_2SO_4 at 40° C, 27 volts, 5.4 amperes, about 8×.

of tube and then gently heating the tube with the thermocouple in place. Thermal emf was measured with a potentiometer.

The photographs were made with a bench camera equipped with a 42-mm Micro-Summar lens. The illuminant was an Identification Flash Outfit used by the Signal Corps, and consisted of a power supply and two gas-discharge flash-lamps. The flash intensity is reported as eleven times more intense than sunlight and the duration about 1/10,000 second.

DISCUSSION

Description of Aqueous Anode-Effect

The discussion of the main body of the data and the development of a hypothesis for the aqueous anode-effect will be followed with greater ease if preceded by a description of a typical electrolysis which results in the anode effect.

Fig. 1 records in graphical form the volt-ampere relationships for a cell consisting of a sheet-platinum cathode (4 x 4 cm) and a platinum-wire anode (0.31 cm² immersed area), with an electrolyte of normal H_2SO_4. The following description applies to the behavior of the wire anode, when the bulk temperature is maintained at 66° ± 4°C. With a low voltage impressed on the cell, bubbles of oxygen are evolved at the anode in a perfectly normal manner. The volt-ampere relation for the cell is that given by the region A-B in Fig. 1; the current increases almost linearly with increased voltage. Fig. 2 is a photograph of the gas evolution at the wire anode during this normal operation of the cell (compare with Fig. 3 which shows the wire anode when no current is flowing). The oxygen bubbles form rapidly, break away from the electrode, and rise quickly to the surface of the electrolyte where they break. The operation of the cell is quiet and steady.

When a current density represented by the point B on Fig. 1 is reached, a new behavior begins. The volt-ampere relation of the cell is erratic. Spitting and hissing noises arise from the anode, and many of the gas bubbles are projected down and away from the anode by the sudden "spits." The electrolyte close to the anode is hot as evidenced by the presence of condensed water vapor in the evolved gases. A further increase in impressed voltage causes no increase (or even a decrease) in current through the cell, as shown by B-C on Fig. 1. Fig. 4 is a photograph of the wire anode during this behavior, which the writer has called the "transition period."

When the voltage is raised to a critical value (near C in Fig. 1), an instantaneous change takes place. The voltage rises suddenly and the current drops to a low value (point D in Fig. 1). The loud spitting and hissing, which accompanied the previous stage, cease. The wire anode is completely surrounded by a gaseous film. Occasional tiny sparks can be seen to form in the film. Fig. 5 is a photograph of the anode during this behavior. This is the phenomenon which the writer has called "aqueous anode-effect."

Increase of voltage to point E on Fig. 1 does not

alter the behavior described for point D, except that a dull red glow can be seen at the lower tip of the anode. The writer has taken this glow to indicate that the temperature of the electrode is high—probably 750°C. Further indication that the electrode is hot is that, if the circuit is suddenly opened while the anode is operating anywhere in the E-F region

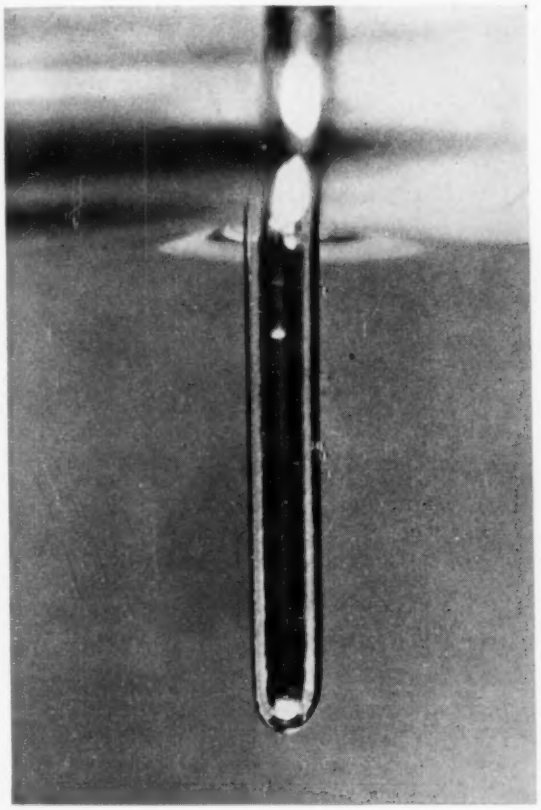

FIG. 3. Platinum-wire anode. No current flowing, immersion 0.8 cm, about 8×.

of Fig. 1, the anode gives forth a sharp hissing noise (like that obtained when a hot object is quenched in water) and water vapor rises from the surface of the electrolyte close to the electrode.

If the voltage is slowly decreased, the anode effect persists at lower voltages than point D. Finally, when the voltage reaches point F there is an instantaneous destruction of the gaseous film and the anode reverts to the behavior at point G.

Mechanism of Aqueous Anode-Effect

In order to investigate quantitatively the temperature of the anode before and during the anode effect, the alloy-steel electrode with the imbedded thermocouple (see EXPERIMENTAL) was used with an electrolyte of normal NaOH[2]. Fig. 6, 7, and 8 summarize the volt-ampere relations and the anode temperature for three different bulk-electrolyte temperatures. The behavior for each electrolyte temperature can again be conveniently divided into three periods: (*a*) normal operation, A-B in Fig. 6, 7, and 8; (*b*) transition period, B-C; (*c*) anode effect, F-D-E.

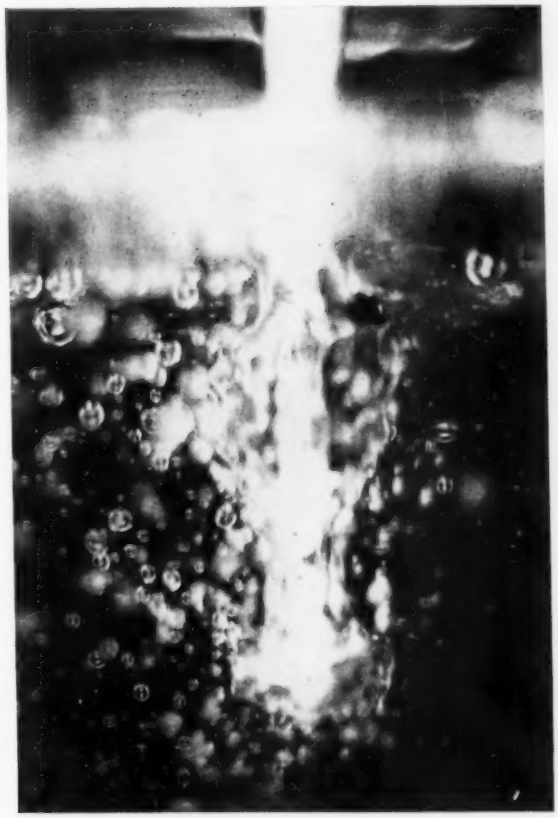

FIG. 4. "Transition period" with platinum-wire anode. 1*N* H_2SO_4 at 88° C, 44 volts, 1.5 amperes, about 8×.

In the following paragraphs each of these periods will be discussed along with the reasons for the transition from one period to another.

1. Normal Operation

When no current is flowing, the electrode temperature coincides with the electrolyte temperature. As the current density is raised in the "normal operation" region (A-B in Fig. 6, 7, and 8), the surface of the electrode becomes hotter than the electrolyte. The reason for this behavior is to be found in the great number of gas bubbles which armor the surface of the electrode (see Fig. 2). The only paths for the

[2] NaOH was used to increase the passivity of the alloy-steel anode.

passage of current from the bulk of the electrolyte to the electrode surface are the bubble walls of the evolving gas. The current density in these bubble walls is correspondingly high, and the heat dissipated by "I^2R" heating in the bubble walls is higher than elsewhere in the electrolyte.

The temperature of the bulk electrolyte has only a minor effect on the volt-ampere relations in this "normal operation" period. For a given voltage, the current is slightly higher for the hot electrolyte than for the cool, as would be expected from the higher conductivity of the hot electrolyte.

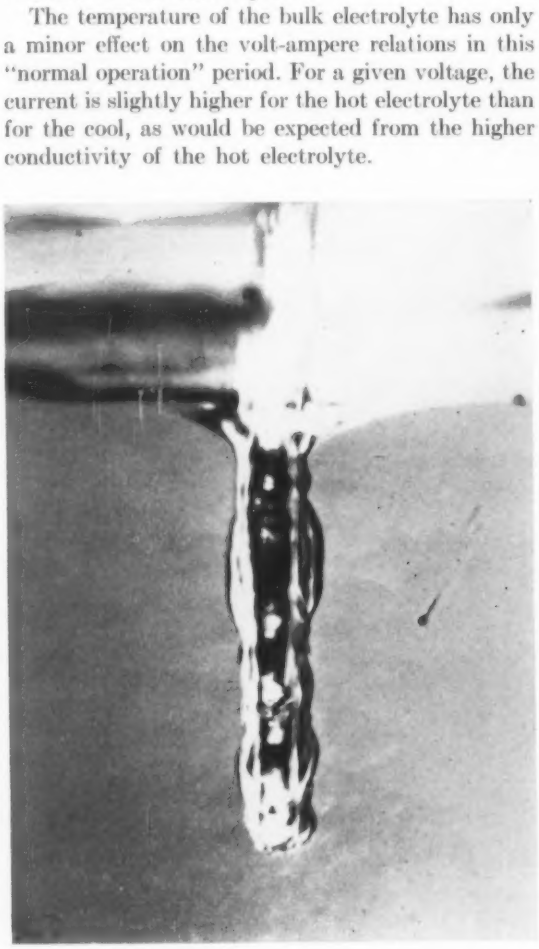

FIG. 5. "Aqueous anode-effect" with platinum-wire anode. 1*N* H_2SO_4 at 40° C, 70 volts, 1.1 amperes, about 8×.

2. *Transition Period*

For all three electrolyte temperatures the change from the "normal operation" to the "transition period" is coincident with the point at which the electrode temperature reaches 100° ± 2°C. The region close to the electrode has become sufficiently hot to vaporize the electrolyte, and the spitting and hissing noises which accompany the "transition period" are evidence that vaporization does take place.

Fig. 6, 7, and 8 show that the current density at which the "normal operation" ends and the "transition period" begins is higher the lower is the bulk-electrolyte temperature. This is readily explained since the cold electrolyte will offer better conditions for heat transfer away from the electrode, and, consequently, a higher current density will be required to

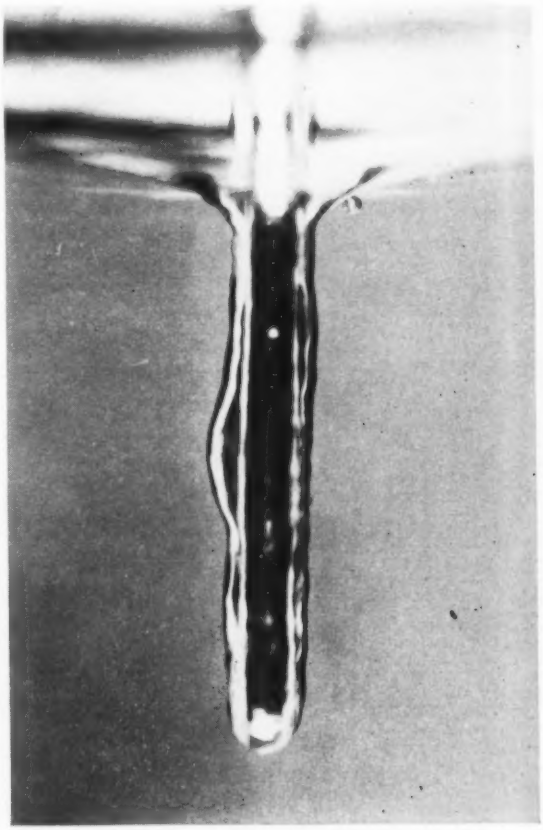

FIG. 7a. "Aqueous anode-effect" with platinum-wire anode. 1*N* H_2SO_4 at 90° C, 74 volts, 0.12 amperes, about 8×.

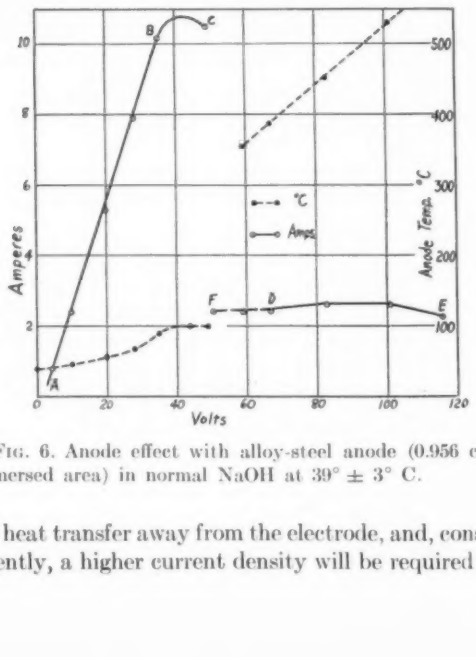

FIG. 6. Anode effect with alloy-steel anode (0.956 cm² immersed area) in normal NaOH at 39° ± 3° C.

raise the electrode temperature to the boiling point of the electrolyte.

Fig. 6, 7, and 8 show that during the "transition period" the current fails to increase and even falls as the voltage is further increased. The explanation of this behavior is found by examination of the electrode surface during the "transition period." Fig. 4 shows that the vaporization of the bubble walls during the "transition period" results in the formation of a wide vapor film which encloses a large section of the electrode. During the "transition period" these films have a very short life and are constantly

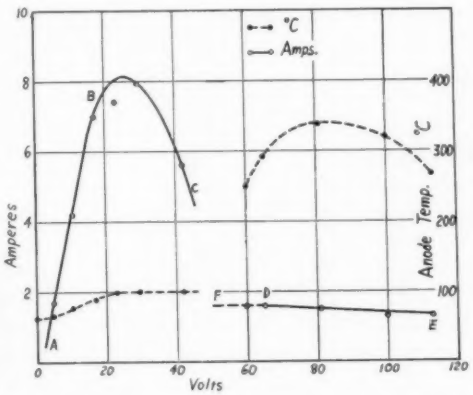

FIG. 7. Anode effect with alloy-steel anode (0.956 cm² immersed area) in normal NaOH at 66° ± 4° C.

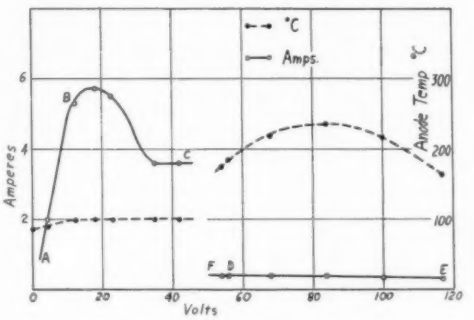

FIG. 8. Anode effect with alloy-steel anode (0.956 cm² immersed area) in normal NaOH at 89° ± 2° C.

forming and breaking—a behavior which is responsible for the unsteady readings of voltage and current during this period. The presence of these vapor films which partially enclose the anode results in a large increase in the resistance of the electrolyte path near the anode and, hence, the current may drop even though the voltage increases.

During the "transition period" the electrode temperature remains constant at 100° ± 2°C. There remains some direct contact between the anode and the electrolyte with the result that the electrode temperature is prevented from rising above the boiling temperature of the electrolyte. The gas evolved by the electrolysis continues to evolve as bubbles, though the force of the sudden vaporizations often projects the gas bubbles far away from the electrode.

3. Anode-Effect Region

The chain of events that leads to the instantaneous change from the "transition period" to the anode effect will be better understood if the characteristics of the already formed anode effect film are first discussed.

The most striking facts, shown in Fig. 6, 7, and 8, are the very high electrode temperatures which prevail when the anode-effect film is present. The lowest anode temperature recorded under these circumstances was 165°C; the highest was about 620°C.[3] These high anode temperatures, together with the facts on the vaporization of the electrolyte during the transition period, suggest a simple and compelling explanation for the forces which maintain the gaseous envelope during the anode effect.

The anode-effect film is primarily a water-vapor film surrounding a hot wire. The electrolyte is pushed back from the electrode surface by the vapor pressure of the electrolyte, which exceeds one atmosphere as a result of the high electrode temperature. If the film attempts to collapse under the influence of hydrostatic forces when the electrolyte surface approaches close to the anode, further vaporization will take place and push the electrolyte back.

This hypothesis of the forces which maintain the film is in accordance with the visual observation of the anode-effect film. The surface of the film is not stationary, but vibrates rapidly toward and away from the electrode surface (see Fig. 5). Since the electrode can lose heat by conduction up through its length, the bottom tip of the wire is the hottest part (this was established experimentally by the observation on the platinum-wire anode that the bottom section could be made to glow at a red heat, while the top gave no visible radiation).

In order to prove that a hot wire is capable of supporting a film, such as is formed during the anode effect, the following experiment was performed: A nichrome wire, 0.10 cm diameter and 12 cm long, was formed into a loop and connected to a direct-current source; a current of 30 amperes was passed through the wire. As soon as the wire was red hot it was plunged into a beaker of water, without disconnecting the current source. A vapor film was seen to surround the entire length of the wire. Fig. 9 is a photograph of that part of the wire close to the surface of the water.

[3] By use of a nickel wire, 0.81 mm diameter, as an anode the author was able to obtain such a high electrode temperature the nickel melted (mp = 1452 C).

In this experiment there is no question but that the gaseous envelope around the hot wire is a water vapor film. There is no electrolysis during this experiment and no other possible source of large quantities of gas other than water vapor. The striking similarity between the hot-wire film (Fig. 9) and the aqueous anode-effect film (Fig. 5) is strong evidence that the anode-effect film is also maintained by the vaporization of water.

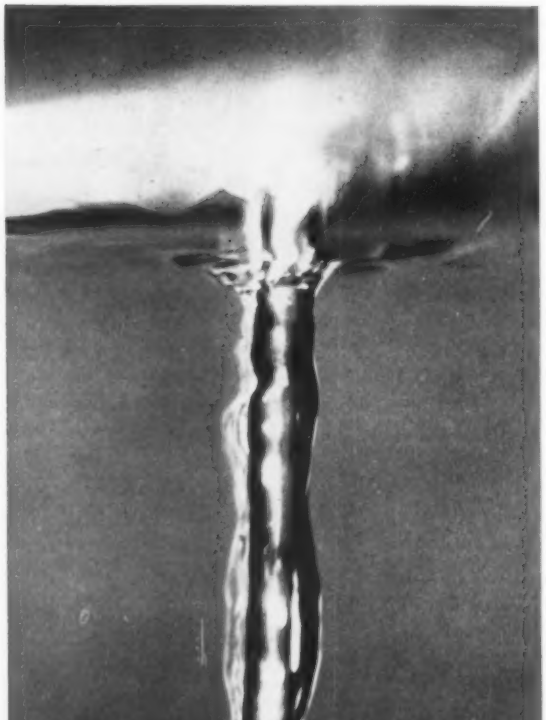

FIG. 9. Vapor film surrounding hot wire (about 8×). A nichrome wire (0.10 cm diam) was heated to red heat by passing 29 amperes through it; the red hot wire was then plunged into distilled water at 72° C, without disconnecting the current source. Wire passes through the surface of the water at the top of the picture.

Another point of similarity between the anode-effect film and the hot-wire film is that the thermal energy which must be dissipated in order to maintain these films is of the same order of magnitude for both films. With water at 87°C, the critical current required to maintain the hot-wire film is about 29 amperes. This corresponds to a heat dissipation of about 40 watts per square centimeter of surface area of the wire. To just maintain the anode effect, with an electrolyte temperature of 87°C, requires about 45 volts and 0.35 amperes, when the platinum-wire anode, immersed to a depth of 0.8 cm, is used. Not all of this voltage drop occurs at the anode film, however. The approximate voltage drop at the film can be obtained by subtracting from the total voltage drop, the voltage drop of the cell when it is operating without anode effect at the same current.

Thus, with normal H_2SO_4 at 87°C:

Total voltage drop to just maintain anode effect = 45 volts.

Voltage drop for normal operation at 0.35 amperes = 3.5 volts.

Voltage drop at film = 45 − 3.5 = 41.5 volts.

Immersed area of electrode = 0.314 cm² (Pt wire immersed 0.8 cm).

$$\text{Heat dissipated by film} = \frac{41.5 \times 0.35}{0.314} = 46 \text{ watts/cm}^2.$$

The close agreement of these two figures for the power required to maintain the two kinds of film also supports the water-vapor theory of the anode-effect film.

A property of the anode-effect film which is of considerable interest and importance is its ability to conduct electric current. The anode effect would be impossible if the film were a nonconductor, since it is the heat dissipated by the current that heats the electrode surface and maintains the vapor film. The mechanism of conduction through the vapor film is by no means clear, but the following observations and discussion throw some light on it.

When the platinum-wire anode is used in an electrolyte of sulfuric acid, the only visible signs of current conduction are rather infrequent and tiny sparks across the anode film. On the other hand, if a little sodium sulfate is added to the electrolyte (or if sodium hyroxide is the electrolyte), the anode film is seen to emit a yellow glow, characteristic of sodium emission. With a cell voltage of 70 volts and an electrolyte temperature of 40°C, the anode surface is covered with a great many (perhaps 100) bright yellow spots, but there is no general glow. When the voltage is raised to 110 volts a yellow glow pervades most of the anode surface. The intensity of the glow varies on any one position of the surface with a periodicity that is similar to the vibration of the vapor film described earlier. The glow does not exist out in the wide portions of the film; it is confined close to the anode surface.

Based upon the above observations, and without rigorous proof, the following hypothesis regarding current conduction across the film is offered:

Very little conduction can take place across the wide portions (0.2 to 2.0 mm thick) of the film, as evidenced by the lack of sodium glow in the wide portion of the film. In those portions of the film

which are sufficiently thin (perhaps 0.2 mm judging from the photograph in Fig. 5), the potential gradient is sufficiently high to cause ionization of the gases within the film and current conduction will take place by migration of the gaseous ions. This ionization may be sufficiently intense to cause a visible discharge in the gas, as evidenced by the sodium glow noted above. Since any one position on the film is periodically approaching closer to the electrode and then receding, the conduction across the film at that point will also vary and the intensity of the glow will vary, thus, the flickering aspect of the glow is described.

Since appreciable current still flows during the anode effect, there must be some electrolytic reaction taking place at the anode. On the other hand, visual observation of the anode during the anode effect shows no formation of gas bubbles. The seat of the electrolytic reaction must now be the electrolyte-gas interface. This type of electrolysis, where the metal electrode is separated from the electrolyte by a gaseous region, has been described as long ago as 1887 by Gubkin (5) and studied at length by Klemenc (6). However, these studies involved low pressures (5–15 mm of Hg) in the gas phase and real glow-discharge conduction was obtained.

To prove that during the anode effect oxygen gas is evolved into the water-vapor envelope and exits through the neck of this envolope to the atmosphere, the following experiment was performed: The upper portion of the platinum-wire anode was sheathed with a close-fitting ceramic insulator, so that a tip about 0.5 cm long of platinum was exposed. The upper end of the sheath was cemented to the wire to prevent gas leakage. The electrode was immersed so that the 0.5 cm of bare platinum and about 0.2 cm of the sheath were below the electrolyte surface. When the anode effect was developed with this electrode a large bubble of noncondensable gas formed at the top of the bare platinum and broke off from time to time when it grew too large. Tests proved the gas to be oxygen. Fig. 10 shows the anode effect under these conditions.

Fig. 6, 7, and 8 show that the electrolyte temperature has a marked effect on both the current and the electrode temperature during the anode effect. A low electrolyte temperature gives rise to a high current and a high electrode temperature during the anode effect. The explanation of this peculiar relationship is to be found in the thickness of the vapor films formed at different electrolyte temperatures. Fig. 5 and Fig. 5a show the anode film at electrolyte temperatures of 40°C and 90°C, respectively. With the high electrolyte temperature the film is quite uniform and it vibrates only slightly. With the low electrolyte temperature the film vibrates violently and is very wide (1–2 mm) in some places and extremely thin in others. It is reasonable to expect that the cooler the electrolyte, the more closely the film can approach the electrode before it is heated sufficiently by the hot surface to cause vaporization. As discussed previously, the main conduction through the film occurs at the very thin sections; thus, the cold electrolyte makes possible a larger current because the film approaches closer to the electrode surface.

As would be expected, the intensity of agitation of the electrolyte also affects the current during the anode effect. At a given electrolyte temperature, increased agitation causes an increased current to flow. Agitation makes possible a more rapid rate of heat transfer away from the electrolyte-gas interface, with the result that this interface remains cooler, can approach more closely to the electrode surface, and can allow a larger current to flow.

FIG. 10. "Aqueous anode-effect with partly insulated platinum wire. The top part of the electrode is sheathed with a ceramic insulator. The large bubble breaks off periodically when it grows too large. 1*N* H_2SO_4 at 67° C, 77 volts, 0.15 amperes, about 8×.

The high electrode temperature obtained with the cold electrolyte is a secondary effect. Since the cold electrolyte allows a large current to flow, and the large current will dissipate more heat than the small one, the electrode will become hotter. In brief, the

electrode temperature is a function of, among other factors, the rate of heat dissipation.

4. Change from "Transition Period" to Anode-Effect

With the foregoing discussion of the anode-effect film after it is formed, it is now possible to discuss the critical factors which result in the change from the "transition period" to the anode effect.

It is evident that the aqueous anode-effect begins at a critical voltage rather than at a critical current density. Fig. 1, 6, 7, and 8 show that for the evolution of oxygen the critical voltage is about 45–50 volts. If hydrochloric acid is the electrolyte and chlorine is evolved, the critical voltage for anode effect is about 30–35 volts. Apparently, therefore, the nature of the gas evolved at the anode has some bearing on the critical voltage. These facts suggest the following hypothesis for the chain of events which lead from the "transition period" to the anode effect.

During the "transition period" there is sufficient heat dissipated to vaporize much of the electrolyte; however, an anode-effect film cannot form unless the

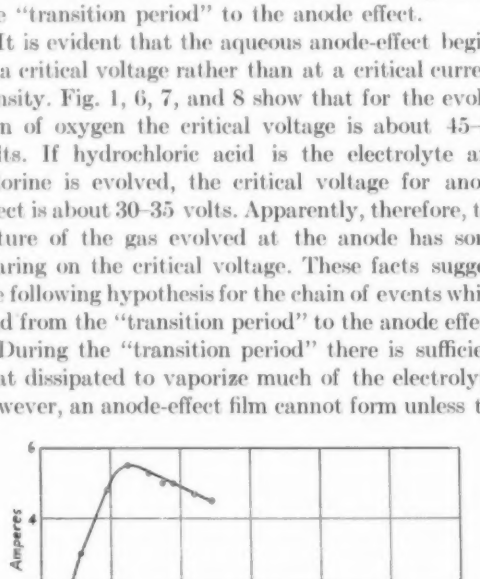

FIG. 11. Cathode effect with platinum-wire cathode (0.314 cm² immersed area) in normal H_2SO_4 at 66° ± 3° C.

anode temperature rises appreciably above the boiling point of the electrolyte. The type of conduction during the "transition period" that results in the vaporization of the bubble walls can never give a temperature above the boiling point of the electrolyte, since as soon as a particular bubble wall is vaporized completely the circuit is broken at that point and the current ceases for that particular path. However, as the voltage is progressively increased, a point is reached where there is sufficient potential drop across some thin section of one of the transient films to cause conduction through the gas film. As soon as this occurs, the heat dissipated by this current can result in a local electrode-temperature in excess of 100°C. The heat can be conducted along the metal electrode and cause the vapor film to spread and be stable as a complete envelope. In short, it is suggested that for aqueous anode-effect under the conditions cited, the critical factor for the onset of anode effect is a sufficient potential drop across a transient vapor film to cause an appreciable conduction through the gas phase.

Aqueous Cathode-effect

In all of the experiments and hypotheses discussed above there is no factor which is peculiar to anodes alone. If the hypotheses are correct, then one could predict that a cathode which evolved gas, and which is operated at a high current density should show a similar behavior and develop a vapor film under proper conditions. Such is found to be the case. If the platinum-wire electrode is made a cathode in a 1*N* sulfuric-acid electrolyte, it follows a behavior exactly similar to that of the anode. Fig. 11 records

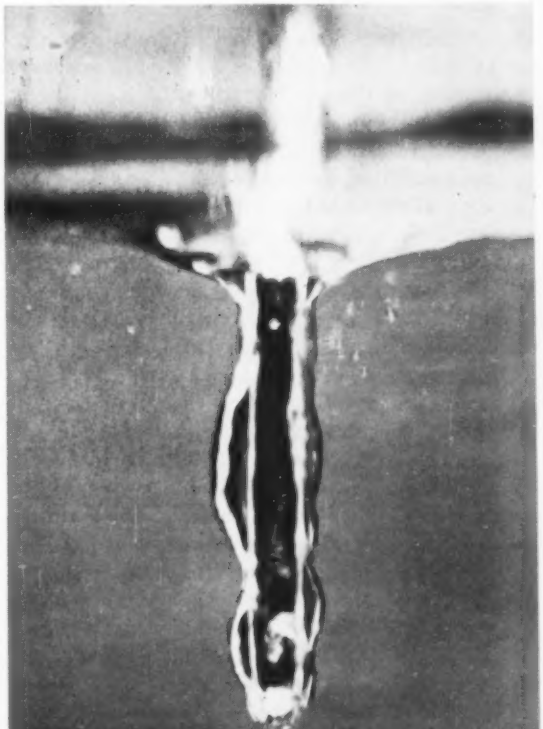

FIG. 12. "Aqueous cathode-effect" with platinum-wire cathode. 1*N* H_2SO_4 at 40° C, 70 volts, 1.0 amperes, about 8×.

the volt-ampere characteristics for the platinum cathode and Fig. 12 is a photograph of aqueous "cathode-effect." The cathode emits a bright blue glow, characteristic of hydrogen emission, if the voltage is raised to 110 volts.

With cathodes, however, there is yet another phenomenon that takes place. If the solution contains sodium sulfate, or if sodium hydroxide is used as the electrolyte, the "cathode effect" is not obtained. Instead, the cathode surface is covered with a multitude of what appear to be spark discharges (blue color), no wide vapor film develops, and the sur-

face of the cathode remains at 100°C or slightly lower. Apparently some kind of film does form around the cathode because the meniscus at the electrolyte surface dips down, just as during the "cathode effect" or anode effect. However, the wide vapor-envelope which can be clearly seen during the true "cathode effect" is absent in this case. The explanation of this phenomenon lies out of the scope of this paper, but the writer feels that a different mechanism of electric conduction between electrolyte and the electrode surface is probably responsible for this phenomenon.

Relation Between Anode Effect in Aqueous and Molten Electrolysis

The writer does not claim that the explanations found valid for aqueous anode-effect are necessarily valid for anode effect in molten media. In particular, the chain of events which leads to molten anode-effect is very likely different. In molten media with a graphite anode, the electrolyte usually has a high contact-angle against graphite (7, 8). On the other hand, platinum and the alloy steel used in this paper are completely wet (have 0° contact angle) by the electrolyte used. The non-wettability of the graphite anode by the molten media may contribute to the incidence of anode effect by making it possible for gas bubbles to adhere strongly to the anode. Moreover, the high temperatures found in molten electrolysis undoubtably have some effect upon the ease with which the gas film can ionize and thus conduct current.

The writer does feel, however, that the concept of the gaseous envelope stabilized by the vaporization of the electrolyte close to the surface of a hot anode should be closely investigated for molten anode-effect. The explanations for the stability of the gaseous envelope to be found in the literature all center about a *gaseous film*—one stabilized by a rush of noncondensable gases (O_2, CO, CO_2) (9). There are at least two considerations that make such an explanation untenable. In the first place, in a laboratory cell, when the anode effect starts, the current will usually drop to $\frac{1}{5}$ or $\frac{1}{10}$ of its previous value. This means that during anode effect only $\frac{1}{5}$ or $\frac{1}{10}$ as much gas is being evolved as before anode effect. Thus, one is forced to explain how a small amount of gas will cause a gaseous envelope to form, where five or ten times that amount of gas was unable to do so. Second, it is not hard to show by means of hydrodynamics that the velocity of gas required to hold back the electrolyte from the anode, at any reasonable depth in the electrolyte, is very large and far more than one could obtain from molten electrolysis.

The writer is planning a future paper which will attempt to apply the vapor-film theory of aqueous anode-effect to anode effect in molten electrolysis. At this time, however, it can be pointed out that it is entirely possible that the electrolyte in the Hall aluminum cell could vaporize if in contact with a hot anode. Waddington and Pearson (10) have recently pointed out that the current carriers in cryolite are Na^+ and possibly $AlF_6^{\equiv}$. The transference of these ions will result in an anode layer of electrolyte which is impoverished in NaF and rich in AlF_3. AlF_3 is a relatively unstable compound and volatilizes with decomposition around 1000 to 1100° C (11). Thus, the anode may be surrounded with an electrolyte which can volatilize at a temperature about 100°C higher than the operating temperature of the cell (1000°C), and it is possible that a vapor film could be formed if the anode became overheated.

Conclusions

1. A phenomenon which occurs when electrodes which evolve gas in aqueous media are operated at high current densities has been described and named "aqueous anode-effect" because of its similarity to anode effect in molten electrolysis.

2. Normal operation of the anode was found to cease when the electrode temperature reached the boiling point of the electrolyte. Under these conditions, the anode enters a so-called "transition period" where vaporization of the bubble walls leads to an increased electrical resistance at the anode and the current through the cell falls as the voltage is increased.

3. The "transition period" behavior instantaneously changes to the "aqeueous anode-effect" when the voltage is raised to a critical value that will permit conduction through the gas phase.

4. The gaseous envelope which encloses the anode during "aqueous anode-effect" is maintained by the vaporization of the electrolyte close to the surface of the anode, which surface was found to be at a temperature far above the boiling point of the electrolyte.

5. It was also shown that an "aqueous cathode-effect," entirely similar to the anode effect, could be obtained.

6. The relation between "aqueous anode-effect" and anode effect in molten media was discussed and it was pointed out that there is a possibility that the anode-effect film in molten media is also stabilized by vaporization of the electrolyte.

Acknowledgements

The writer is indebted to Professors M. D. Hassialis, T. A. Read, and A. F. Taggart for helpful criticisms and suggestions. Mr. M. A. Kaci, Asso-

ciate in Metallurgy, aided with much of the experimental work.

Any discussion of this paper will appear in a Discussion Section, to be published in the December 1950 issue of the JOURNAL.

REFERENCES

1. C. S. TAYLOR, *Trans. Electrochem. Soc.*, **47**, 301 (1925).
2. G. OESTERHELD AND E. BRUNER, *Z. Electrochem.*, **22**, 38 (1916).
3. K. ARNDT AND H. PROBST, *Z. Electrochem.*, **29**, 323 (1923).
4. H. WARTENBERG, E. MANTHEY, AND W. CONZELMANN, *Z. Electrochem.*, **32**, 330 (1926).
5. J. GUBKIN, *Ann. Physik*, **32**, 114 (1887).
6. A. KLEMENC AND H. F. HOHN, *Z. physik. Chem.*, **154A**, 385 (1931).
7. H. V. WARTENBERG, *Z. Electrochem.*, **41**, 448 (1935).
8. H. H. KELLOGG AND K. K. BHASIN, Unpublished Research.
9. J. D. EDWARDS, F. C. FRARY, AND Z. JEFFRIES, "Aluminum and its Production," pp. 310-312, McGraw-Hill Book Co., Inc., New York (1930).
10. T. G. PEARSON AND J. WADDINGTON, *Discussion Faraday Soc.*, **1**, 307 (1947).
11. E. BAUD, *Ann. chim. et. phys.* Series 8, **1**, 60 (1904).

Conditioning Aluminum Alloys for Electroplating[1]

FRED KELLER AND WALTER G. ZELLEY

Aluminum Research Laboratories, Aluminum Company of America, New Kensington, Pennsylvania

ABSTRACT

Successful use of the zinc immersion process for plating aluminum alloys is dependent on the effectiveness of the surface conditioning treatments used prior to the immersion zinc dip. Various conditioning treatments are described for removing constituents that may cause difficulty during plating and for obtaining a uniform and active surface for deposition of the zinc layer. The manner in which the conditioning treatments and variations in the zinc immersion layer may affect the performance of plated aluminum alloys is described.

Of the many processes that have been developed for electroplating aluminum alloys, the zinc-immersion method is considered to be one of the most practical and economical processes for commercial application. Furthermore, it can be employed for plating all of the different aluminum alloys with various other metals. Successful use of this method, however, is dependent to a large degree on the type and effectiveness of the cleaning and conditioning treatments that are used for the various aluminum alloys (1).

Ordinarily, aluminum alloys do not respond to the cleaning and etching treatments usually employed for other metals; thus, the conditioning treatments that are required are different from those commonly employed in plating shops and may be somewhat more important. The objective of this paper, therefore, is to describe the various conditioning treatments that are required for different aluminum alloys and to show how variations in the zinc-immersion layer affect the performance of electroplated samples.

From the metallurgical viewpoint, many different types of aluminum alloys are used for producing various cast and wrought products. Because of this fact, it has been difficult to find conditioning treatments that would give equally satisfactory results for all types and tempers of aluminum alloys. In addition to the metallurgical differences which may affect response to conditioning treatments, all aluminum products have an ever-present natural oxide film. This film can be removed by acid and alkaline treatments, but after rinsing the surface will still have an oxide film which reformed during the treatment. For best results with the zinc immersion process, this new film should be thinner and more uniform and provide a more active surface for deposition of the zinc layer.

[1] Manuscript received October 11, 1949. This paper prepared for delivery before the Chicago Meeting, October 12 to 15, 1949.

THE ZINC IMMERSION PROCESS

Aluminum alloys, because they are less noble than most of the common metals, will readily replace many other metals from solutions of their salts. This forms a basis for the use of the zinc immersion process in the electroplating of aluminum alloys (6) (7). In principle, the alkaline zincate solution that is used to obtain an immersion coating of zinc dissolves the surface oxide film and some of the underlying aluminum and replaces the latter with an equivalent amount of metallic zinc. The thin and adherent layer of zinc provides a surface on which many other metals can be electrodeposited readily.

For the immersion treatment (1), a highly alkaline solution containing the following is used at room temperature:

Sodium hydroxide (NaOH)	500 grams
Zinc oxide (ZnO)	100 grams
Water to make	1 liter
Immersion time (at 60°–80°F) (15–27°C)	1 minute

Since the thickness, continuity, and compactness of the immersion deposit appear to be dependent on the conditioning treatments that are used, the operating conditions for the zinc immersion treatment, and on the type of alloy and product, the effects of these variables are of considerable interest. Failure to recognize the importance of some of these factors may have been responsible in part for the inconsistent and unsatisfactory results that have been experienced in the plating of aluminum alloys.

CLEANING AND CONDITIONING TREATMENTS

To obtain good results with the zinc immersion process for plating aluminum alloys, it is essential that the various cleaning and conditioning treatments provide a clean and more uniformly active surface for the deposition of the zinc layer. First, the surface should be free of any oil or grease. For re-

moving oil or grease, vapor degreasing or solvent cleaning may be necessary. Usually, a mild alkaline cleaner can be used. One can be made conveniently by using 3 per cent each of sodium carbonate and trisodium phosphate. This solution should be used at a temperature of 140°–180°F (60°–82°C) for 1 to 3 minutes.

After appropriate cleaning, further conditioning of the surface is generally required. For the conditioning to be most effective, it must accomplish two things: (*a*) remove the original surface oxide film and replace it with a thinner and more uniform oxide film, and (*b*) remove any microconstituent which may interfere with the formation of a continuous zinc layer or which may react with subsequent plating solutions.

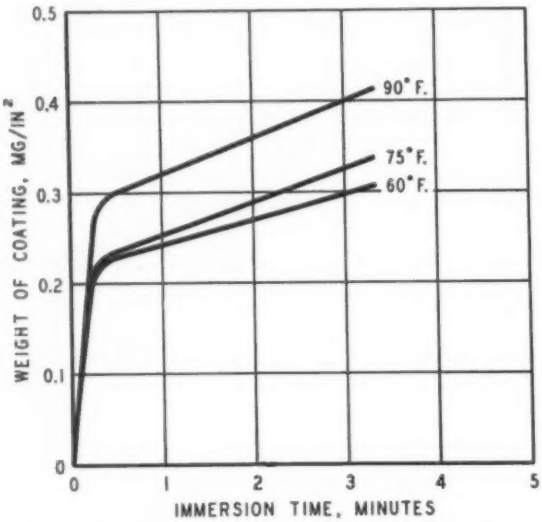

FIG. 1. Effect of temperature of the zincate solution on the weight of coating deposited on 2S alloy sheet during different immersion periods.

One of the more effective treatments for removing the surface oxide film and any undesirable microconstituents comprises using a hot acid etch containing 25 per cent sulfuric acid (by weight) for about 5 minutes at a temperature of 180°F (82°C) (1). This treatment has been found satisfactory for all wrought and most cast aluminum alloys. It not only leaves the surface in an excellent condition for the formation of the immersion zinc layer, but it also eliminates the undesirable effects of the magnesium-containing constituents in alloys of the 52S, 61S, and 63S types.

For wrought alloys of the 2S and 3S types, fairly good conditioning may be obtained by employing the carbonate-phosphate etch, followed by a treatment in a 1:1 nitric acid solution. These alloys do not contain interfering constituents, and the use of the hot sulfuric acid treatment is not essential.

Another conditioning treatment which has considerable merit consists of a double zinc-immersion treatment with the first zinc layer being removed by a dip in 1:1 nitric acid. This treatment has been described by Korpiun (2), Armstrong (3), and Ehrhardt and Guthrie (4). It has been found to be very effective for use with many cast alloys and with wrought alloys which do not contain appreciable amounts of magnesium. With this procedure, the first immersion dip removes the original surface oxide and

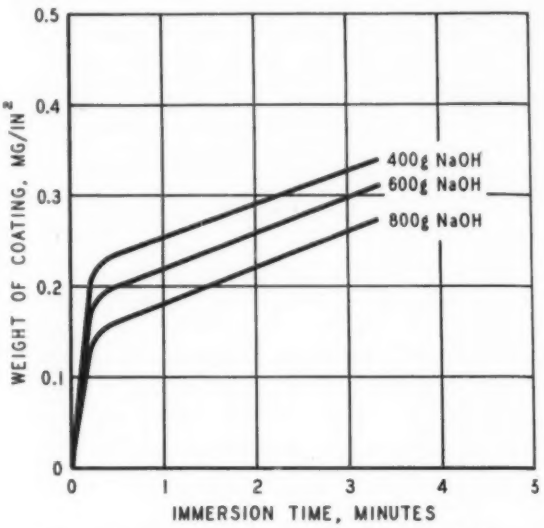

FIG. 2. Effect of concentration of the zincate solution on the weight of deposit formed on 2S alloy sheet at a temperature of 70°F. The weights shown refer to concentration in g/l.

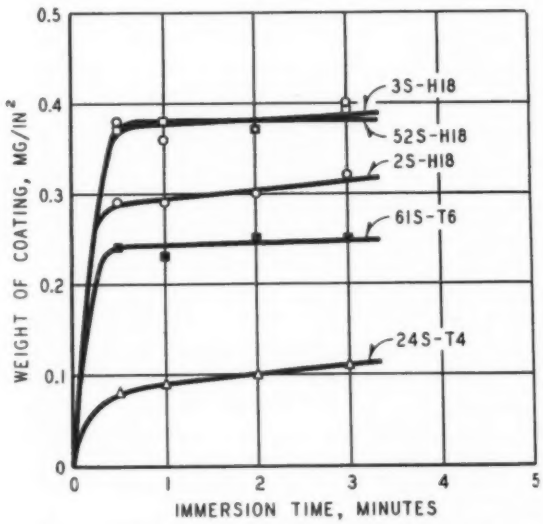

FIG. 3. Weight of zinc immersion coating obtained on different wrought alloys when the same conditioning treatment was used.

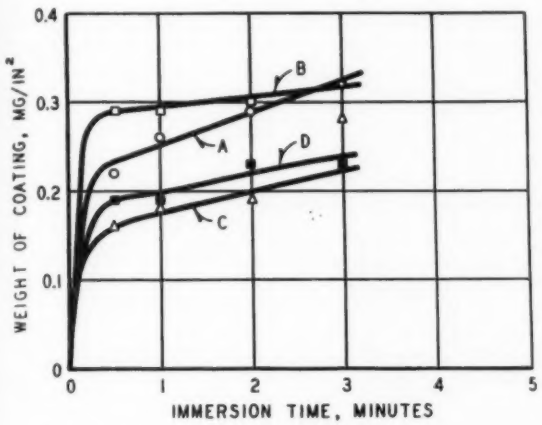

FIG. 4. Effect of different conditioning treatments on the weight of zinc immersion coating on 2S alloy. Treatment "A"—carbonate-phosphate cleaner + zinc dip; "B"—same cleaner + 25% sulfuric acid etch + zinc dip; "C"—same cleaner + double zinc dip; "D"—Alcoa R5 Bright Dip + zinc dip.

Dip.[2] For this treatment, a hot mixture of commercially available acids is used. This treatment is very effective in removing the surface oxide film and in leaving a smooth, bright, and uniformly active surface. It is especially useful in obtaining very thin and uniform zinc immersion deposits and compares favorably, in this respect, with the double zinc immersion treatment.

CONTROL OF IMMERSION TREATMENT

To get smooth, uniform, and adherent zinc coatings, the temperature of the solution should be maintained in the range from 60° to 80°F (15°–27°C). The character of the coating is influenced by the rate of replacement, and, when the rate of deposition is too rapid, the coatings tend to be heavier and less satisfactory from the plating standpoint. The effects of temperature of the zincate solution are illustrated by Fig. 1. The sodium hydroxide content of the solution is also a factor in the formation of the immersion coating as shown by Fig. 2.

TABLE I. *Treatments to obtain different thicknesses of zinc on 2S, 3S, and 24S alloys*

Sample number	Alloy and temper	Conditioning treatments	Zinc immersion treatment	Weight of deposit Mg/in² (mg/dm²)	Calculated thickness of deposit mil (mm)
1	2S-H16	(a) 1 min carbonate-phosphate etch (b) 1 min zinc immersion dip (c) Strip in 1:1 nitric acid	1 min at 74°F (23.3°C)	0.10 (1.5)	0.0008 (0.00002)
2	2S-H16	(a) 1 min carbonate-phosphate etch (b) ½ min dip in 1:1 nitric acid	½ min at 76°F (24.4°C)	0.23 (3.5)	0.0019 (0.00005)
3	2S-H16	(a) 1 min carbonate-phosphate etch (b) ½ min dip in 1:1 nitric acid	3 min at 76°F (24.4°C)	0.39 (6.0)	0.0033 (0.00008)
4	3S-H16	(a) 1 min carbonate-phosphate etch (b) 1 min zinc immersion dip (c) Strip in 1:1 nitric acid	1 min at 78°F (25.5°C)	0.14 (2.2)	0.0012 (0.00003)
5	3S-H16	(a) 1 min carbonate-phosphate etch (b) ½ min dip in 1:1 nitric acid	1 min at 76°F (24.4°C)	0.34 (5.2)	0.0029 (0.00007)
6	3S-H16	(a) 1 min carbonate-phosphate etch (b) ½ min dip in 1:1 nitric acid	3 min at 76°F (24.4°C)	0.48 (7.4)	0.0041 (0.0001)
7	24S-T4	(a) 1 min carbonate-phosphate etch (b) 5 min in 25% sulfuric acid (175°F)(80°C) (c) ½ min in 1:1 nitric acid	1 min at 75°F (23.9°C)	0.09 (1.4)	0.0007 (0.00002)
8	24S-T4	(a) 1 min carbonate-phosphate etch (b) 5 min in 25% sulfuric acid (175°F)(80°C) (c) ½ min in 1:1 nitric acid	3 min at 90°F (32.2°C)	0.12 (1.8)	0.0011 (0.00003)

replaces it with a zinc layer. Removal of the zinc layer by the nitric acid dip leaves the surface in a very satisfactory condition for deposition of the final zinc immersion coating.

A new treatment which will satisfactorily condition the surface of many aluminum alloys for the zinc immersion treatment is the Alcoa R5 Bright

Thinner and more uniform deposits are obtained from solutions having the higher percentages of sodium hydroxide. Since the zincate solution is very viscous, losses are due mainly to "drag-out." This is advantageous, as it limits the accumulation of impurities resulting from solution of the aluminum

[2] Process licensed by Aluminum Company of America.

during treatment. The specific gravity of this solution should be checked occasionally and any losses should be made up by adding more of the components. From the data shown in Fig. 1 and 2, it is evident that most of the deposition takes place during the very first part of the immersion period. Thus, an immersion period of 30 seconds to 1 minute is adequate in all cases.

The type and temper of aluminum alloy have been mentioned as factors influencing the weight and other characteristics of the immersion coating (1). The manner in which the weight of coating will differ on several wrought aluminum alloys treated by the same procedure is illustrated by Fig. 3. On these samples, the weight of deposit with a 1 minute immersion treatment ranged from about 0.1 to 0.4 mg/in.^{2} (1.5 to 6.2 mg/dm^2) depending on the alloy. Our previous experience with electroplated alloys of these types has indicated that alloys which had the thinner zinc immersion coatings before plating resisted corrosive conditions better than those plated in the same manner, but which had heavier immersion coatings.

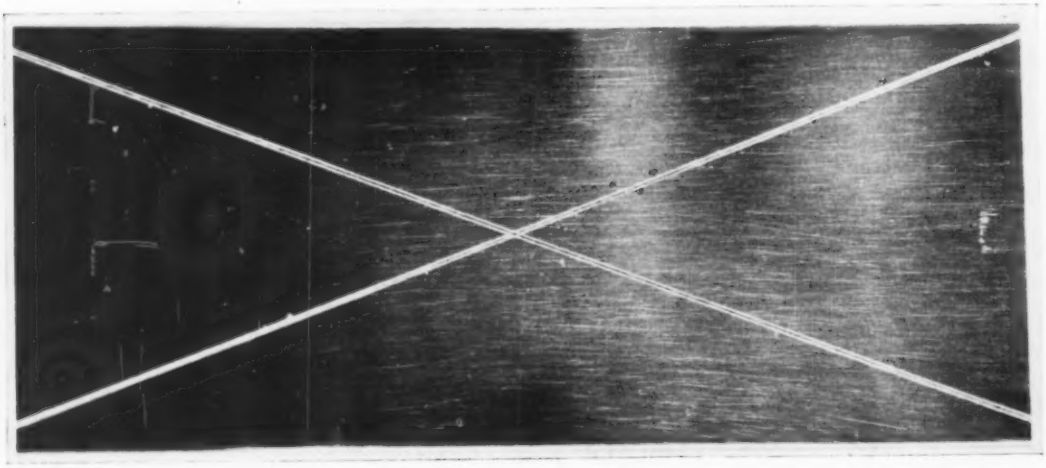

FIG. 5. Grooved-type of test specimen used for evaluation of plated samples by salt spray and atmospheric exposure Grooves are machined through the plating as shown by Fig. 6.

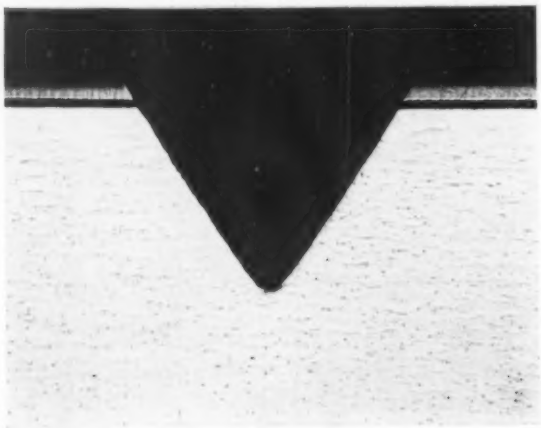

FIG. 6. A cross section through the machined grooves in the above plated test specimen, showing the extent to which the underlying aluminum alloy is exposed.

The weight of coating also is significantly affected by the conditioning treatments used prior to the immersion treatment. The effects, for example, of the four conditioning treatments described previously in this paper are shown by Fig. 4. In this case, the treatments were employed for conditioning 2S-H16 alloy sheet. When the double zinc immersion treatment or the Alcoa R5 Bright Dip is used, appreciably lower weights of zinc coating are obtained, and samples prepared in this manner have exhibited excellent resistance to corrosion after electroplating.

In view of the various factors that may influence the weight and other characteristics of the zinc immersion coating and of the fact that samples with the thinner zinc immersion coatings may be more satisfactory for electroplating, further investigation of the effect of the thickness of the immersion zinc coating on the behavior of electroplated aluminum samples was undertaken.

Effect of Thickness of Immersion Coating

For this investigation, samples of aluminum alloys 2S-H16, 3S-H16, and 24S-T4 were prepared by different conditioning and immersion procedures to obtain different amounts of zinc deposit. The procedures that were employed for the three alloys are listed in Table I. After the zinc immersion coating was applied, all of the samples were electroplated by

the following procedures: (*a*) plated in a Rochelle-type copper cyanide solution to obtain a copper plate about 0.2 mil (0.005 mm) thick; (*b*) plated in a Watts'-type nickel bath to obtain a plate 1.5 mils (0.04 mm) in thickness; (*c*) plated in a standard chromium bath to obtain a final plate from 0.01 to 0.02 mil (0.00025 to 0.0005 mm) in thickness.

satisfactory for rapidly evaluating electroplated coatings on aluminum alloys in both salt spray and atmospheric exposure tests. The test samples are 6 in. x $2\frac{1}{2}$ in. (15 x 6.3 cm) in size and, after plating, are grooved as shown by Fig. 5 by machining two grooves about $\frac{1}{32}$ in. (0.8 mm) deep with a V-shaped threading tool in such a manner as to form an X-

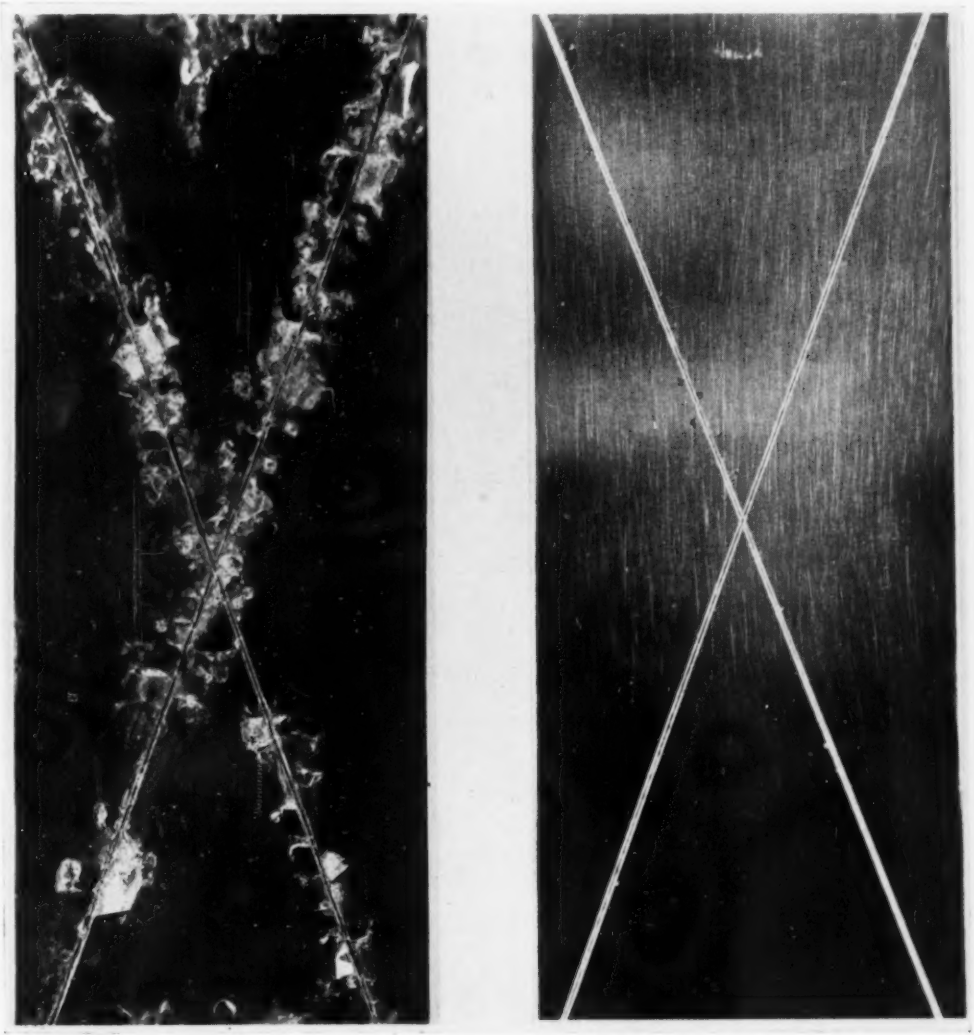

FIG. 7. Two of the grooved-type test specimens of plated 24S-T4 sheet after a 300-hour salt spray test. These samples were prepared by different conditioning and plating practices. On the one sample, considerable blistering and lifting of the plating occurred along the grooves; on the other, little change took place.

TYPE OF SAMPLE

In order to obtain a rapid evaluation of the samples of the various aluminum alloys conditioned for plating by the different procedures, a grooved-type of sample suggested by C. E. Heussner of the Chrysler Corporation and described in a recent paper (1) was used. Samples of this type have been found very

pattern. These machined grooves extend through the plating and expose a portion of the underlying aluminum alloys as illustrated by Fig. 6. Machining of the grooves provides an incidental check on the adhesion of the plated coatings as lifting of the plating at points of intersection and along the sides of the grooves will occur on samples having poor adhesion.

When specimens of this type are exposed to salt spray or to the atmosphere, plating that is inadequate or that has not been satisfactorily applied will soon develop blisters and will lift along the grooves as shown by Fig. 7. In this photograph, two samples of plated 24S-T4 sheet are shown after a 300-hour salt spray test. These samples had the same thickness

this corrosion test is shown by Fig. 8 to 10, inclusive. On this group of samples, the weight of zinc deposits ranged from about 0.1 to 0.5 mg/in.^{2} (1.5 to 7.7 mg/dm^2). Assuming that these coatings were metallic zinc, the zinc deposit would range from about 0.0008 to 0.004 mil (0.00002 to 0.0001 mm) in thickness.

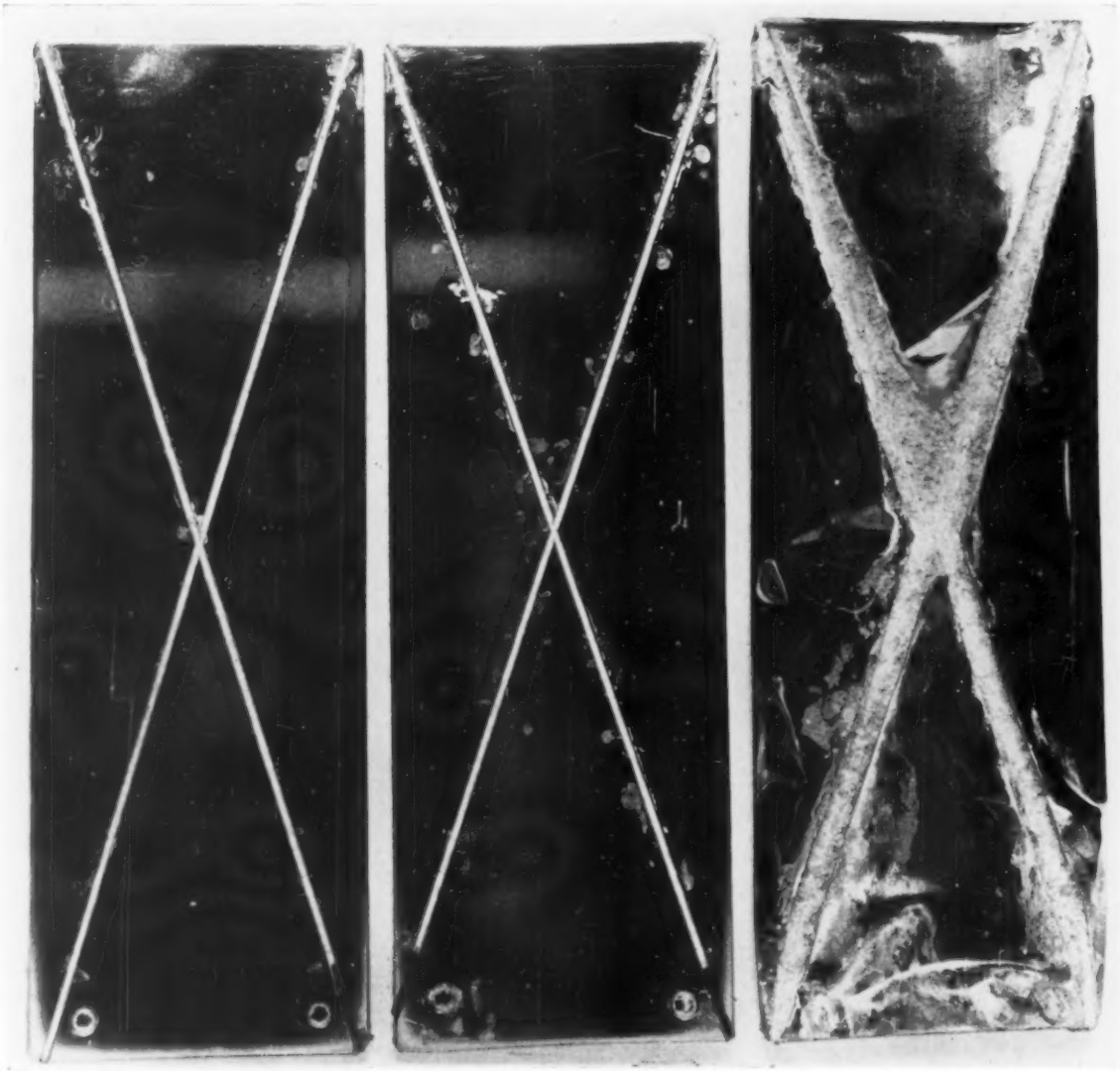

Sample 1. 0.10 mg/in.^{2} (1.5 mg/dm^2) Sample 2. 0.23 mg/in.^{2} (3.5 mg/dm^2) Sample 3. 0.39 mg/in.^{2} (6.0 mg/dm^2)

FIG. 8. Influence of amount of zinc immersion coating on the behavior of plated 2S-H16 alloy sheet samples in a 300-hour salt spray test. The plating was the same on all samples, but the amount of zinc deposit differed as indicated.

of plating, but were prepared by different conditioning and plating practices.

To evaluate the effect of various thicknesses of zinc immersion deposit on the behavior of the plated samples described in Table I under corrosive conditions, these samples were subjected to a 300-hour salt spray test. The appearance of the samples after

RESULTS OF CORROSION TESTS

The results from this corrosion test are very interesting since they indicate rather definitely that the samples having the thinner zinc deposits withstood the 300-hour salt spray test without developing appreciable blistering or lifting of the plating or appreciable corrosive attack at the interface, whereas

those with the heavier zinc deposits showed considerable blistering and lifting of the plating and severe corrosive attack on the underlying aluminum alloy base. The behavior in relation to the thickness of the zinc layer appears to be consistent for the several different alloys included in this test, although it would appear that the thickness of the zinc coating alloy, however, the weight of zinc deposit obtained with the normal immersion treatment is of the order of 0.1 mg/in.^{2} (1.5 mg/dm^2), and it is difficult to obtain a heavier immersion layer on this alloy. To obtain the heavier zinc layer on the sample illustrated, an immersion treatment of 3 minutes at 90°F (32°C) had to be used.

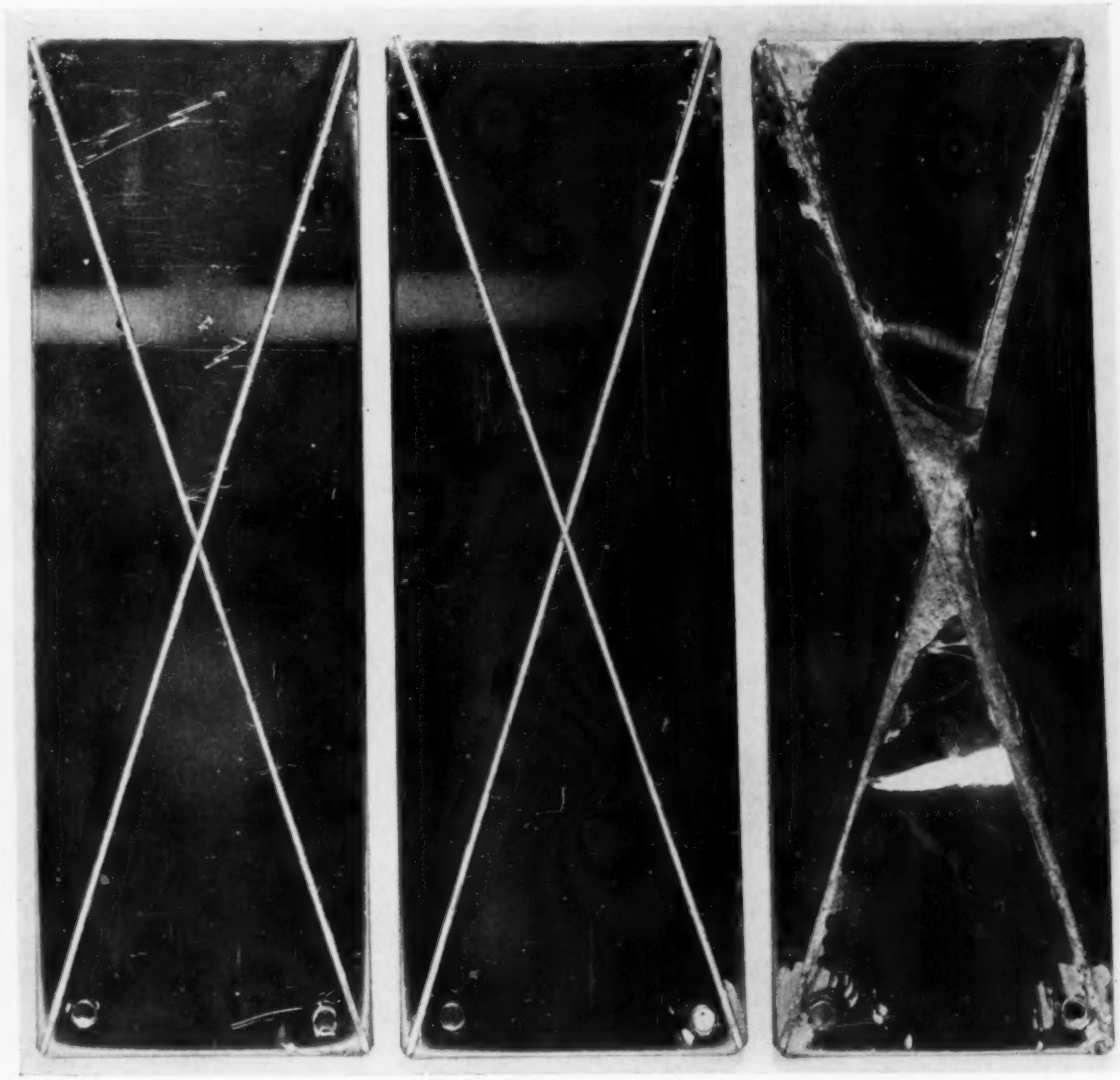

Sample 4. 0.14 mg/in.^{2} (2.2 mg/dm^2) Sample 5. 0.34 mg/in.^{2} (5.2 mg/dm^2) Sample 6. 0.48 mg/in.^{2} (7.4 mg/dm^2)

FIG. 9. Effect of the amount of immersion zinc coating on the behavior of plated 3S-H16 alloy sheet samples in a 300-hour salt spray test. The weight of zinc deposit on each sample is indicated.

which will give similar results will probably vary with the alloy and temper of the base metal. This is illustrated by the samples of plated 24S-T4 sheet shown in Fig. 10. Here the weight of zinc coating varied from 0.09 to 0.12 mg/in.^{2} (1.4 to 1.8 mg/dm^2), yet the corrosion test showed an appreciable difference in the behavior of the two samples. On 24S-T4

PLATING ALUMINUM ALLOYS

After a satisfactory zinc immersion layer has been formed on an aluminum alloy article, silver, brass, zinc, nickel, or chromium may be deposited directly on the zinc layer provided that the plating procedures are suitable for plating on zinc and do not penetrate the zinc layer or cause attack on the underlying

aluminum alloy (5). Usually, however, a copper strike is applied over the zinc immersion layer before other metals are deposited. For many decorative applications, the copper strike is followed by a 0.5 to 1.5 mil (0.013 to 0.038 mm) nickel plate and a 0.01 to 0.02 mil (0.00025 to 0.0005 mm) chromium plate. Aluminum alloys plated with this system have been exposed for as long as 800 hours in a salt spray test and for more than 1 year in the atmosphere without showing any lifting or blistering of the plated coatings or significant corrosion on the aluminum alloy exposed by grooving the samples.

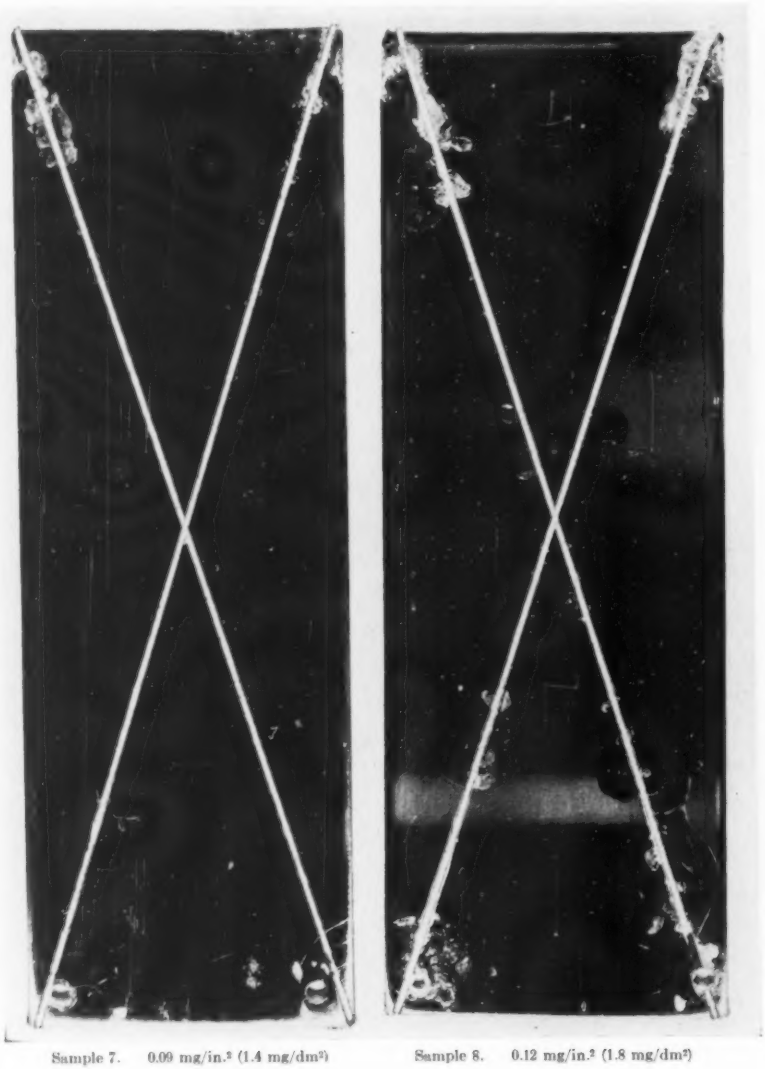

Sample 7. 0.09 mg/in.^{2} (1.4 mg/dm^2) Sample 8. 0.12 mg/in.^{2} (1.8 mg/dm^2)

FIG. 10. Effect of two different weights of immersion zinc coating on the behavior of plated 24S-T4 samples in a 300-hour salt spray test.

Owing to its position in the electromotive series, aluminum will in some degree electrolytically protect all of the usual plated coatings except zinc or cadmium. Thus, it is to be expected that, with most combinations of metals employed for electroplating aluminum alloys, some galvanic action will occur between exposed aluminum and the plated coatings with the aluminum being the sacrificial metal. It would be desirable, for example, to plate nickel directly on aluminum without first applying intermediate coatings of zinc or copper. Although this can be done, direct plating methods are not as practical or economical as the zinc immersion method. Furthermore, by the use of proper conditioning procedures and control of the thickness and character of the zinc deposit, it is possible to obtain decorative and protective electroplated finishes on most wrought and cast aluminum alloys which should meet the ordinary service conditions to which many plated articles will be subjected.

Because of the large electrolytic potential between aluminum alloys and nickel, a nickel electroplate on aluminum should be of good quality and of sufficient thickness and soundness to provide adequate cover-

age for any given application. For applications where resistance to corrosion is not a significant factor, a nickel plate about 0.5 mil (0.013 mm) thick will be satisfactory. Where mechanical damage or moderately severe corrosive conditions may be encountered, the nickel plate should be from 1.5 to 2.0 mils (0.038 to 0.050 mm) in thickness. Ordinarily, nickel plating by itself is not recommended as a protective finish for aluminum alloys where even moderately corrosive conditions may be encountered. The application of a final chromium plate 0.01 to 0.02 mil (0.00025 to 0.0005 mm) in thickness will passivate the surface and extend the service life to a much greater extent than would be expected from a thin plate of this order of thickness.

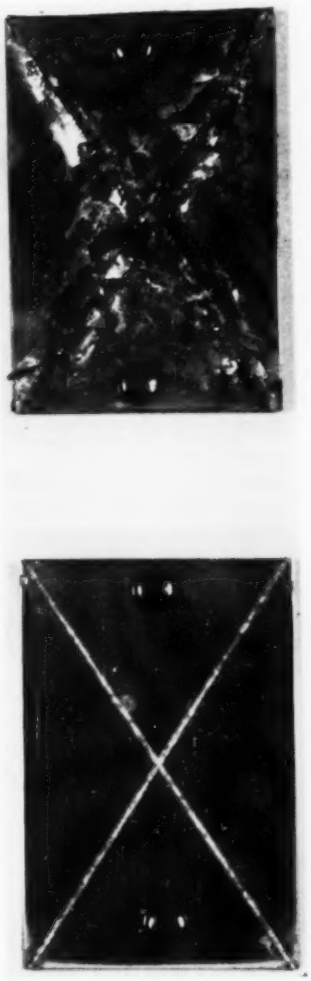

FIG. 11. Effectiveness of thin chromium plate in reducing galvanic action at grooves in plated samples of 14S-T6 alloy sheet exposed 350 hours in salt spray test. Both samples were plated by the same procedure. Sample (a), however, did not have a final chromium plate; sample (b) had a 0.01-0.02 mil (0.00025 to 0.0005 mm) coating of chromium.

The amount of galvanic attack that will occur when any underlying aluminum is exposed on a plated aluminum sample will be dependent not only on the potential between the aluminum and the plated coatings, but also on the amount of current that flows in the galvanic cell which is formed when an electrolyte is present. The amount of current flow is probably the more important factor and is influenced by many variables.

The very thin chromium layer ordinarily applied for appearance greatly reduces the amount of current flowing from any exposed aluminum areas on plated samples. The beneficial effect of the thin chromium plating over nickel is illustrated by the two grooved samples shown in Fig. 11.

SUMMARY

The various conditioning treatments employed for the different aluminum alloys have a significant influence on the quality and performance of electroplates on these alloys. These treatments affect the weight of zinc deposit obtained in the immersion step. Control of the temperature of the zincate solution and the duration of the immersion treatment are important factors also in obtaining thin and uniform zinc deposits.

By corrosion tests on grooved electroplated samples, the important influence of the thickness of the zinc immersion layer is demonstrated. With the thinner zinc coatings the performance of plated aluminum samples is greatly superior to that obtained from samples where the plating was applied over the heavier immersion coatings.

By employing suitable conditioning and immersion procedures, it has been possible to finish various wrought aluminum alloys by plating with a copper-nickel-chromium system which should satisfactorily withstand the service conditions ordinarily encountered by most electroplated articles.

Any discussion of this paper will appear in a Discussion Section, to be published in the December 1950 issue of the JOURNAL.

REFERENCES

1. F. KELLER AND W. G. ZELLEY, "Proc. 36th Annual Convention, Am. Electroplaters' Soc., 1949."
2. J. KORPIUN, U. S. Pat. 2,142,564, Jan. 3, 1939.
3. E. ARMSTRONG, *Metal Treatment*, **6**, 153 (1940).
4. R. A. EHRHARDT AND J. N. GUTHRIE, *Monthly Rev. Am. Electroplaters' Soc.*, **34**, 421 (1947).
5. W. R. MEYER, *Monthly Rev. Am. Electroplaters' Soc.*, **33**, 269 (1946).
6. E. H. HEWITSON (To Eastman Kodak Co.) U. S. Pat. 1,627,900, May 10, 1927.
7. H. BENGSTON, *Trans. Electrochem. Soc.*, **88**, 307 (1945).

An X-Ray Method for Determining Tin Coating Thickness on Steel[1]

H. F. Beeghly

Division of Metallurgical Research, Jones & Laughlin Steel Corporation, Pittsburgh, Pennsylvania

ABSTRACT

The thickness of tin coatings on steel can be measured rapidly and nondestructively on either side of the sheet by application of a simple x-ray technique. The method is based on the selection of an x-ray beam of a wavelength that excites significant amounts of secondary radiation in the base metal but not in the coating. With this method, results were obtained that are comparable in accuracy and reproducibility to those obtained with the usual chemical methods for measuring the coating thickness of tin on steel.

The investigation placed emphasis on use of a commercial x-ray spectrometer for measurement of tin coating thickness on a laboratory scale, but enough work was done to show that the principle used for measuring tin coating weights on steel is applicable to other coatings and to the continuous indication and control of tin coating weights on the electrotinning line. Such a unit has been designed and built.

Introduction

The measurement and control of tin coating thickness during application is of great economic importance. The commonly used methods for measurement of tin coating weight are based on volumetric determination of the tin after solution of the tin plate or after stripping the tin coating. These methods are destructive and have other limitations which restrict their value, especially for use on thin electrodeposited coatings. At best, they give a picture only of the average amount of tin on both sides of a given area of the sheet.

The various common methods for measuring coating weights of tin were compared by McKenzie (1) who recommended the determination of the loss in weight resulting from stripping the tin with hydrochloric acid inhibited with antimony chloride as being the most dependable. These methods are of no value to operating personnel in controlling deposition of the tin.

Measurement of coating weight by x-ray diffraction methods was investigated by Friedman and Birks (2) who compared the intensities of selected x-ray lines diffracted by the uncoated base metal with the intensities of these same lines after the coating was applied. Gray (3) and Eisenstein (4) also studied the measurement of coating thickness by x-ray diffraction methods in which they compared the intensities of diffraction lines from the surface and base materials and expressed the ratio of line intensities of the two materials as a function of coating weight. These methods utilized the diffracted primary x-ray beam and the relation between the ratio of line intensities and coating weight was found to conform to the well-known absorption equation (I):

$$I = I_o e^{-\frac{\mu}{\rho} \times \chi} \qquad \text{(I)}$$

in which I_o is the intensity of the initial (incident) radiation; I the transmitted intensity; $\frac{\mu}{\rho}$ = the mass absorption coefficient, and χ = the transmitted thickness of the absorber. These methods did not appear to be suitable for use in controlling application of tin on the electrolytic line.

Thus, although the manufacture of tin plate has been an industrial operation of great economic importance for many years, no method has been available to the operator of the tinning line for determining at the time of application the thickness of tin applied. Some of the data obtained in developing such a nondestructive control method are presented here.

A specimen irradiated by x-rays becomes a secondary source of energy when exposed to radiation less than some critical wavelength. When this happens, the specimen "fluoresces" and the secondary radiation is emitted in all directions as illustrated in Fig. 1. This radiation from the specimen is generally considered objectionable since it raises the background level and tends to obscure the pattern of constituents in the specimen being studied. Therefore, x-ray diffraction workers avoid it by purposely choosing an x-ray target material whose radiation is of a wave-

[1] Manuscript received July 28, 1949. This paper prepared for delivery before the Chicago Meeting, October 12 to 15, 1949.

length that will not produce "fluorescence" from the given specimen. In the work to be described it was found that this secondary radiation could be used effectively as a source of radiant energy for measuring the thickness of metallic coatings on steel economically and rapidly. The procedure is not subject to some of the limitations imposed by previously described methods utilizing the diffracted x-ray beam.

Fig. 2 shows the x-ray spectrometer manufactured by the North American Philips Company used in developing the fluorescence method. For the problem of thickness measurement an x-ray target is selected which produces an adequate background from the base metal without exciting significant secondary radiation from the coating. A typical curve made for black plate[2] with copper K radiation is shown in the upper portion of Fig. 3. The lower curve in this figure was made from the same sample with iron K radiation. The equipment was adjusted

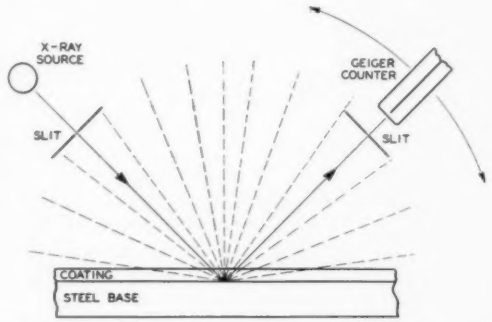

FIG. 1. Schematic arrangement for measuring coating thickness by absorption of fluorescent x-radiation.

without regard to background intensity so that approximately the same peak heights were obtained in each case. A nickel filter was used at the Geiger counter window with the copper target and a manganese filter with the iron target. The background intensity with copper K radiation was approximately three times that obtained with iron K radiation. The fluorescent radiation from the iron base is absorbed in passing through tin in much the same way that light is absorbed in passing through a solution. The insertion of a tin coating should then result in a loss in background intensity that should be in proportion to the thickness of the tin. The intensity of the primary beam striking the base metal would be decreased also with increased thickness of coating and this would increase the rate at which background intensity falls off with increase in coating weight.

It appeared that if a consistent correlation could be established between the intensity of the radiation transmitted through the tin and the tin thickness, a continuous, nondestructive method for controlling the application of tin to steel by the electrolytic process could be devised.

[2] Black plate is the term used in the steel industry to describe the bare steel sheet on which tin is applied to make tin plate.

EXPERIMENTAL METHODS AND RESULTS

The variation in background intensity with tin coating thickness was explored by preparing a series of x-ray curves of black plate, tin, and a series of commercial tin plate specimens with different known coating weights. Copper K radiation was used with a rapid scanning rate (two degrees θ per minute). A nickel filter was used between the specimen and the

FIG. 2. The direct reading x-ray spectrometer

Geiger counter window. The irradiated area of the specimen was $\frac{3}{16}$ in. x $\frac{5}{16}$ in. (4.7 x 8 mm). X-ray curves typical of those obtained are shown in Fig. 4.

For any given angle of reflection (other than those at which a diffraction peak of the base metal or coating occurred) the background intensity decreased with increasing thickness of coating. These exploratory trials indicated that the intensity of the radiation transmitted from the background decreased in a regular way as the thickness of the tin coating increased. The relationship between the intensity and the coating thickness appeared to be independent of the method by which the coating was applied.

X-ray curves similar to the top one in Fig. 4 were made over a period of several days under iden-

tical conditions on a series of steel coupons cut from commercial black plate. Intensity values were tabulated at several angles; the deviation from the mean of eight readings was +2.4, −1.3; +0.6, −0.9; +2.9, −1.7; and +1.0, −1.0 for 2θ values of 82.2°, 76.0°, 44.8°, and 38.0°, respectively. The deviation from the mean of all readings was appreciably less for background (at $2\theta = 38°$ and 76°) than for iron lines (at 44.8° and 82.2°). Values obtained in the same way on tin plate and on commercially pure tin substantiated the reproducibility obtained on bare steel. The background intensity from commercially pure tin was low and did not vary significantly from one sample to another.

than from some function of the diffraction peak intensity has the added advantage of avoiding error from differences in intensity due to preferred orientation. Intensity values at an angle of $2\theta = 76°$ with copper K radiation showed the best correlation with coating weights in these preliminary trials.

The intensity of the transmitted radiation from a series of tin plate coupons selected to give a range of coating weights from approximately 0.5 to 1.5 pounds (0.23–0.67 kg) per base box was measured. Then the coating weights were determined by the usual chemical method. Typical x-ray data obtained at $2\theta = 76°$ and the corresponding coating weights for a typical series of coupons are shown in Table I.

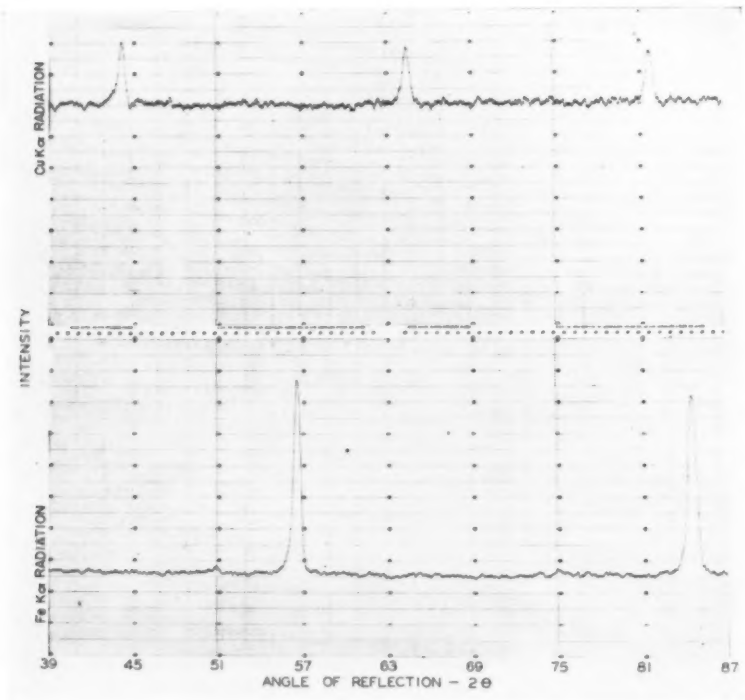

FIG. 3. X-ray curves of steel made with copper and iron K radiation.

Coating weights were correlated with intensity values by plotting some function of the intensity values at a given angle against the coating weight.[3] The empirical relationship so established with tin plate of known coating weight provided a basis for determining the thickness of tin on specimens of unknown coating weight. The actual angle selected for the intensity measurement was not critical provided it was not one at which occurred a diffraction peak from either the coating or base metal. Use of the transmitted energy from the background rather

These may be plotted empirically against the ratio of background intensity of the coated specimens at some given angle to that of bare steel at the same angle to give a working curve for relating background intensity with coating weights. Intensity ratios are shown so that the automatically recorded data can be compared readily with manually recorded data. In practice it is more convenient to plot the instrument reading directly against the coating weight. The correlation of coating weights with both manually recorded and automatically recorded values indicates that either method is capable of a satisfactory degree of accuracy. For routine use in the laboratory it is convenient to set up for manual operation so that a counting error of 1 per cent will

[3] Coating weights in pounds per base box were used. By definition, a base box contains 62,720 square inches (40.4 m²) of surface. This is the unit used by industry in the manufacture and sale of tin plate.

be obtained in a 64-second counting interval. This may be done with the equipment used by irradiating a specimen area sufficiently great to give approximately 6000 counts in 64 seconds from the heaviest coating to be measured. A coating weight then may be determined in approximately 70 seconds. If a large number of determinations is necessary on a particular material, it would be desirable to adjust

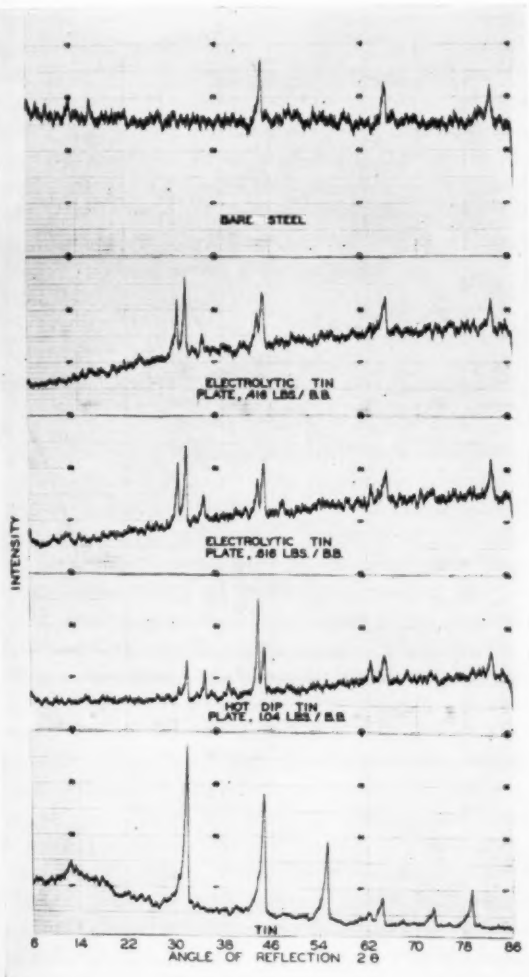
BARE STEEL
ELECTROLYTIC TIN PLATE, .418 LBS./ B.B.
ELECTROLYTIC TIN PLATE, .616 LBS./ B.B.
HOT DIP TIN PLATE, 1.04 LBS./ B.B.
INTENSITY
TIN
6 14 22 30 38 46 54 62 70 78 86
ANGLE OF REFLECTION 2θ

FIG. 4. X-ray curves obtained with copper K radiation

the equipment so an equivalent count will be obtained in 32 (or perhaps 16) seconds.

Fig. 5 shows a calibration curve based on a 64-second count at 76.0° using a nickel filter and an irradiated area of $\frac{3}{16}$ in. x $\frac{5}{16}$ in. (4.7 x 8 mm) and with data recorded manually. Coating weights are measured by placing a specimen in the holder and registering counts over the time interval necessary (from the statistics of the counting circuit) to give the desired counting accuracy under the conditions for which a calibration curve such as this has been established and at a rate that does not exceed the resolving or registering ability of the recording circuit. The intensity (counts per standard time interval) is converted to coating weight by means of the curve.

TABLE I. *Comparison of manually and automatically recorded intensity ratios*

Coating weights lb/BB*	Background intensity ratio at 76°	
	Manual recording	Automatic recording
0.305	0.720	0.755
0.475	0.634	0.662
0.655	0.522	0.555
1.250	0.308	0.344
1.525	0.262	0.283
0.870	0.465	0.462

* Tin plate coating thickness is commonly expressed in pounds per base box. A base box is defined as a number of sheets having an area over both faces of 62,720 square inches. One pound per base box equals approximately 11g/m².

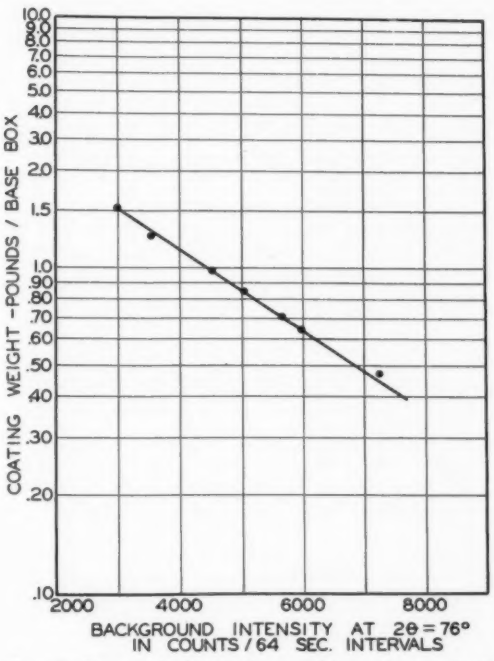

FIG. 5. Curve relating background intensity to tin plate coating weights.

DISCUSSION

Precautions in Use of the Method

Energy is transmitted from the steel base through the coating in a random manner and sufficient counts must be recorded to reduce the probable error from this random fluctuation to the desired value, e.g., if a probable counting error of 1 per cent (exclusive

of experimental error and other errors inherent in the method) is required, about 6000 counts must be taken. Also, a counting rate must be used that does not exceed the resolving power of the counter tube or the registering ability of the recording device. If counting accuracy is the only requirement, a slow counting rate may be used over a relatively long period of time.

TABLE II. *Comparison of coating weights obtained by standard method with those obtained with x-ray method*

Sample	Type	Side	Coating weight (Pounds/base box)	
			std. method	x-ray method
1	Electrolytic	A		0.49
		B		0.54
		avg*	0.52	0.52
2	Electrolytic	A		0.41
		B		0.39
		avg	0.42	0.40
3	Electrolytic	A		0.54
		B		0.51
		avg	0.52	0.525
4	Electrolytic	A		0.50
		B		0.47
		avg	0.50	0.485
5	Electrolytic	A		0.73
		B		0.70
		avg	0.70	0.715
6	Electrolytic	A		0.81
		B		0.83
		avg	0.83	0.82
7	Hot Dip	A		1.21
		B		1.08
		avg	1.03	1.145
8	Hot Dip	A		1.55
		B		1.31
		avg	1.25	1.43

* Values obtained by standard method are true averages. Averages shown for x-ray method are average of two readings one on each side of test coupon and are not necessarily true averages.

In general, it is advisable to use a large angle between the incident primary beam and the coating and between the axis of the counter tube and the coating; thus, errors resulting from surface imperfections are minimized. Small angles may be necessary for coatings that are relatvely transparent to the fluorescent radiation in order to lengthen the path through the coating (note Fig. 1). The calibration curve, once established, is permanent, but intensity readings should be checked regularly with a piece of bare steel since the intensity of the x-ray beam may change as the tube ages. It is convenient to have a set of coupons of tin plate with a range of known coating weights so that a working curve for a new set of conditions can be prepared quickly if needed. The specimen requires no special preparation but should be reasonably clean and flat. Its size may vary within wide limits. Variations in surface condition encountered in the usual commercial grades of tin plate do not affect reliability of results; nor does the method of application, since equally satisfactory values may be obtained on base metal coated by the hot-dip or the electrolytic process. If the coating is not uniform, as is particularly true with hot-dip tin plate, then samples must be selected from different areas and the results averaged in the same manner as when chemical methods are used. The size of the irradiated area may also be increased for such coatings so that a given reading will indicate the average coating weight over a larger area.

Other Applications of the X-Ray Method to Coating Problems

The present method is useful for the routine measurement of coating weights on each surface and for determination of the variation in coating weight from edge to center of sheets. The differences that may be obtained on opposite sides of standard test coupons are shown in Table II. These values were obtained under conditions which gave excellent reproducibility of readings. Thus, the method has been helpful in explaining some of the variations in performance of articles fabricated from coated steel.

The method is not limited to tin on steel, but appears to be generally useful for metal coatings such as lead, silver, or cadmium where the base metal can be made to fluoresce by an x-ray beam which does not produce fluorescence from the coating. Fig. 6 shows curves for three samples of cadmium coated steel. These are typical of the change in diffraction patterns that occurs as the coating weight increases. The background decreases in intensity as the coating weight increases, while the diffraction peaks of the coating increase and those of the base metal decrease. With heavy coatings, little or no evidence of the pattern of the base metal is obtained. Thus, there is an upper limit to the thickness that can be measured by the fluorescence method.

The actual thickness that can be measured is a function of the coating and base metal elements, as well as of the characteristics of the x-ray equipment. The common commercial weights of tin on steel can be handled by the method described. The actual ranges for other coatings or base metals for

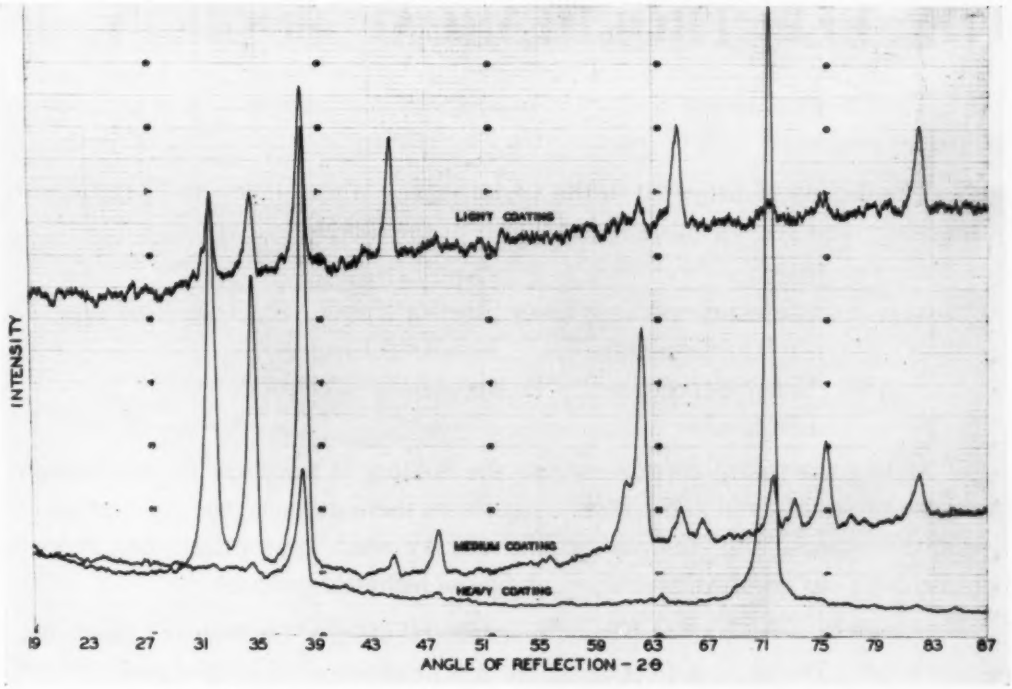
LIGHT COATING
MEDIUM COATING
HEAVY COATING
INTENSITY
19 23 27 31 35 39 43 47 51 55 59 63 67 71 75 79 83 87
ANGLE OF REFLECTION - 2θ

FIG. 6. X-ray curves for cadmium coated steel made with copper K radiation

a given set of requirements can be most conveniently determined by actual trial.

One of the most valuable potential applications of the nondestructive fluorescence method is for the continuous recording and control of the amount of tin coating applied to steel by the electrolytic process. The principle of the method described has been used for such a unit designed and built in the research laboratory specifically for utilization on the mill electrotinning line. It is now in experimental operation.

SUMMARY

An x-ray fluorescence method developed for measuring tin coating weights on steel and for other coatings has been investigated. Applications of this method, including use of the principle for continuously recording and controlling of coatings deposited electrolytically, have been outlined. The accuracy of the method is comparable to that of conventional methods for measuring tin plate coating weights.

ACKNOWLEDGMENTS

The writer acknowledges his appreciation to the management of Jones & Laughlin Steel Corporation for permission to publish these results and to his associates for assistance in the work reported here.

Any discussion of this paper will appear in a Discussion Section, to be published in the December 1950 issue of the JOURNAL.

REFERENCES

1. H. A. MCKENZIE, *J. Soc. Chem. Ind. London*, **66**, 312–319 (1946).
2. H. FRIEDMAN AND L. S. BIRKS, *Rev. Sci. Instruments*, **17**, 99–101 (1946).
3. R. B. GRAY, *Phys. Rev.*, **69**, 49 (1946).
4. A. EISENSTEIN, *J. Applied Phys.*, **17**, 874–8 (1946).

THE ELECTROCHEMICAL SOCIETY, INC.

The Electrochemical Society is an international organization of individuals and companies concerned with or interested in Electrochemistry and allied subjects.

The Society is dedicated to the advancement of the theory and practice of Electrochemistry and related subjects, as shown in the following divisions:

Battery	Electro-Organic
Corrosion	Electrothermic
Electric Insulation	Industrial Electrolytic
Electrodeposition	Theoretical Electrochemistry
Electronics	

Among the means to this end are the holding of meetings for the reading and discussion of professional and scientific papers on these subjects, the publication of such papers, discussions, and communications as may seem appropriate, and cooperation with chemical, electrical, and other scientific and technical societies.

It is an incorporated society without capital stock. The affairs of the Society are managed by a Board of Directors under a Constitution and By-Laws. Officers are nominated by a nominating committee appointed by the Board of Directors and elected by the members.

Direct all general correspondence and inquiries regarding membership to Society headquarters at 235 West 102nd Street, New York 25, N. Y., c/o Mr. W. J. Holian, Assistant Secretary.

Officers of the Society

President ..... ALFRED L. FERGUSON
Past President ..... JAMES A. LEE
Vice-President ..... CHARLES L. FAUST
Vice-President ..... RALPH M. HUNTER
Vice-President ..... J. C. WARNER
Treasurer ..... E. GIDEON WIDELL
Secretary ..... H. B. LINFORD

UMI

UMI